universe

Review

Vector Quarkonia at the LHC with JETHAD: A High-Energy Viewpoint

Francesco Giovanni Celiberto

Departamento de Física y Matemáticas, Campus Universitario, Universidad de Alcalá (UAH), E-28805 Alcalá de Henares, Spain; francesco.celiberto@uah.es

Abstract: In this review, we discuss and extend the study of the inclusive production of vector quarkonia, J/ψ and Υ, emitted with large transverse momenta and rapidities at the LHC. We adopt the novel ZCW19$^+$ determination of fragmentation functions to depict the quarkonium production mechanism at the next-to-leading level of perturbative QCD. This approach is based on the non-relativistic QCD formalism well adapted to describe the formation of a quarkonium state from the collinear fragmentation of a gluon or a constituent heavy quark at the lowest energy scale. We rely upon the NLL/NLO$^+$ hybrid high-energy and collinear factorization for differential cross-sections, where the collinear formalism is enhanced by the BFKL resummation of next-to-leading energy logarithms arising in the t-channel. We employ the JETHAD method to analyze the behavior of the rapidity distributions for double-inclusive vector quarkonium and inclusive vector quarkonium plus jet emissions. We discover that the natural stability of the high-energy series, previously seen in observables sensitive to the emission of hadrons with heavy flavor detected in the rapidity acceptance of LHC barrel calorimeters, becomes even more manifest when these particles are tagged in forward regions covered by endcaps. Our findings present the important message that vector quarkonia at the LHC via hybrid factorization offer a unique chance to perform precision studies of high-energy QCD, as well as an intriguing opportunity to shed light on the quarkonium production puzzle.

Keywords: precision QCD; high-energy resummation; vector quarkonia; NRQCD fragmentation

Citation: Celiberto, F.G. Vector Quarkonia at the LHC with JETHAD: A High-Energy Viewpoint. *Universe* **2023**, *9*, 324. https://doi.org/10.3390/universe9070324

Academic Editors: Deliang Yao and Zhi Yang

Received: 23 May 2023
Revised: 30 June 2023
Accepted: 2 July 2023
Published: 7 July 2023

Contents

1. Introduction

It is widely recognized that the emissions of heavy-quark flavored objects in high-energy hadron collisions represent gold-standard channels to access the core dynamics of fundamental interactions. Quarks with heavy masses are *sentinels* of long-awaited imprints of New Physics, since they might couple with Beyond the Standard Model (BSM) particles. At the same time, since the values of their masses lie in a region where Quantum Chromo-Dynamics (QCD) perturbative calculations are possible, they give a unique opportunity to perform precision studies of strong interactions.

QCD is the well-established quantum field theory that describes the strong interaction sector. It relies upon the non-Abelian $SU(N_c)$ gauge group, with $N_c \equiv 3$ being the number of colors [1–4]. Quarks are the spin-1/2 fermions that make up the matter part of hadrons. There exist six species of quarks and of their anti-matter counterparts, grouped into three families. In the QCD Lagrangian, they are described by fermionic fields belonging to the fundamental triplet representation of $SU(3)$. Conversely, gluons are the spin-1 massless bosons that mediate the strong force. They bind quarks together to form hadrons. In the QCD Lagrangian, they are described by bosonic fields belonging to the adjoint octet representation of $SU(3)$.

While QCD represents one of the founding pillars of the Standard Model (SM) of fundamental interactions, it can also serve as a "support basis" in relevant searches for New Physics (see Ref. [5] for a recent and comprehensive resource letter). An incomplete list of possible QCD portals beyond SM is as follows: *axions*, namely hypothetical elementary particles, originally proposed by R. Peccei and H. Quinn to resolve the strong Charge-Parity (CP) problem [6–9]; Non-Abelian *dark gauge forces* [10,11]; *quarkyonic matter* [12–14]; and *higher-dimension* QCD operators, effectively included in the Lagrangian (see, e.g., Refs. [15–18] and references therein).

Unraveling the production mechanisms of heavy-quark flavored hadrons plays a key role in understanding the true dynamics of strong interactions. Mesons whose lowest Fock state contains a heavy quark (Q) and its antiquark ($\bar{Q}$) are known as (heavy) *quarkonia*. The origins of quarkonium studies date back to the so-called *November Revolution*. On 11 November 1974, a new vector meson, whose mass was around 3.1 GeV, carrying photon quantum numbers, was discovered. It was named J/ψ after the two groups that contemporaneously observed it: the collaboration headed by B. Richter [19] at the Stanford Linear Accelerator Center (SLAC) and one led by S. Ting [20] at the Brookhaven National Laboratory (BNL). A few days after the announcements by SLAC and BNL, the discovery of the J/ψ was confirmed by the Frascati ADONE experiment, directed by G. Bellettini [21]. The fact that the J/ψ was a hadron became clear from the analysis of the ratios of the cross-sections between hadrons and $\mu^+\mu^-$ in e^+e^- inclusive annihilations, which eventually were much larger at the resonance, thus pointing out that J/ψ-like objects directly decay into lighter hadrons. At the same time, evidence was found that the charm quark exists and that quarks are real particles of which hadrons are made, and not simply mathematical artifacts. The concept of charm flavor was proposed for the first time by Bjorken and Glashow in 1964 [22], but its experimental evidence was scarce. Then, in 1970, the Glashow–Iliopoulos–Maiani (GIM) mechanism [23] proposed the existence of a new quark species, the charm flavor , which became necessary to explain the suppression of Flavor-Changing Neutral Currents (FCNCs) in Feynman diagrams embodying a loop.

Studies on quarkonium properties and formation mechanisms have been relevant to validate our knowledge of the fundamental properties of QCD, such as *asymptotic freedom*. In particular, the discovery of the first excited radial state of the J/ψ, called $\psi(2S)$, brought clear evidence that the strong force lowers at short distances. The J/ψ represents the first discovered *charmonium*. This name reflects an affinity with the e^+e^- bound pair, called the *positronium*, and it stands for an entire species of hadrons comprehending all the $c\bar{c}$

meson states. A few years after the first J/ψ observation, other charmonia were discovered (such as the P-wave χ_c and the pseudoscalar η_c), as well as hadrons with open charm, such as D mesons [24]. The first *bottomonium* particle was observed in 1977 and was named Υ. It represents a vector meson equivalent to the J/ψ, but with bottom quarks instead of charm quarks [25]. Excited $b\bar{b}$ states, such as the $\Upsilon(2S)$, and open-bottom B mesons were subsequently observed [26].

Toponium systems are hypothetical $t\bar{t}$ mesons whose lowest Fock state consists of a top and an anti-top quark. As for charmonia and bottomonia, toponia should also appear as vectors, called θ mesons, or scalars, called η_t mesons (for a short overview, see Ref. [27] and references therein). At variance with lighter, observed quarkonia, $t\bar{t}$ mesons are thought to decay instantly since top quarks are short-lived [28–32]. Hence, they possess a very large decay width [33,34]. Estimates for toponium emission rates at the LHC were presented in Refs. [35–38]. Possible mechanisms for spin-1 and spin-0 toponium production at future lepton colliding machines were proposed in Refs. [39–41] and Ref. [42], respectively. Ref. [43] reports deviations between predictions and observations related to the production of top pairs at the LHC, followed by double-lepton decays. It also proposes a novel method to unveil toponium formation by reconstructing both top and anti-top constituents in dilepton hadroproduction. Ref. [44] focuses on probing CP violation via toponium leptoproduction.

A clear advantage in studying quarkonia comes from the fact that they can be easily detected, particularly vector mesons, which can be easily identified in lepton-initiated processes. At the same time, however, describing their production rates is a challenge. Difficulties encountered in attempting to describe quarkonium formation in distinct kinematic ranges give rise to the so-called *quarkonium production puzzle*. Several models attempting to capture the core features of the quarkonium formation mechanism have been proposed so far (see Refs. [45,46] for a review). The Color Evaporation Model (CEM) [47,48] was perhaps the first mechanism proposed. It assumes that the original $(Q\bar{Q})$ pair, from which the final quarkonium stems, goes through a very large number of soft interactions, which eventually permits it to be a color singlet, after hadronization. These soft subprocesses completely decorrelate the initial $(Q\bar{Q})$ color state with the final meson one. The predictive power of CEM is limited by the inability to provide us with a distinct description of the production rates of different quarkonia, such as J/ψ and χ_c states [49,50].

The second model proposed was the Color Singlet Mechanism (CSM) [51–54]. In contrast with CEM, it postulates that the $(Q\bar{Q})$ pair does not undergo any soft evolution. This happens because gluon emissions are suppressed with powers of $\alpha_s(m_Q)$, with $\alpha_s(\mu)$ the QCD running coupling and m_Q the mass of the constituent heavy quark. Both the quark polarization and its color state do not change during the hadronization phase. Thus, the originating pair must be generated in a color-singlet configuration. Moreover, since the measured quarkonium mass, $m_{\mathcal{Q}}$, is slightly larger than $2m_Q$, the two constituent heavy quarks are almost at rest in the hadron frame, namely with almost zero relative velocity, $v_{\mathcal{Q}}$. The only nonperturbative contribution to the formation mechanism is a nonrelativistic Schrödinger wave function at the origin, labeled as $\mathcal{R}_{\mathcal{Q}}(0)$. While the CSM genuinely possesses high predictive power (its only free parameter is $\mathcal{R}_{\mathcal{Q}}(0)$, which can be extracted from experimental data on leptonic decay widths), it presents infrared divergences emerging at higher perturbative order in P-wave decay channels [55,56].

To overcome these divergence issues associated with the CSM, it was argued that higher Fock states, such as $|Q\bar{Q}g\rangle$ and so on, could play a role in the production mechanism. Contextually, they could solve Next-to-Leading Order (NLO) divergences. The $(Q\bar{Q})$ subsystem contained in a $|Q\bar{Q}g\rangle$ state is clearly in a Color Octet (CO) state. More generally, the physical quarkonium is built up as a linear combination of all the possible Fock states. All these terms are ordered within a double expansion in powers of both α_s and $v_{\mathcal{Q}}$. In this picture, the CSM represents the leading contribution in $v_{\mathcal{Q}}$ for S-wave channels (for higher waves, this term might vanish). The $(\alpha_s \otimes v_{\mathcal{Q}})$ expansion constitutes the building block of NonRelativistic QCD (NRQCD) [57–63]. According to this effective field theory, high-energy distributions sensitive to quarkonium emissions are cast as sums of partonic subprocess hard factors producing a given Fock state in the final state, each of them being multiplied by a Long-Distance Matrix Element (LDME) embodying the nonperturbative hadronization mechanism. Despite giving an elegant solution to the quarkonium production puzzle, the NRQCD introduces many new nonperturbative parameters, which can make the comparison with data cumbersome.

What makes the overall picture even more intricate is the possibility of having a quarkonium produced through the decay or de-excitation of heavier particles. Thus, J/ψ production can follow the decay of a B meson [64]. This channel is labeled as *nonprompt*, since it features a visible time delay. In some circumstances, the nonprompt contribution can be experimentally isolated by measuring the distance between the creation vertex of the B and its subsequent decay or de-excitation. In this way, one obtains the *prompt* component. Within the prompt channel, a charmonium, e.g., the J/ψ, can still be emitted as the decay product of a χ_c, or via the de-excitation of a $\psi(2S)$. This represents the *indirect* production component. The total number of quarkonia produced in hard subprocesses is called the *direct fraction* and it is generally not measurable alone but can be accessed by subtraction methods.

All the models introduced above are based on the assumption that the dominant formation mechanism is the production of a $(Q\bar{Q})$ pair in the hard scattering, namely at *short distances*, followed by its hadronization into the physical quarkonium state. The two constituent heavy quarks are generated with a relative transverse-momentum separation of order $1/|\vec{p}_T|$. Therefore, short-distance mechanisms are expected to be suppressed at large $|\vec{p}_T|$. Furthermore, the two quarks have a separation of order $1/\mu$, with μ any process-typical energy scale [65]. At large transverse momenta, one has $\mu \sim |\vec{p}_T| \gg m_Q$. In this way, since the exchanges of particles with virtualities of the order of $|\vec{p}_T|$ are related to the scatterings of particles in a small volume, $1/|\vec{p}_T|^3$ [66,67], they act as suppression factors for the probability amplitude.

The authors of Ref. [68] pointed out that, in moderate or large transverse-momentum regimes, an additional mechanism is at work. It relies upon the *fragmentation* of a single parton, which then inclusively hadronizes into the observed quarkonium. According to *collinear factorization*, which is the most appropriate formalism to describe these regimes, the full hadronization must be encoded in collinear Fragmentation Functions (FFs), whose time-like evolution [69,70] is naturally governed by the Dokshitzer–Gribov–Lipatov–Altarelli–Parisi (DGLAP) system of equations [71–75]. Here, NRQCD turns out to be a powerful tool to perturbatively calculate nonevolved, initial scale inputs for these FFs. Now, the heavy-quark pair has a separation of order $1/m_Q$. On the one hand, fragmentation production is often of a higher perturbative order than the short-distance mechanism. On the other hand, fragmentation is magnified by powers of $(\mu/m_Q)^2$. Thus, it becomes dominant at large energy scales, $\mu \gg m_Q$.

NRQCD calculations of the gluon FF to an S-wave particle in the CSM were presented in Ref. [68] for J/ψ and η_c at Leading Order (LO), and in Ref. [76] for η_c with higher accuracy (NLO). The corresponding calculation for the $(c \to J/\psi + c + \mathcal{X})$ FF was given in Ref. [77] at LO and in Ref. [78] at NLO. Refs. [79–83] contain phenomenological analyses aimed at shedding light, at the LO, on the intersection range between the short-distance and the fragmentation approximations. Functions portraying the fragmentation of constituent heavy quarks into S- and P-wave quarkonia were studied in Refs. [84,85]. We refer to Refs. [86,87] for some FF advancements at next-to-NLO. FFs for polarized quarkonia were investigated in Refs. [88–93] (see Ref. [94] for a digression). The authors of Ref. [95] analyze quarkonium factorization and evolution at large energies.

All the issues found on the path towards capturing the correct production mechanism(s) do not prevent quarkonium studies from providing gold-standard tools to access the inner dynamics of QCD. Pioneering analyses of quarkonium emissions within collinear factorization at NLO were performed in Refs. [32,96–104]. Refs. [105,106] study the NLO transverse-momentum spectrum in the CEM approximation. NRQCD advancements in quarkonium polarization can be found in Refs. [107–109]. The possible emergence of Multi-Parton Interaction (MPI) dynamics in quarkonium observables was quantified in Refs. [110,111]. The weight of nuclear modifications of the gluon density on quarkonium was gauged for the first time in Refs. [112–114]. Automated NRQCD calculations were recently implemented [115–118]. Problems in the NLO description of J/ψ distributions at large transverse momenta can spread from an over-subtraction in the factorization of collinear singularities inside collinear Parton Distribution Functions (PDFs) [119–121]. Matching high-energy (low-x) resummation effects on top of NLO calculations recently emerged as a promising means to solve these issues [122,123]. Color reconnection effects in J/ψ hadroproduction have been recently investigated [124]. Some recent results on forward and central quarkonium production in (ultra-peripheral) hadron and lepton–hadron scatterings can be found in Refs. [125–142]. The formation mechanism of hidden heavy-flavored *tetra-* and *penta-quarks* was studied [143,144] by means of the *hadro-quarkonium* approach [145,146]. NRQCD-based studies have been used to model tetra-quark fragmentation [147–150].

Observables sensitive to the single forward production of quarkonium states, as well as those for forward light vector mesons [151–156] and forward Drell–Yan pairs [157–159], are useful tools to extensively scan the intersection kinematic corners between the Transverse-Momentum-Dependent (TMD) and the high-energy dynamics. Studies given in Refs. [154,156] unambiguously pointed out that spin-dependent distributions for the single forward electroproduction of a ρ meson at HERA and the Electron-Ion Collider (EIC) give us a unique opportunity to access the content and properties of low-x gluons in the proton. There, transverse-momentum factorized cross-sections are sensitive to the scattering of color dipoles with a small transverse distance. Contrariwise, forward detections of excited states, such as $\psi(2S)$ and $\Upsilon(2S)$ quarkonia, might probe dipoles with larger transverse sizes [160–162], thus calling for a low-$|\vec{p}_T|$ improvement in the pure small-x picture.

Quarkonium emissions at low transverse momenta in lepton–hadron and hadron–hadron collisions offer a unique opportunity to perform 3D reconstructions of the nucleon content by means of *transverse-momentum-dependent* gluon densities [163–166]. We refer to Refs. [167–178] for recent phenomenological advancements. The validity of TMD factorization in the presence of quarkonium detections was recently questioned via a Soft and Collinear Effective Theory (SCET) [179,180] and then evaluated for di-jet and heavy-meson pair tags in lepton–proton reactions [181]. An SCET approach turns out to be useful to access jet fragmenting functions, a basic component to study quarkonia inside jets [182–186]. Quarkonium TMD distributions were recently investigated in Ref. [187].

In this review, we consider the inclusive hadroproduction, at LHC energies and kinematic configurations, of a forward vector quarkonium (J/ψ or Υ in the *direct* channel) in association with a backward particle, which can be another vector quarkonium or a light-flavored jet. The two final-state objects have transverse momenta and are largely separated in rapidity. On the one hand, moderate values of partons' longitudinal-momentum fractions make a description in terms of collinear PDFs valid. On the other hand, large rapidity intervals translate into significant exchanges of transverse momenta in the t-channel, which call for a $|\vec{p}_T|$-factorization treatment aimed at resumming large logarithmic contributions in energy, associated with rapidity-ordered gluon emissions. As a last step, we must select the most adequate mechanism for the quarkonium formation in the kinematic sector of our interest. From a collinear factorization perspective, large transverse momenta permit us to adopt a Variable-Flavor Number Scheme (VFNS) approach [188,189]. Here, the hard factor for the production of a light parton is convoluted with an FF that describes the hadronization into the vector quarkonium.

Following the recent scheme proposed in Ref. [190], we first make use of NRQCD to build initial-scale FF inputs, and then we encode the resummation of DGLAP-type logarithms. We take the NRQCD input from a recent NLO computation of the constituent heavy-quark FF channel [78], together with the gluon one [68]. We stress that these NRQCD FFs describe a vector quarkonium in a color-singlet state. In other words, they embody

${}^3S_1^{(1)}$ LDMEs (we refer to Section 3.1 for more details). Putting together all the components, we define a hybrid high-energy and collinear factorization, already set as the reference formalism for the study of semi-inclusive forward–backward hadroproduction [191–195], now enriched with a novel element: the single-parton quarkonium fragmentation [190].

Another formalism, close in spirit to our hybrid factorization and suitable for single forward detections, was proposed in Refs. [196–200]. We also refer to Refs. [201,202] for analyses of small-x resummed inclusive or differential distributions for Higgs and heavy-flavor hadroproduction via the HELL method [203–205], which relies upon the Altarelli–Ball–Forte (ABF) approach [206–212], aimed at combining collinear factorization with small-x resummation, based upon high-energy factorization theorems [213–220]. We believe that a strong formal connection between our hybrid factorization and the ABF formalism exists. Studies along this direction are relevant, but they go beyond the scope of this review. We postpone them for a future work.

Our study is complementary to the one presented in Ref. [221], where the inclusive semi-hard J/ψ plus jet process was investigated within the short-distance approximation and with partial NLO accuracy. In the future, matching between the two approaches will certainly improve the description of quarkonium detections at high energies. For the sake of completeness, we mention the computation of doubly off-shell LO coefficient functions for inclusive quarkonium production in central rapidity regions [222,223].

This review is structured as follows. In Section 2.2, we introduce the NLL/NLO$^{(+)}$ hybrid high-energy and collinear factorization, while Section 3 contains technical details on the vector quarkonium collinear fragmentation mechanism, based on constituent heavy-quark and gluon initial-scale inputs on top of which standard DGLAP evolution is switched on. In Section 4, we present our phenomenological analysis of rapidity-differential distributions. Then, in Section 5, we draw our conclusions and highlight future perspectives.

2. Vector Quarkonia at the LHC with JETHAD

This part of the manuscript contains a brief review of recent key advancements in the phenomenology in the semi-hard sector of QCD (Section 2.1), as well as technical details of the hybrid high-energy and collinear factorization for inclusive vector quarkonium and vector quarkonium + jet hadroproduction at NLL/NLO$^+$ (Section 2.2).

2.1. A Glance at High-Energy QCD Phenomenology

One of the greatest results in high-energy particle physics is the possibility to decouple, in the context of hadron scatterings, the long-distance from the short-distance dynamics. This decoupling allows us to factorize nonperturbartive components from perturbative computations through the well-established *collinear* picture. At the same time, there exist kinematic regions where large logarithms arise. They can become so large as to compensate for the smallness of the QCD running coupling, thus spoiling the convergence of the perturbative series. Therefore, the standard collinear factorization needs to be enhanced by the inclusion of one or more all-order resummations.

We turn our attention to the so-called *semi-hard* regime [224] (see Refs. [225–227] for relevant applications), where the scale hierarchy $\sqrt{s} \gg \{Q\} \gg \Lambda_{\rm QCD}$ stringently holds. Here, s is the center-of-mass energy squared, $\{Q\}$ a set of process-characteristic hard scales, and $\Lambda_{\rm QCD}$ the QCD scale. While the second inequality simply tells us that the use of perturbation techniques is allowed, the first highlights that we have entered the *Regge limit* of QCD. In this case, large logarithms of the form $\ln s/Q^2$ enter the perturbative series with a power growing with the order. When $\alpha_s(Q^2)\ln(s/Q^2) \sim 1$, pure fixed-order perturbative calculations are no longer reliable, but it must be improved by resumming these large-energy logarithms to all orders. The most powerful mechanism for this high-energy resummation is represented by the Balitsky–Fadin–Kuraev–Lipatov (BFKL) formalism [228–231], which tells us how to resum all the contributions proportional to $(\alpha_s \ln s)^n$, the so-called Leading Logarithmic (LL) approximation, as well as the ones proportional to $\alpha_s(\alpha_s \ln s)^n$, the so-called Next-to-Leading Logarithmic (NLL) approximation. In the BFKL formalism, a given scattering amplitude can be written as a convolution of a process-independent Green's function with two singly-off-shell coefficient functions depicting the transition from each colliding particle to the respective final-state object. Using the BFKL jargon, these coefficients are known as forward-production *impact factors*. The BFKL Green's function is controlled an integral evolution equation, whose kernel is known at the NLO for any fixed, not growing with energy, momentum transfer, t, and for any possible two-gluon color exchange in the t-channel [232–238]. Recent, partial advancements of the BFKL next-to-NLL level can be found in Refs. [239–243].

Despite the full NLO accuracy of the kernel, the predictive power of the BFKL at NLL is limited by the number of impact factors computed within NLO: (1) colliding parton (quarks and gluons) impact factors [244,245], namely the core component for (2) forward jet [246–251] and (3) forward light hadron [252] impact factors, then (4) γ^* to Light Vector Meson (LVM) transition [253] and (5) γ^* to γ^* impact factors [254–259], and finally (6) the impact factor depicting the emission of a forward Higgs boson in the infinite top-mass limit [260–262] (see also Refs. [263,264]). The forward production impact factors known at LO only are those for (7) Drell–Yan pairs [157,265], (8) heavy-quark pairs hadro- and photo-produced [266–268], and (9) forward J/ψ emitted low transverse momentum in the short-distance approximation [221] (see also Refs. [269–271]).

On the one hand, these off-shell coefficient functions have been employed for phenomenological studies of several semi-inclusive reactions featuring forward plus backward two-particle final states. An incomplete list is as follows: the diffractive exclusive electroproduction of two light vector mesons [272–276], the inclusive hadroproduction of two jets with large transverse momenta and well separated in rapidity (Mueller–Navelet channel [277]), for which several analyses have been conducted so far (see, e.g., Refs. [191,249,251,278–290]), the inclusive emission of two light-charged hadrons [291–295], three- and four-jet hadroproduction [296–308], J/ψ plus jet [221], hadron plus jet [192,309–313], Higgs plus jet [314–318], heavy-light dijet systems [193,319], forward Drell–Yan pairs with a possible backward-jet detection [320], and heavy-flavored hadrons' hadroproduction [190,194,221,266–268,321–327].

On the other hand, single forward emissions permit us to unveil the proton content at low x via the BFKL Unintegrated Gluon Distribution (UGD), whose evolution is driven by Green's function. Gold-standard channels for the testing of the UGD are the exclusive light vector–meson leptoproduction at HERA [151–155,328–331] and the EIC [156,332–335], the exclusive quarkonium photoemission [162,336,337], and the inclusive detection of Drell–Yan dilepton systems [157–159,338]. Then, the information on the gluon content at small x carried by the BFKL UGD has allowed us to enhance the collinear description via the first determination of small-x resummed PDFs [339–341], as well as to model low-x improved gluon TMD densities at leading twist, namely within the lowest level of the operator product expansion of the gluon correlator [342–350]. We refer to Refs. [351,352] for recent investigations of the interplay between the BFKL dynamics and the TMD factorization, and to Ref. [353] for a study of the connection between the deep-inelastic-scattering dipole cross-section and the UGD.

A major issue emerging from the study of Mueller–Navelet distributions is the size of the NLL corrections, which are of the same order but generally with an opposite sign with respect to the LL background. This leads to heavy instabilities in the high-energy series arising when renormalization and factorization scale variations are moved from their natural values, suggested by process kinematics. Thus, the differential cross-sections can easily become negative when the rapidity interval between the two jets increases. Furthermore, azimuthal-angle correlations turn out to be unphysical, both in small and large rapidity interval ranges. Several strategies have been proposed to solve these issues. Among them, the Brodsky–Lepage–Mackenzie (BLM) method [354–357], as specifically designed for semi-hard processes [282], has become quite popular, since it permits us to lightly suppress these instabilities on azimuthal correlations and to moderately improve the agreement with experimental data. However, the use of BLM is almost ineffective on cross-sections for light di-hadron and light hadron jet observables. This happens because the optimal renormalization scales are substantially higher than the natural scales [192,225,309]. As a result, one observes a significant loss of statistics for total cross-sections. Therefore, any effort at reaching the precision level is unsuccessful.

First, unambiguous imprints of fair stability of the high-energy resummation under higher-order corrections and energy-scale variations were observed only recently in Large Hadron Collider (LHC) semi-inclusive final states featuring the tags of objects possessing large transverse masses, such as Higgs bosons [314,358–361]. Subsequently, a very remarkable result at NLL was obtained by studying semi-hard correlations for a singly heavy-flavored hadron species, namely Λ_c baryons. A strong stabilization pattern emerged from an analysis of double Λ_c and Λ_c plus jet productions at the LHC [194], and also from similar distributions sensitive to single-bottomed hadrons [321]. Indisputable evidence was provided that the characteristic trend of VFNS collinear FFs describing the formation of those heavy hadrons at large transverse momenta translates into the *natural stabilization* of the high-energy series, with the fair dampening of those instabilities associated with higher-order corrections. Analogous patterns were then observed for vector quarkonium [190] and charmed *B*-meson [325] semi-hard observables built up by combining the high-energy resummation with collinear PDFs and DGLAP-evolved FFs with an NRQCD initial-scale input. This suggests that the found natural stability is an *intrinsic* feature globally shared by heavy-flavor observables.

2.2. NLL/NLO$^+$ Hybrid Factorization

We consider the reactions as in Figure 1:

$$\begin{aligned} \mathrm{p}(P_a) \;+\; \mathrm{p}(P_b) \;&\to\; \mathcal{Q}(p_{\mathcal{Q}_1}, y_{\mathcal{Q}_1}) \;+\; \mathcal{X} \;+\; \mathcal{Q}(p_{\mathcal{Q}_2}, y_{\mathcal{Q}_2}) \;, \\ \mathrm{p}(P_a) \;+\; \mathrm{p}(P_b) \;&\to\; \mathcal{Q}(p_{\mathcal{Q}}, y_{\mathcal{Q}}) \;+\; \mathcal{X} \;+\; \mathrm{jet}(p_J, y_J) \;, \end{aligned} \tag{1}$$

with $\mathrm{p}(P_{a,b})$ being an incoming proton with four-momentum $P_{a,b}$, $\mathcal{Q}(p_{\mathcal{Q}_{(1,2)}}, y_{\mathcal{Q}_{(1,2)}})$ denoting a vector quarkonium (J/ψ or Υ) produced with four-momentum $p_{\mathcal{Q}_{(1,2)}} \equiv p_{1,2}$ and rapidity $y_{\mathcal{Q}_{(1,2)}} \equiv y_{1,2}$, and the light-favored jet being detected with four-momentum $p_J \equiv p_2$ and rapidity $y_J \equiv y_2$. The inclusive, undetected remnant is $\mathcal{X}$. The large final-state transverse momenta, $|\vec{p}_{1,2}|$, together with the high rapidity interval, $\Delta Y \equiv y_1 - y_2$, are necessary conditions to make the final state diffractive and semi-hard. Moreover, the transverse-momentum ranges must to be large enough to preserve the validity of the single-parton collinear fragmentation as a leading mechanism for quarkonium production.

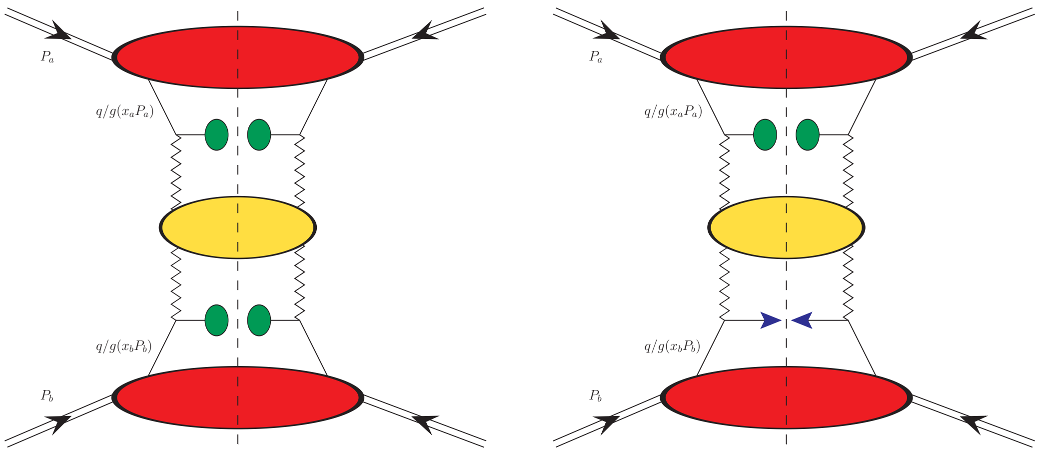

Figure 1. Hybrid high-energy and collinear factorization for the double-inclusive vector quarkonium (**left**) and for the inclusive vector quarkonium + jet production (**right**). Red blobs describe proton collinear PDFs, green blobs denote quarkonium FFs, and blue arrows denote light-flavored jets. The BFKL ladder, depicted by the yellow blob, is connected to impact factors via Reggeon (zigzag) lines. Diagrams realized with `JaxoDraw 2.0` [362].

Incoming protons' four momenta can be taken as Sudakov vectors obeying $P_a^2 = P_b^2 = 0$ and $2(P_a \cdot P_b) = s$, so that the four momenta of the observed object can be decomposed in the following way:

$$p_{1,2} = x_{1,2} P_{a,b} + \frac{\vec{p}_{1,2}^{\,2}}{x_{1,2} s} P_{b,a} + p_{1,2\perp} \,, \quad p_{1,2\perp}^2 = -\vec{p}_{1,2}^{\,2} \,. \tag{2}$$

Here, outgoing particle longitudinal momentum fractions, $x_{1,2}$, are related to the corresponding rapidities through $y_{1,2} = \pm\frac{1}{2}\ln\frac{x_{1,2}^2 s}{\vec{p}_{1,2}^{\,2}}$, so that $\mathrm{d}y_{1,2} = \pm\frac{\mathrm{d}x_{1,2}}{x_{1,2}}$, and $\Delta Y \equiv y_1 - y_2 = \ln\frac{x_1 x_2 s}{|\vec{p}_1||\vec{p}_2|}$.

A purely collinear treatment in QCD would cause the LO cross-sections of our reactions (Equation (1)) to be written as a convolution among the partonic hard factor, the proton PDFs, and the quarkonium FFs. In the double quarkonium channel (panel a) of Figure 1), one has

$$\begin{aligned} \frac{\mathrm{d}\sigma^{\mathrm{LO}}_{[p+p\,\to\,\mathcal{Q}+\mathcal{Q}]}}{\mathrm{d}x_1\mathrm{d}x_2\mathrm{d}^2\vec{p}_1\mathrm{d}^2\vec{p}_2} &= \sum_{a,b}\int_0^1 \mathrm{d}x_a \int_0^1 \mathrm{d}x_b\; f_a(x_a,\mu_F) f_b(x_b,\mu_F) \\ &\times \int_{x_1}^1 \frac{\mathrm{d}z_1}{z_1}\int_{x_2}^1 \frac{\mathrm{d}z_2}{z_2}\, D_a^{\mathcal{Q}}\left(\frac{x_1}{z_1},\mu_F\right) D_b^{\mathcal{Q}}\left(\frac{x_2}{z_2},\mu_F\right) \frac{\mathrm{d}\hat{\sigma}_{a,b}}{\mathrm{d}x_a\mathrm{d}x_b\mathrm{d}z_1\mathrm{d}z_2\mathrm{d}^2\vec{p}_1\mathrm{d}^2\vec{p}_2}\,, \end{aligned} \tag{3}$$

where the (a,b) indices run over quarks, antiquarks, and the gluon; $f_{a,b}(x,\mu_F)$ denote parent protons' PDFs; $D^{\mathcal{Q}}_{a,b}\left(\frac{x}{z},\mu_F\right)$ denote quarkonium FFs; $x_{a,b}$ are the longitudinal-momentum fractions of the process-initiating partons; $z_{1,2}$ are the longitudinal-momentum fractions of fragmenting partons; and $\mathrm{d}\hat{\sigma}_{a,b}(x_a,x_b)$ is the partonic hard factor. In the same way, in the quarkonium plus jet channel (panel b) of Figure 1), one writes

$$\begin{aligned} \frac{\mathrm{d}\sigma^{\mathrm{LO}}_{[p+p\,\to\,\mathcal{Q}+\mathrm{jet}]}}{\mathrm{d}x_1\mathrm{d}x_2\mathrm{d}^2\vec{p}_1\mathrm{d}^2\vec{p}_2} &= \sum_{a,b}\int_0^1 \mathrm{d}x_a \int_0^1 \mathrm{d}x_b\; f_a(x_a,\mu_F) f_b(x_b,\mu_F) \\ &\times \int_{x_1}^1 \frac{\mathrm{d}z}{z} D_a^{\mathcal{Q}}\left(\frac{x_1}{z}\right) \frac{\mathrm{d}\hat{\sigma}_{\alpha,\beta}}{\mathrm{d}x_1\mathrm{d}x_2\mathrm{d}z\,\mathrm{d}^2\vec{p}_1\mathrm{d}^2\vec{p}_2}\,. \end{aligned} \tag{4}$$

Conversely, to obtain the formula for the high-energy resummed cross-section in our hybrid factorization, we first apply the high-energy factorization that is genuinely embodied in the BFKL framework, and then we complement the description by plugging collinear inputs, PDFs, and FFs. It is convenient to rewrite the differential cross-section as a Fourier sum of azimuthal-angle coefficients

$$\frac{\mathrm{d}\sigma^{\mathrm{NLL/NLO}^+}}{\mathrm{d}y_1\mathrm{d}y_2\mathrm{d}\vec{p}_1\mathrm{d}\vec{p}_2\mathrm{d}\varphi_1\mathrm{d}\varphi_2} = \frac{1}{(2\pi)^2}\left[\mathcal{C}_0^{\mathrm{NLL/NLO}^+} + 2\sum_{n=1}^{\infty}\cos(n(\Phi-\pi))\,\mathcal{C}_n^{\mathrm{NLL/NLO}^+}\right], \tag{5}$$

where $\varphi_{1,2}$ are final-state particle azimuthal angles and $\Phi \equiv \varphi_1 - \varphi_2$. The azimuthal coefficients are calculated in the BFKL approach and they embody the resummation of energy logarithms up to the NLL level. Working in the $\overline{\mathrm{MS}}$ renormalization scheme [363], one obtains (for the technical derivation see, e.g., Ref. [249])

$$\begin{aligned} \mathcal{C}_n^{\mathrm{NLL/NLO}^+} &= \int_0^{2\pi}\mathrm{d}\varphi_1\int_0^{2\pi}\mathrm{d}\varphi_2\,\cos(n(\Phi-\pi))\,\frac{\mathrm{d}\sigma^{\mathrm{NLL/NLO}^+}}{\mathrm{d}y_1\mathrm{d}y_2\,\mathrm{d}|\vec{p}_1|\,\mathrm{d}|\vec{p}_2|\mathrm{d}\varphi_1\mathrm{d}\varphi_2} \\ &= \frac{e^{\Delta Y}}{s}\int_{-\infty}^{+\infty}\mathrm{d}\nu\, e^{\Delta Y \bar{\alpha}_s(\mu_R)\chi^{\mathrm{NLO}}(n,\nu)} \\ &\times\; \alpha_s^2(\mu_R)\left\{c_1^{\mathrm{NLO}}(n,\nu,|\vec{p}_1|,x_1)[c_2^{\mathrm{NLO}}(n,\nu,|\vec{p}_2|,x_2)]^* \right. \\ &+ \left.\bar{\alpha}_s^2(\mu_R)\,\Delta Y\frac{\beta_0}{4N_c}\chi(n,\nu)f(\nu)\right\}, \end{aligned} \tag{6}$$

where $\bar{\alpha}_s(\mu_R) \equiv \alpha_s(\mu_R) N_c/\pi$ with N_c the number of colors; then, $\beta_0 = 11N_c/3 - 2n_f/3$ as the first coefficient of the QCD β-function with n_f the number of flavors. A two-loop running-coupling setup with $\alpha_s(M_Z) = 0.11707$ and a dynamic n_f is adopted. The BFKL kernel at the exponent of Equation (6) encodes the resummation of leading and next-to-leading energy logarithms. It reads

$$\chi^{\rm NLO}(n,\nu) = \chi(n,\nu) + \bar{\alpha}_s \hat{\chi}(n,\nu) \;, \tag{7}$$

with

$$\chi(n,\nu) = -2\gamma_{\rm E} - 2\,{\rm Re}\left\{\psi\left(\frac{1+n}{2} + i\nu\right)\right\} \tag{8}$$

being the LO BFKL eigenvalues, $\gamma_{\rm E}$ the Euler–Mascheroni constant, and $\psi(z) \equiv \Gamma'(z)/\Gamma(z)$ the logarithmic derivative of the Gamma function. Then, the $\hat{\chi}(m,\nu)$ function in Equation (7) denotes the NLO correction to the BFKL kernel

$$\hat{\chi}(n,\nu) = \bar{\chi}(n,\nu) + \frac{\beta_0}{8N_c}\chi(n,\nu)\left(-\chi(n,\nu) + 10/3 + 2\ln\frac{\mu_R^2}{\mu_C^2}\right) . \tag{9}$$

Here, $\mu_C \equiv \sqrt{m_{1\perp} m_{2\perp}}$, with $m_{(1,2)\perp}$ being the transverse masses of the two final-state objects. For the quarkonia, one has $m_{\mathcal{Q}\perp} = \sqrt{m_{\mathcal{Q}}^2 + |\vec{p}_{\mathcal{Q}}|^2}$, with $m_{\mathcal{Q}} \equiv m_{J/\psi} = 3.0969$ GeV or $m_{\mathcal{Q}} \equiv m_{\Upsilon} = 9.4603$ GeV. The light-jet transverse mass coincides with its transverse momentum, $m_{\mathcal{Q}\perp} = |\vec{p}_J|$. The characteristic $\bar{\chi}(n,\nu)$ function was calculated in Ref. [364] and reads

$$\begin{aligned}\bar{\chi}(n,\nu) \;=\; & -\frac{1}{4}\left\{\frac{\pi^2-4}{3}\chi(n,\nu) - 6\zeta(3) - \frac{{\rm d}^2\chi}{{\rm d}\nu^2} + 2\,\phi(n,\nu) + 2\,\phi(n,-\nu)\right. \\ & \left. + \frac{\pi^2\sinh(\pi\nu)}{2\,\nu\,\cosh^2(\pi\nu)}\left[\left(3 + \left(1+\frac{n_f}{N_c^3}\right)\frac{11+12\nu^2}{16(1+\nu^2)}\right)\delta_{n0} - \left(1+\frac{n_f}{N_c^3}\right)\frac{1+4\nu^2}{32(1+\nu^2)}\delta_{n2}\right]\right\},\end{aligned} \tag{10}$$

with

$$\begin{aligned}\phi(n,\nu) \;=\; & -\int_0^1 {\rm d}x\,\frac{x^{-1/2+i\nu+n/2}}{1+x}\left\{\frac{1}{2}\left(\psi'\left(\frac{n+1}{2}\right) - \zeta(2)\right) + {\rm Li}_2(x) + {\rm Li}_2(-x)\right. \\ & \left. + \ln x\left[\psi(n+1) - \psi(1) + \ln(1+x) + \sum_{k=1}^{\infty}\frac{(-x)^k}{k+n}\right] + \sum_{k=1}^{\infty}\frac{x^k}{(k+n)^2}\left[1-(-1)^k\right]\right\} \\ = & \sum_{k=0}^{\infty}\frac{(-1)^{k+1}}{k+(n+1)/2+i\nu}\Big\{\psi'(k+n+1) - \psi'(k+1) \\ & + (-1)^{k+1}\left[\beta_\psi(k+n+1) + \beta_\psi(k+1)\right] - \frac{\psi(k+n+1) - \psi(k+1)}{k+(n+1)/2+i\nu}\Big\},\end{aligned} \tag{11}$$

where

$$\beta_\psi(z) = \frac{1}{4}\left[\psi'\left(\frac{z+1}{2}\right) - \psi'\left(\frac{z}{2}\right)\right] , \tag{12}$$

and

$${\rm Li}_2(x) = -\int_0^x {\rm d}y\,\frac{\ln(1-y)}{y} \;. \tag{13}$$

The two quantities

$$c_{1,2}^{\rm NLO}(n,\nu,|\vec{p}_{1,2}|,x_{1,2}) = c_{1,2}(n,\nu,|\vec{p}_{1,2}|,x_{1,2}) + \alpha_s(\mu_R)\,\hat{c}_{1,2}(n,\nu,|\vec{p}_{1,2}|,x_{1,2}) \tag{14}$$

represent the forward impact factors depicting the emission of a quarkonium and of a light jet. In the LO limit, we have

$$c_{\mathcal{Q}}(n,\nu,|\vec{p}_{\mathcal{Q}}|,x_{\mathcal{Q}}) = 2\sqrt{\frac{C_F}{C_A}}(|\vec{p}_{\mathcal{Q}}|^2)^{i\nu-1/2}\int_{x_{\mathcal{Q}}}^{1}\frac{\mathrm{d}z}{z}\left(\frac{z}{x_{\mathcal{Q}}}\right)^{2i\nu-1} \times \left[\frac{C_A}{C_F}f_g(z)D_g^{\mathcal{Q}}\left(\frac{x_{\mathcal{Q}}}{z}\right)+\sum_{a=q,\bar{q}}f_a(z)D_a^{\mathcal{Q}}\left(\frac{x_{\mathcal{Q}}}{z}\right)\right] \tag{15}$$

and

$$c_J(n,\nu,|\vec{p}_J|,x_J) = 2\sqrt{\frac{C_F}{C_A}}(|\vec{p}_J|^2)^{i\nu-1/2}\left(\frac{C_A}{C_F}f_g(x_J)+\sum_{b=q,\bar{q}}f_b(x_J)\right), \tag{16}$$

respectively. Here, $C_F \equiv (N_c^2-1)/(2N_c)$ and $C_A \equiv N_c$ correspond to Casimir constants related to a gluon emission from a quark and a gluon, correspondingly. The $f(\nu)$ function contains the logarithmic derivative of LO impact factors

$$f(\nu) = \frac{i}{2}\frac{\mathrm{d}}{\mathrm{d}\nu}\ln\left(\frac{c_1}{c_2^*}\right)+\ln(|\vec{p}_1||\vec{p}_2|)\,. \tag{17}$$

What remains in Equation (6) is the NLO corrections to the forward impact factors, $\hat{c}_{1,2}$. The NLO correction to the vector quarkonium impact factor is obtained in the light-quark limit [252] and its expression is given in Appendix A. This choice is fully consistent with our VFNS scheme, provided that the observed transverse momenta of the quarkonium are sufficiently larger than the mass of the constituent heavy quark. Our selection for the light-jet NLO impact factor is based on studies performed in Refs. [250,252], suited to numeric analyses, which embody a jet algorithm calculated in the "small-cone" limit (SCA) [365,366] with a cone-type selection [251]. Its analytic formula is reported in Appendix B.

We compare our NLL predictions with current LL predictions, which can be obtained by neglecting all the NLO pieces of the BFKL kernel and the impact factors. One obtains

$$\mathcal{C}_n^{\mathrm{LL/LO}} = \frac{e^{\Delta Y}}{s}\int_{-\infty}^{+\infty}\mathrm{d}\nu\, e^{\Delta Y\bar{\alpha}_s(\mu_R)\chi(n,\nu)}\,\alpha_s^2(\mu_R)\,c_1(n,\nu,|\vec{p}_1|,x_1)[c_2(n,\nu,|\vec{p}_2|,x_2)]^*\,. \tag{18}$$

Equations (6)–(18) highlight the way in which the hybrid factorization is constructed. The cross-section is high-energy factorized *à la* BFKL as a convolution between Green's function and the two impact factors. Then, the latter contain the collinear inputs. The NLL/NLO$^+$ label highlights that the complete resummation of the energy logarithms is performed at NLL and within the NLO perturbative order. The '+' superscript in Equation (6) indicates that some next-to-NLL contributions arise from the cross-product of the two NLO impact factor corrections.

We employ the formulæ presented in this Section at the *natural* scales provided by the process. In particular, we set $\mu_F = \mu_R = \mu_N \equiv m_{\mathcal{Q}_1\perp} + m_{\mathcal{Q}_2\perp}$, or $\mu_F = \mu_R = \mu_N \equiv m_{\mathcal{Q}\perp} + |\vec{p}_J|$, according to the considered final state (see Figure 1). Collinear PDFs are obtained from the `NNPDF4.0` NLO parametrization [367,368] as implemented in `LHAPDF v6.5.4` [369]. The `NNPDF4.0` PDF determination is obtained from global fits and via the so-called *replica* method originally derived in Ref. [370] in the context of neural network techniques (for more details of the ambiguities arising from *correlations* between different PDF sets, see Ref. [371]). All results are obtained in the $\overline{\mathrm{MS}}$ renormalization scheme [363].

3. NRQCD Collinear Fragmentation for Vector Quarkonia

In Section 3.1, we give technical details regarding the way that we construct DGLAP-evolved, collinear FFs for vector J/ψ and Υ states, starting with ${}^3S_1^{(1)}$ NRQCD inputs at the initial energy scale. In Section 3.2, we discuss the *natural stabilization* property emerging from the gluon fragmentation channel. We compare this pattern with corresponding patterns obtained for other hadron species.

3.1. DGLAP-Evolved NRQCD FFs

NLO collinear FFs describing the direct inclusive emission of a vector, J/ψ or Υ, can be constructed by starting from initial-scale NRQCD inputs. According to NRQCD factorization, the function describing the collinear fragmenting process of a parton a into a quarkonium state $\mathcal{Q}$ having longitudinal fraction z can be cast as

$$D_a^{\mathcal{Q}}(z,\mu_F) = \sum_{[n]} \mathcal{D}_a^{\mathcal{Q}}(z,\mu_F,[n]) \langle \mathcal{O}^{\mathcal{Q}}([n]) \rangle \; . \tag{19}$$

where $\mathcal{D}_a(z,\mu_F,[n])$ represents a short-distance, perturbative coefficient embodying DGLAP-type logarithms to be resummed through collinear evolution; $\langle \mathcal{O}^{\mathcal{Q}}([n]) \rangle$ denotes a nonperturbative NRQCD LDME; and $[n] \equiv {}^{2S+1}L_J^{(\mathcal{C})}$ denotes the comprehensive set of quarkonium quantum numbers in the spectroscopic notation [372], with the $(\mathcal{C})$ superscript labeling the color state, singlet (1) or octet (8). In our study, we consider a spin-triplet state, namely a vector, taken in color singlet, so that ${}^{2S+1}L_J^{(\mathcal{C})} \equiv {}^3S_1^{(1)}$.

The first building block is the heavy-quark fragmentation, $c(\bar{c}) \to J/\psi$ or $b(\bar{b}) \to \Upsilon$. The left plot of Figure 2 is one of the representative diagrams for this channel, with the green blob depicting the $\langle \mathcal{O}^{\mathcal{Q}}({}^3S_1^{(1)}) \rangle$ nonperturbative NRQCD LDME. Here, a standard color-triplet heavy quark, $Q \equiv c$ or $Q \equiv b$, is emitted from the hard subprocess. It radiates collinear gluons via DGLAP (not shown in the picture), thus losing energy. Then, when its energy is around $3m_Q$, it perturbatively fragments, according to NRQCD, into a $(Q\bar{Q}Q)$ state. At this stage, the $(Q\bar{Q})$ subsystem, carrying color-singlet quantum numbers, nonperturbatively hadronizes into the observed vector quarkonium, $\mathcal{Q} \equiv J/\psi$ or $\mathcal{Q} \equiv \Upsilon$. The LO FF for the $Q \to \bar{Q}$ transition in color singlet was calculated in Ref. [77], whereas its NLO correction was recently obtained in Ref. [78]. We write [1]

$$D_Q^{\mathcal{Q}}(z,\mu_F = 3m_Q) = D_Q^{\mathcal{Q},\,\mathrm{LO}}(z) + \frac{\alpha_s^3(\mu_R = 3m_Q)}{m_Q^3} \, |\mathcal{R}_{\mathcal{Q}}(0)|^2 \, \Gamma_Q^{\mathcal{Q},\,\mathrm{NLO}}(z) \; , \tag{20}$$

where $m_c = 1.5$ GeV or $m_b = 4.9$ GeV and $|\mathcal{R}_{J/\psi}(0)|^2 = 0.810$ GeV^3 or $|\mathcal{R}_{\Upsilon}(0)|^2 = 6.477$ GeV^3 is the NRQCD radial wave function at the origin of the heavy quarkonium, according to potential model studies [380]. The LO initial-scale function in Equation (20) reads

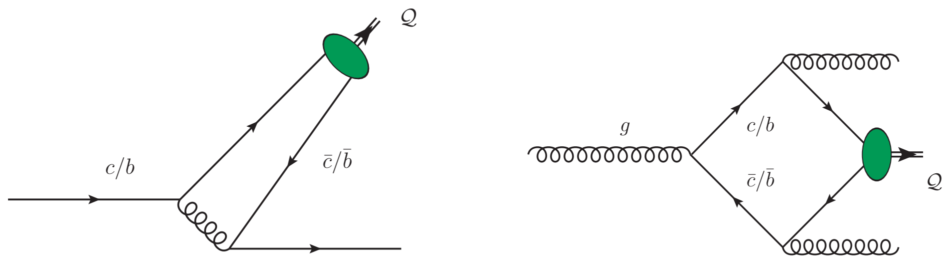

Figure 2. (**Left**): one of the leading diagrams depicting the fragmentation of a heavy quark Q into a ${}^3S_1^{(1)}$ vector quarkonium $\mathcal{Q}$ at order α_s^2. (**Right**): one of the leading diagrams for the fragmentation of a gluon g into a ${}^3S_1^{(1)}$ vector quarkonium $\mathcal{Q}$ at order α_s^3. The green blob denotes the corresponding nonperturbative NRQCD LDME. Diagrams realized with `JaxoDraw 2.0` [362] and taken from Ref. [190].

$$D_Q^{\mathcal{Q},\mathrm{LO}}(z) = \frac{\alpha_s^2(3m_Q)}{m_Q^3}\,\frac{8z(1-z)^2}{27\pi(2-z)^6}\,|\mathcal{R}_{\mathcal{Q}}(0)|^2\,(5z^4-32z^3+72z^2-32z+16)\,, \tag{21}$$

while

$$\begin{aligned}\Gamma_Q^{J/\psi,\mathrm{NLO}}(z) = {} & -9.01726z^{10}+18.22777z^9+16.11858z^8-82.54936z^7 \\ & +106.57565z^6-72.30107z^5+28.85798z^4-6.70607z^3 \\ & +0.84950z^2-0.05376z-0.00205\end{aligned} \tag{22}$$

or

$$\begin{aligned}\Gamma_Q^{\Upsilon,\mathrm{NLO}}(z) = {} & -14.00334z^{10}+46.94869z^9-55.23509z^8+16.69070z^7 \\ & +22.09895z^6-26.85003z^5+13.41858z^4-3.50293z^3 \\ & +0.46758z^2-0.03099z-0.00226\end{aligned} \tag{23}$$

are the NLO FF core parts suitably cast in the form of fitted polynomial functions. From a perturbative QCD perspective, the LO heavy-quark FF starts at $\mathcal{O}(\alpha_s^2)$, while its NLO correction starts at $\mathcal{O}(\alpha_s^3)$.

The second building block is the gluon fragmentation, $g \to J/\psi$ or $g \to \Upsilon$, whose leading channel is portrayed in the right plot of Figure 2. Here, from the hard subprocess, a standard gluon is extracted. As for the heavy-quark case, it emits collinear radiation through DGLAP (not shown in the diagram), thus losing energy. Then, when its energy is around $2m_Q$, it perturbatively fragments into a $(Q\bar{Q}gg)$ state, according to NRQCD. The $(Q\bar{Q})$ subsystem nonperturbatively hadronizes into the final-state quarkonium, $\mathcal{Q}$. We note that two extra gluon emissions are encoded in the NRQCD mechanisms. Indeed, being the parent gluon a colored object, in order to produce a colorless $(Q\bar{Q})$ pair, at least another gluon needs to be emitted. However, due to the Landau–Yang selection rule [381,382], a spin-1 massive particle, such as our quarkonium, cannot be produced via a fermion triangle with two other on-shell vectors, such as gluons. Therefore, another secondary gluon must be emitted. One immediately recognizes that, from a perturbative QCD point of view, the leading gluon to vector quarkonium fragmentation channel is opened at $\mathcal{O}(\alpha_s^3)$. Thus, to be consistent with the perturbative level of the heavy-quark FF, we do not need any higher-order correction for the gluon function. The FF for the $g \to \mathcal{Q}$ transition was calculated in Ref. [68] and reads [2]

$$\begin{aligned}D_g^{\mathcal{Q}}(z,\mu_F=2m_Q) = {} & \frac{5\alpha_s^3(\mu_R=2m_Q)}{36(2\pi)^2}\,\frac{|\mathcal{R}_{\mathcal{Q}}(0)|^2}{m_{\mathcal{Q}}^3}\int_0^z \mathrm{d}v\int_{(1+z^2)/2z}^{(1+v)/2}\frac{\mathrm{d}\omega}{(1-\omega)^2(\omega-v)^2(\omega^2-v)^2} \\ & \sum_{l=0}^{2} z^l\left[f_l^{(g)}(v,\omega)+g_l^{(g)}(v,\omega)\frac{1+v-2\omega}{2(\omega-v)\sqrt{\omega^2-v}}\ln\left(\frac{\omega-v+\sqrt{\omega^2-v}}{\omega-v-\sqrt{\omega^2-v}}\right)\right],\end{aligned} \tag{24}$$

where $f_{l=0,1,2}^{(g)}$ and $g_{l=0,1,2}^{(g)}$ are analytic functions calculated in Ref. [385]. We remark that, here, we consider the quarkonium's direct production from the parent gluon. Another channel for high-energy J/ψ emissions, not considered in our study, is the production of a P-wave charmonium χ_c, followed by its radiative decay, given by the $\chi_c \to J/\psi + \gamma$ subprocess [77,386].

A major outcome of the phenomenological study of Ref. [80] is that the $c \to J/\psi$ and $g \to J/\psi$ fragmentation channels are similar in weight. Their relative size also depends on the hard scattering producing these partons. In particular, the number of gluons emitted at large transverse momentum might be of the same order or larger than the number of heavy quarks. Including the gluon channel is also relevant for our hadroproduction reactions (Figure 1), since the gluon FF is magnified by the collinear convolution with the corresponding gluon PDF, which is diagonal at LO (see Equation (15)).

Starting from the NRQCD inputs in Equations (20)–(24), we generate a first and novel DGLAP-evolved set of collinear FFs for ${}^3S_1^{(1)}$ vector quarkonia. Several tools, such as `QCD-PEGASUS` [387], `HOPPET` [388], `QCDNUM` [389], `APFEL(++)` [390–392], and `EKO` [393], have been released as publicly available interfaces for DGLAP evolution. In contrast with collinear PDFs, whose evolution is space-like, the one for collinear FFs is time-like [69,70]. We employ `APFEL++`, in which the time-like evolution has been already implemented. According to the diagrams in Figure 2, the threshold for switching on the DGLAP evolution of gluons is set to $\mu_F = 2m_Q$, whereas constituent heavy-quark and anti-quark FFs start to evolve at $\mu_F = 3m_Q$. Light-quark and nonconstituent heavy-quark species are generated by evolution only. In this way, for each quarkonium species, J/ψ and Υ, we generate a phenomenology-ready FF set in `LHAPDF` format, named `ZCW19`$^+$ [190], which encodes both the gluon NRQCD input and the constituent heavy-quark one.

3.2. Natural Stability

In this section, we shed light on the stabilization pattern arising from the fragmentation mechanism depicting the production of heavy-flavored hadrons in the VFNS. The connection between the behavior of DGLAP-evolving VFNS FFs and the stability of the NLL/NLO$^{(+)}$ hybrid high-energy and collinear factorization was discovered for the first time [323] in the context of singly heavy-flavored hadrons, such as D mesons [394–402], Λ_c hyperons [395,403,404], and b-flavored ($\mathcal{H}_b$) hadrons [405–412]. This remarkable property was first seen in observables sensible to the forward inclusive emission of Λ_c [194,195,322], $D^{*\pm}$ [324,326], and $\mathcal{H}_b$ [195,321] particles. Then, further corroborating evidence emerged from the study of vector quarkonia [190,327] and charmed B mesons [325] produced via the NRQCD single-parton fragmentation mechanism [68,77,78,373–376,383,384]. Milder stabilization effects were also observed when s-flavored, cascade $\Xi^-/\bar{\Xi}^+$ baryons were tagged [313].

In the upper plots of Figure 3, we show the μ_F-dependence of `ZCW19`$^+$ collinear FFs describing the production of a J/ψ (left) or a Υ (right). We fix the quarkonium longitudinal-momentum fraction z to a value that roughly corresponds to the average value at which FFs are probed in the kinematic ranges typical of our analyses (see Section 4.3). We have $z = 0.45 \simeq \langle z \rangle$. As expected, the constituent heavy (anti-)quark, $c(\bar{c})$ for J/ψ and $b(\bar{b})$ for Υ, heavily dominates over the other flavors. Notably, the gluon FF smoothly increases as μ_F grows, to reach a plateau. A similar trend characterizes the lower plots in Figure 3, where collinear `ZCFW22` FFs depicting the emission of a $B_c^{\pm}({}^1S_0)$ meson (left) or a $B_c^{*\pm}({}^3S_1)$ one (right) are presented. The VFNS `ZCFW22` sets for charmed B mesons were recently obtained in Ref. [325] by performing a DGLAP evolution of NQRCD initial-scale heavy-quark [376] and gluon [383] inputs at NLO. The strategy adopted there is analogous to the one defined in Ref. [190] for vector quarkonia and presented in Section 3 of this review.

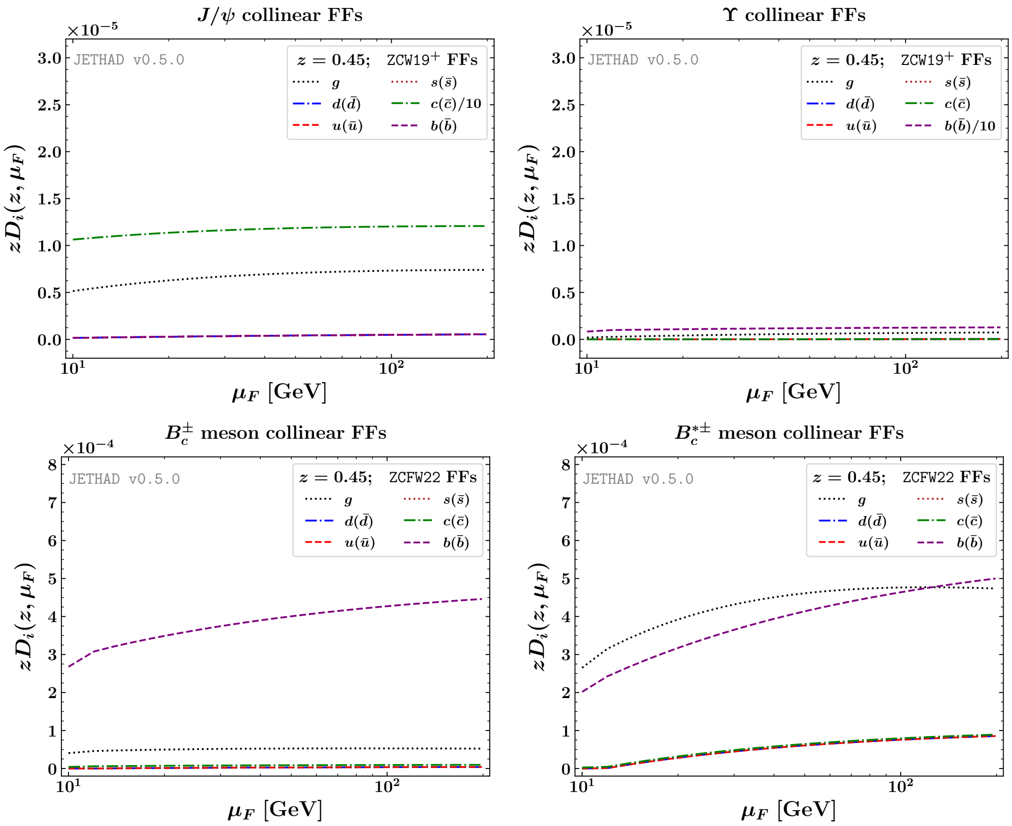

Figure 3. Factorization-scale dependence of ZCW19$^+$ and ZCFW22 NLO collinear FFs, respectively, depicting vector quarkonium (**upper** plots) and charmed B meson (**lower** plots) hadronization, at $z = 0.45 \simeq \langle z \rangle$.

The upper plots of Figure 4 contain the μ_F shape of FFs describing the production of two singly heavy-flavored hadrons, Λ_c baryons (left) and $\mathcal{H}_b$ particles (right). The first FFs are depicted by the KKSS19 determination [403], a VFNS set based on a Bowler-like [413] initial-scale parametrization for charm and bottom (anti-)quark flavors. The second functions are portrayed by KKSS07 FFs [406,409], a VFNS set based on a power-like [414] initial-scale *Ansatz* for the bottom flavor. Moreover, in these two cases, heavy-quark FFs heavily prevail (for b-hadrons, only bottom functions dominate, since charm fragmentation is generated by DGLAP evolution), and the gluon FFs increase with μ_F (for b-hadrons, the growth is stronger). Finally, the lower plots of Figure 4 are for two species of light-flavored hadrons: Λ hyperons (left) and Ξ baryons (right). Hyperons are described by AKK08 FFs [415], while cascade baryons are described by the novel SHKS22 neural network determination [416]. In the Λ case, the strange FF dominates but, more importantly, all parton FF channels decrease with μ_F. Cascade particle FFs present an intermediate situation, with the gluon channel smoothly growing up to roughly $20 \div 40$ GeV, and then slightly falling off.

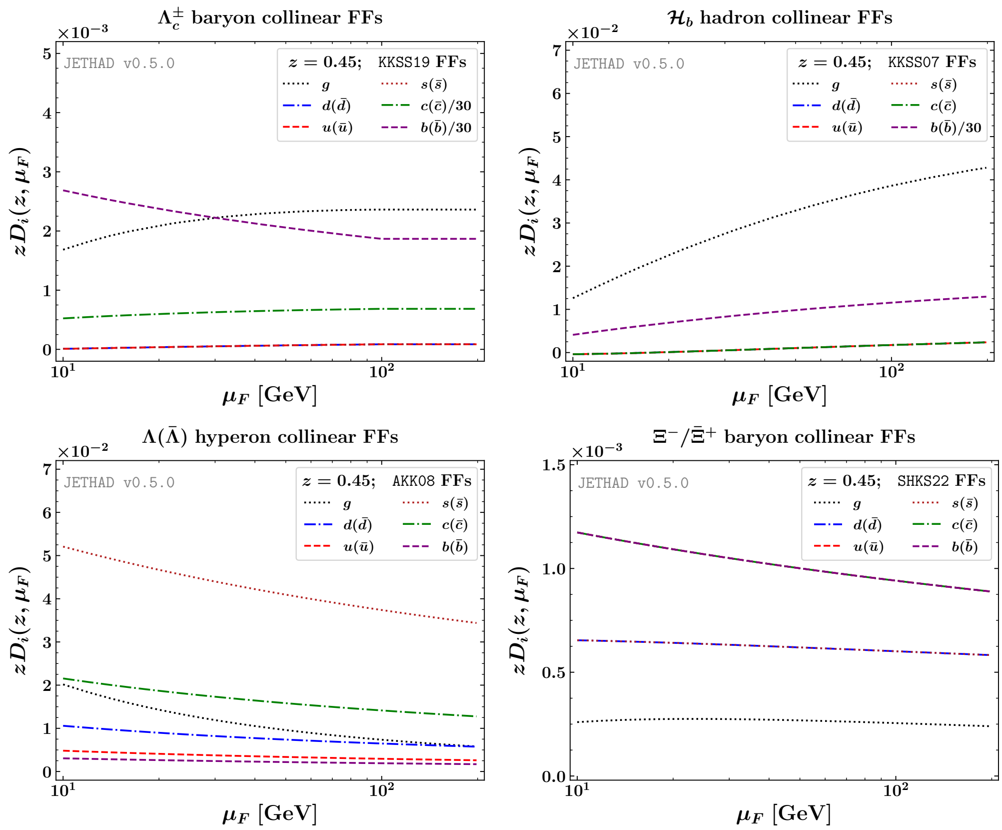

Figure 4. Factorization-scale dependence of KKSS19 and KKSS07, AKK08 and SHKS22 NLO collinear FFs, respectively, depicting Λ_c baryon and $\mathcal{H}_b$ hadron (**upper** plots), and Λ hyperon and Ξ baryon emissions (**lower** plots), at $z = 0.45 \simeq \langle z \rangle$.

As extensively explained in Refs. [190,194,321,323,325], the gluon collinear FF is a key actor in our NLL/NLO$^{(+)}$ hybrid factorization framework. Its energy dependence directly regulates the stability of the high-energy logarithmic series of our observables. Indeed, in the kinematic sectors of interest, i.e., when $10^{-4} \lesssim x \lesssim 10^{-2}$, the gluon PDF strongly prevails over all (anti-)quark channels. Since the gluon FF is diagonally convoluted with the gluon PDF in the LO hadron impact factor (see Equation (15)), its behavior is strongly heightened. As discussed in Ref. [194], this feature is valid also at NLO, namely where the (qg) and (gq) nondiagonal channels are switched on (see Appendix A).

On one hand, the QCD running coupling becomes smaller when μ_R increases, and this happens both in Green's function and in the impact factors (see Section 2.2). On the other, it is well known that the gluon PDF grows with μ_F. When the latter is convoluted in the impact factor with a gluon FF that also grows with μ_F, as happens for heavy-flavored species, the two effects compensate each other. This gives rise to the stability of heavy-hadron distributions under scale variation. The stronger the growth of the gluon FF with μ_F, the clearer the stabilization pattern. Thus, $\mathcal{H}_b$ sensitive distributions are even more stable than Λ_c distributions [321]. Conversely, when the gluon FF falls off with μ_F, as happens for Λ hyperons, no stabilization under scale variation is found. This hampers any possibility of performing precision studies of the high-energy distributions at natural scales [192]. Cascade Ξ baryons present an intermediate situation, with the smooth-behaved μ_F gluon FF leading to a partial and milder stabilization pattern [313].

The rise of the *natural stability* in the presence of both singly heavy-flavored hadrons and quarkonia gives strong evidence that this remarkable property is an *intrinsic* feature of heavy-flavor emissions, which becomes manifest whenever a heavy-hadron species is detected, independently of the *Ansätze* made for the corresponding collinear FFs.

4. Phenomenology

All the presented results were obtained with JETHAD, a PYTHON/FORTRAN hybrid and multimodular interface aimed at the calculation, management, and processing of physical observables defined in the context of different formalisms [192,195]. In particular, numeric computations of rapidity distributions were performed through the FORTRAN 2008 modular routines implemented in JETHAD, while the JETHAD PYTHON 3.0 analysis environment was employed for the elaboration of the results. Section 4.1 encompasses the core features of the current version of the JETHAD technology (`v0.5.0`, not yet public). Details of our strategy to assess the weights of uncertainties for high-energy predictions are given in Section 4.2. The final-state kinematic configurations to which our distributions are tailored can be found in Section 4.3. Numeric analyses and a discussion of the results for the rapidity distributions are presented in Section 4.4.

4.1. JETHAD `v0.5.0`: A Basic Overview

The origins of the JETHAD project date back to the end of 2017, when the constantly increasing number of semi-hard hadron [291,293] or/and jet [284,286,309] sensitive LHC final states, proposed as a testing ground for high-energy resummation, called for the development of a standard and reference interface, suited both to the computation and the elaboration of high-energy distributions. The first (private) recognized version, `v0.2.7`, served as a useful tool to perform a pioneering comparison between NLL/NLO hybrid predictions and fixed-order computations for hadron–jet correlations in the high-energy limit of QCD [192]. The possibility of considering forward heavy-quark pair emissions both in photo- and hadroproduction was implemented in `v0.3.0` [268]. Studies of Higgs emissions as well as transverse-momentum distributions became accessible with `v0.4.2` [314]. The first version of the PYTHON analyzer was combined with the FORTRAN core in `v0.4.3` [193]. The first analyses of heavy-flavored hadrons via VFNS FFs at NLO started with `v0.4.4` [194]. The ΔΥναμις (DYNAMIS) work package, suitable to investigate forward Drell–Yan dilepton emissions [159], was incorporated in JETHAD `v0.4.5`. The possibility of accessing the proton content at low x through the UGD and gluon TMDs become possible after interfacing the previously stand-alone *Leptonic-Exclusive-Amplitudes* (LEXA) modular code [154] with JETHAD `v0.4.6` [156]. Support for quarkonium studies from NRQCD single-parton fragmentation started with `v0.4.7` [190]. The newest features in `v0.5.0` essentially rely on (*i*) an improved system to perform studies of energy-scale variations, (*ii*) the extension of the list of observables that can be analyzed, with particular attention to singly and doubly differential transverse momentum distributions [290,313], and (*iii*) the possibility of removing the NLO expanded contribution from the fully NLL resummed series to support *matching* procedures with collinear factorization (see Equation (1) of Ref. [360]).

From the main core to the service modules and routines, JETHAD has been designed to dynamically reach a high level of computational performance. JETHAD's multidimensional integrators make use of extensive parallel computing to actively select the best integration algorithm, depending on the shape of the integrand. Any process implemented in JETHAD can be actively selected via a user-friendly, *structure*-based smart management interface, where physical final-state particles are portrayed by *object* prototypes (code structures in the working environment). Particle objects encode all the information about the basic and kinematic properties of their physical *Doppelgänger*s, from mass and charge to kinematic ranges and rapidity tags. As a first step, they are loaded from a master database via a dedicated *particle generation* routine (custom particle generation is also possible). Subsequently, they are *cloned* into a final-state object array and therefore *injected* from the integrand routine, differential regarding final-state kinematic variables, to the respective hard-factor module via a suitable *controller*. The strong flexibility characterizing the generation of the physical final states is complemented by a window of possibilities in selecting the initial state. Indeed, a peculiar *particle ascendancy* structure attribute allows JETHAD to dynamically recognize whether a particle is hadroproduced, leptoproduced, photoemitted, and so on. In this way, only the relevant modules will be initialized, thus breaking down computing time lags. JETHAD is structured as an object-based interface, entirely independent of the reaction being investigated. While inspired by high-energy resummation and TMD factorization phenomenology, different approaches can be easily encoded in it by implementing new and customized modules and supermodules, which can be linked to the core structure of the code via a native *point-to-routine* system, thus making JETHAD a general, particle physics environment.

With the aim of providing the scientific community with a standard software program designed for the computation and management of different types of processes described by distinct formalisms, we plan, as a medium-term goal, to release the first public version of JETHAD.

4.2. Uncertainty Estimation

Accurate predictions for our high-energy observables rely upon identifying the main potential uncertainty sources and quantifying their effects. A widely employed strategy to assess the size of higher-order corrections, not accounted for by our formalism, consists in gauging the sensitivity of our distribution on renormalization- and factorization-scale variation. From a recent analysis on semi-inclusive emissions of light and heavy bound states [195], it emerged that the effect of varying energy scales around their *natural* values represents one of the main contributions to the global uncertainty. Therefore, we study the effect of simultaneously varying μ_R and μ_F around their natural values, in the range of $1/2$ to 2. The C_μ parameter in the plots in Section 4.4 refers to the ratio $C_\mu = \mu_R/\mu_N$. We also set $\mu_F = \mu_R$. Another potential source of relevant uncertainty might come from proton PDFs. However, recent studies on semi-hard observables pointed out that the choices of different PDF parametrizations, as well as of different members inside the same set, brings no sizeable impact [192,195,309,321]. Thus, we use the central member of only one PDF determination, the `NNPDF4.0` one. Two further potential sources of uncertainty might be connected to $a)$ a *collinear improvement* in the NLO BFKL Green's function [417–423], which is based on the inclusion of renormalization group (RG) contributions needed to impose a compatibility with the DGLAP equation in the collinear limit, and from $b)$ employing another renormalization scheme. The point $a)$ was studied in detail in Ref. [195]. It was found that the effect of the collinear improvement on rapidity distributions was completely contained by the error bands produced by energy-scale variations, and it was even less relevant when other other azimuthal-angle sensitive observables were considered. In the same work, an estimation of point $b)$, namely the upper limit of the effect of moving from $\overline{\text{MS}}$ to the MOM renormalization scheme, was provided. MOM predictions for rapidity distributions are systematically larger than those for $\overline{\text{MS}}$ predictions, but are still affected by error bands due to scale variations. We remark that a consistent MOM study would rely upon MOM-evolved PDFs, not available so far. In view of these considerations, we generate uncertainty bands for our predictions by considering the net and combined effects of varying energy scales, together with the numeric uncertainty generated by final-state multidimensional integration (Section 4.3). The latter is steadily kept below 1% by the JETHAD numeric integrators.

4.3. Final-State Ranges

In our phenomenological study, we provide NLL/NLO$^+$ predictions for the rapidity distribution, i.e., the cross-section differential in the rapidity distance, ΔY, between the two outgoing objects. Its expression follows from the integration of the $\mathcal{C}_0$ azimuthal angle coefficient, defined in Section 2.2, over the final-state rapidities and transverse momenta, with ΔY being taken to be fixed. One has

$$\frac{d\sigma(\Delta Y, s)}{d\Delta Y} = \int d|\vec{p}_1| \int d|\vec{p}_2| \int_{y_1^{\min},\, \max(\Delta Y + y_2^{\min})}^{y_1^{\max},\, \min(\Delta Y + y_2^{\max})} dy_1 \; \mathcal{C}_0(|\vec{p}_1|, |\vec{p}_2|, y_1, y_2) \Big|_{y_2 \,=\, y_1 - \Delta Y} \tag{25}$$

Here, a $\delta((y_1 - y_2) - \Delta Y)$ function has been used to remove and to enforce the extremes of integration in y_1 accordingly. As proposed in Ref. [190], the transverse momenta of the detected quarkonia lie in the range 20 GeV to 60 GeV. This choice is perfectly consistent with our VFNS treatment, which requires the energy scales to be sufficiently larger than the thresholds controlling the DGLAP evolution of heavy quarks. Conversely, light-flavored jets are reconstructed with transverse-momentum cuts typical of current works at the CMS detector [424], 35 GeV $< |\vec{p}_J| \equiv |\vec{p}_2| <$ 60 GeV. Adopting *asymmetric* transverse-momentum windows allows us to better disengage the core high-energy signal from the DGLAP background [192,284,285]. It also suppresses Sudakov logarithmic contributions rising from almost back-to-back configurations, which would call for another appropriate resummation mechanism [425–429]. Moreover, it dampens possible instabilities emerging in next-to-leading computation [430,431], as well as energy–momentum conservation violations [432].

Concerning rapidity ranges, we select two relevant cases.

- ***Standard*** kinematic configurations, characteristic of the ongoing LHC phenomenology, where the quarkonium is identified in the detector barrel only [433], while the jet is reconstructed also in the endcap calorimeters. We have $|y_{\mathcal{Q}_{(1,2)}}| < 2.4$ and $|y_J| < 4.7$, so that $\Delta Y < 4.8$ in the double quarkonium channel and $\Delta Y < 7.1$ in the quarkonium plus jet channel.
- ***Extended*** kinematic configurations, suitable to test the validity of the *natural stability* at the edges of application of the hybrid factorization, with the quarkonium detected both in the barrel and the endcaps; we have $|y_{\mathcal{Q}_{(1,2)}}| < 4.7$ and $|y_J| < 4.7$, so that $\Delta Y < 9.4$ in the two production channels.

4.4. ΔY-Distribution

Figure 5 shows the behavior of the ΔY-distributions for the double vector quarkonium (left) and the inclusive vector quarkonium plus jet production (right) at NLL/NLO$^+$, for $\sqrt{s}$ = 14 TeV, and in *standard* rapidity configurations. The values of our distributions are all larger than 10^{-2} pb in the vector quarkonium plus jet channel (right). This is a very favorable statistic, which turns out to be lower than the one for heavy-baryon and heavy-light meson emissions [194,321], but substantially higher than the one for the double vector quarkonium channel (left). The falloff of these high-energy resummed cross-sections as ΔY increases is a common pattern of all the hadronic semi-hard processes analyzed so far. It is the net effect of the interplay of two competing features. On the one hand, the pure high-energy dynamics would lead to the well-known growth with the energy of partonic hard factors. On the other hand, collinear DGLAP-evolving PDFs and FFs quench hadronic distributions when ΔY increases.

In particular, the plots of Figure 5 contain a study of the ΔY-distributions under the progressive variation of the μ_R and μ_F scales in a wide range, regulated by the C_μ parameter, which runs from 1 to 30. The ancillary panels below the primary plots exhibit the reduced cross-sections, i.e., divided by their central values taken at $C_\mu = 1$. Notably, the sensitivity of the NLL/NLO$^+$ predictions on C_μ variation is rather weak for all four considered channels (Figure 1) and for all the values of the probed ΔY spectrum. This indicates that our VFNS quarkonium FFs, built in terms of both initial-scale heavy-quark and gluon NRQCD functions, and then evolved via DGLAP, lead to a strong stabilization pattern, as with the one observed for singly heavy-flavored hadrons and for charmed B mesons (see results on the same distributions given in Refs. [190,194,321,325]).

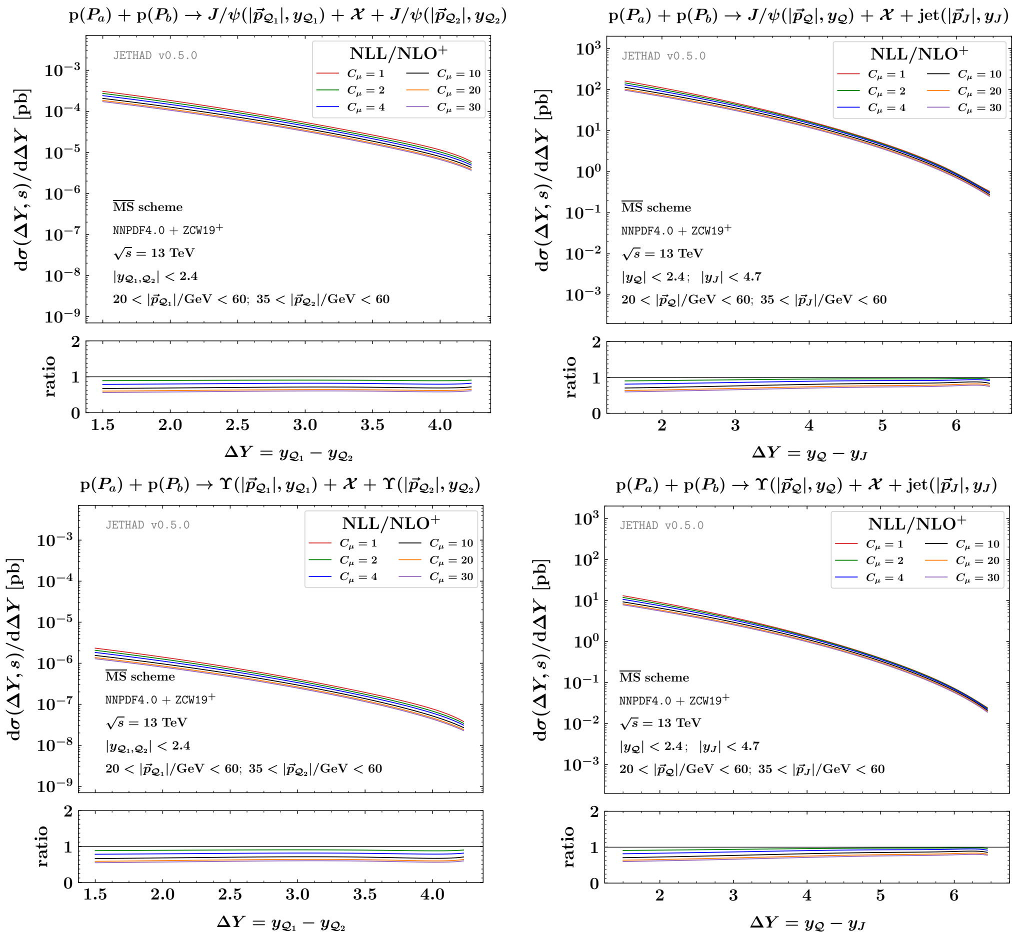

Figure 5. ΔY-distribution for the double vector quarkonium (**left**) and the inclusive vector quarkonium + jet production (**right**) at NLL/NLO$^+$, for $\sqrt{s} = 14$ TeV and in the *standard* rapidity ranges, $\Delta Y < 4.8$ (**left**) and $\Delta Y < 7.1$ (**right**). A study of the progressive variation of the renormalization and factorization scales in the $1 < C_\mu < 30$ range is shown.

Figure 6 shows the behavior of the ΔY-distributions for the double vector quarkonium (left) and the inclusive vector quarkonium plus jet production (right) at NLL/NLO$^+$, for $\sqrt{s} = 14$ TeV, and in *extended* rapidity configurations. Here, as anticipated, we allow the vector quarkonium to be tagged not only in the barrel calorimeter but also in the endcaps, to match the detection range of the light jet. On the one hand, from an experimental point of view, such configurations could be difficult to realize, due to hardware limitations in particle identification at high rapidities. On the other hand, however, this extension offers us a unique opportunity to test, from a phenomenological perspective, the validity of the *natural stability* at the edges of the applicability of our hybrid factorization. Indeed, at a very large rapidity separation between the two detected objects, we enter the so-called *threshold* regions. In this case, forward final-state objects stem from a parton struck with a large longitudinal-momentum fraction x. As a result, the weight of undetected gluon radiation diminishes and, correspondingly, large Sudakov-type double logarithms (threshold double logarithms) appear in the perturbative series. In principle, they could spoil the convergence of the perturbative series, and they should be accounted for to all orders by a proper resummation mechanism [434–451], which is different from our high-energy one. At the same time, large ΔY values probe our distribution in a high-energy regime, which might be "asymptotic", namely where the BFKL dynamics might be the dominant mechanism or, at least, it could strongly modulate the pure fixed-order background.

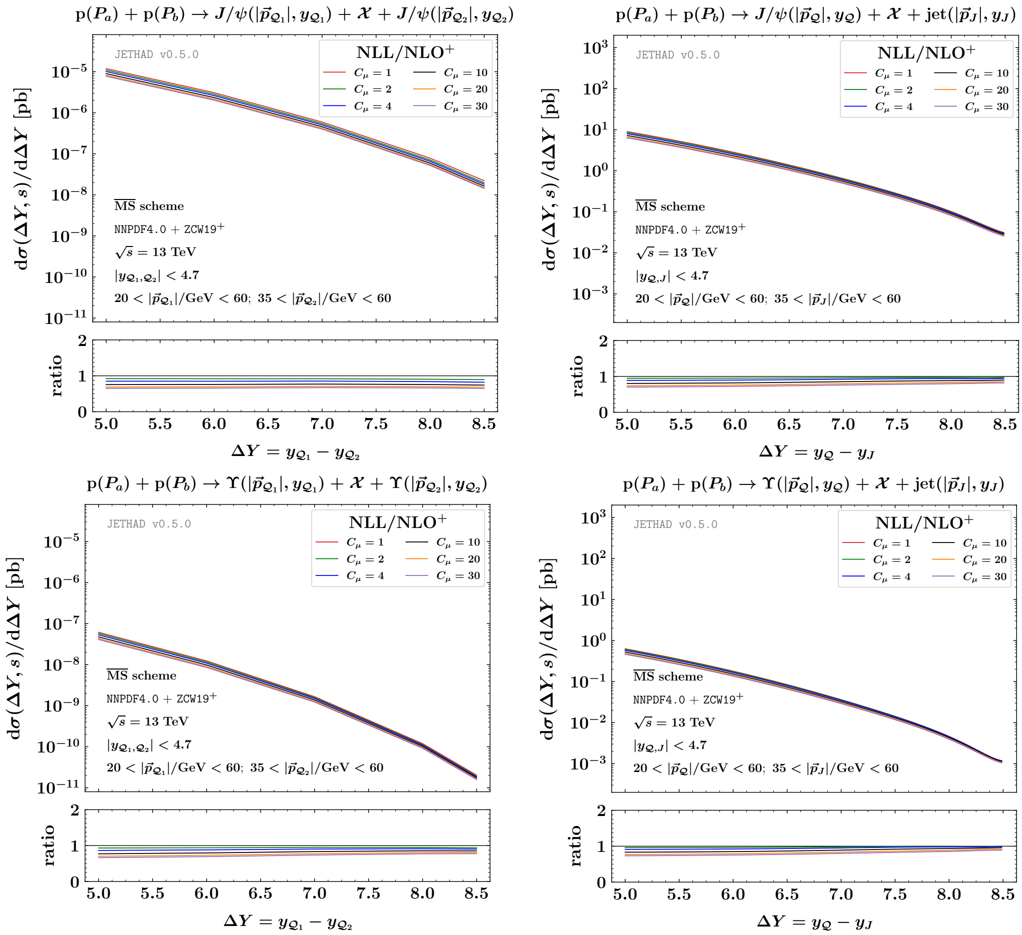

Figure 6. ΔY-distribution for the double vector quarkonium (**left**) and the inclusive vector quarkonium + jet production (**right**) at NLL/NLO$^+$, for $\sqrt{s} = 14$ TeV and in the *extended* rapidity ranges, $\Delta Y < 9.4$. A study of the progressive variation of the renormalization and factorization scales in the $1 < C_\mu < 30$ range is shown.

The global pattern emerging from the inspection of the plots in Figure 6 unambiguously highlights that the ΔY-distributions are very stable under progressive energy-scale variation, in all the investigated channels. The *natural stability* is not spoiled by the *extended* rapidity kinematics, but rather magnified. Finally, we observe that the statistic is lower than that obtained in the *standard* rapidity range, but still favorable for the quarkonium plus jet channel.

We complete the analysis given in this section by providing predictions for NLL/NLO$^+$ ΔY-differential cross-sections as compared with the corresponding ones taken in a pure LL/LO limit. Results for the four channels under investigation (see Figure 1) after applying *standard* and *extended* final-state cuts are, respectively, presented in Figures 7 and 8. The shaded uncertainty bands embody the combined effects of energy-scale variations and numeric multidimensional integrations (see Section 4.2 for details). Additionally, in this case, the lower ancillary panels refer to reduced distributions, namely divided by central values taken at $C_\mu = 1$. The overall pattern is one of fair stability under NLL/NLO corrections, with the NLL/NLO$^+$ bands generally narrower and partially nested inside the corresponding LL/LO ones. Their overlap is weaker in the quarkonium plus jet channel. This is expected, since having only one heavy hadron in the final state, instead of two, clearly halves the stabilizing power coming from the VFNS collinear FFs.

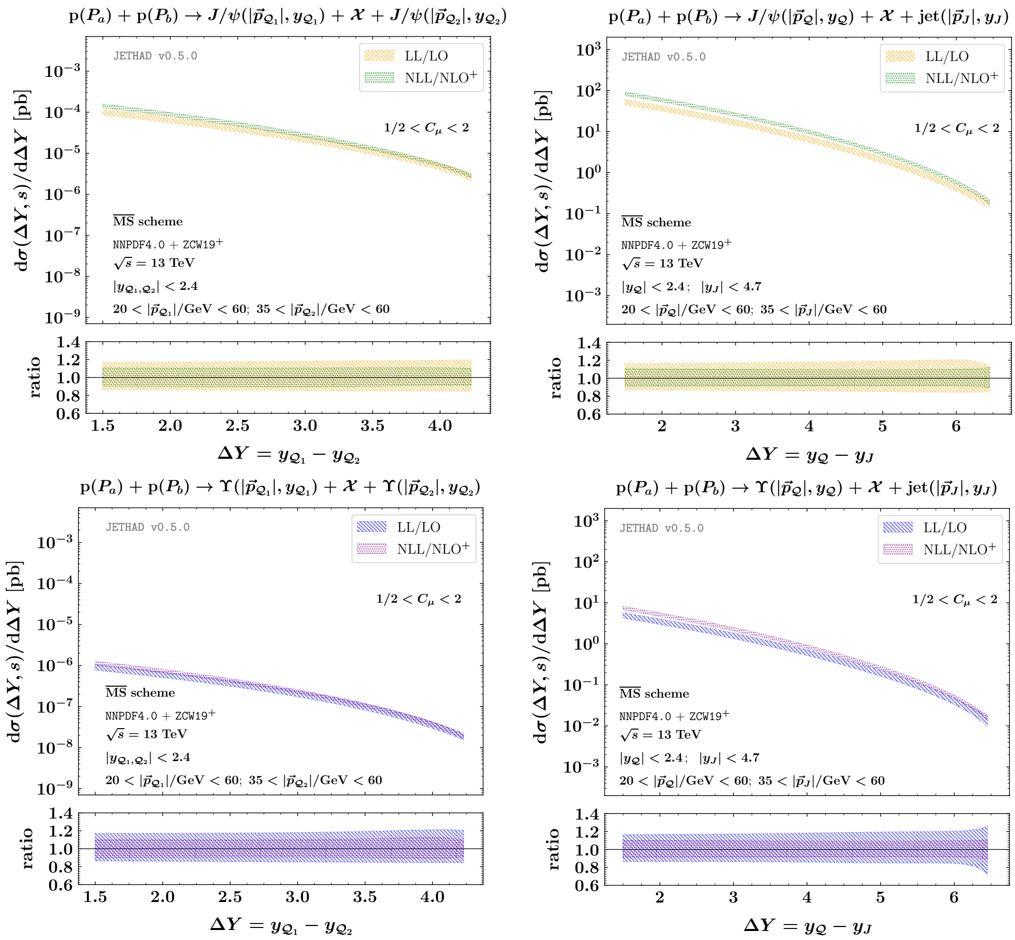

Figure 7. ΔY-distribution for the double vector quarkonium (**left**) and the inclusive vector quarkonium + jet production (**right**) at NLL/NLO$^+$, for $\sqrt{s} = 14$ TeV and in the *standard* rapidity ranges, $\Delta Y < 4.8$ (**left**) and $\Delta Y < 7.1$ (**right**). Uncertainty bands carry the combined effects of renormalization- and factorization-scale variation in the $1 < C_\mu < 2$ range and of phase-space numeric multidimensional integrations.

We conclude this section by mentioning a relevant aspect that goes beyond the aim of this review, but still deserves a discussion. We refer to the impact of MPI effects on the differential distributions at increasing values of ΔY. In particular, we consider the Double-Parton Scattering (DPS), which accounts for two hard-scattering subreactions at most. Ref. [283] deals with a study of DPS corrections to Mueller–Navelet jets, which can be potentially relevant for ΔY-distributions at large center-of-mass energies and moderate transverse momenta. From investigations of double J/ψ [106,111], J/ψ plus Y [106], J/ψ plus Z [105], and J/ψ plus W [452] final states, an important indication emerged that the DPS contribution might be sizeable and it should be considered to improve the description of the moderate transverse-momentum spectrum. Then, MPI imprints could arise also in triple J/ψ events [453,454]. Therefore, the search for MPI signatures in our observables represents an important development that should be carried out in the medium-term future.

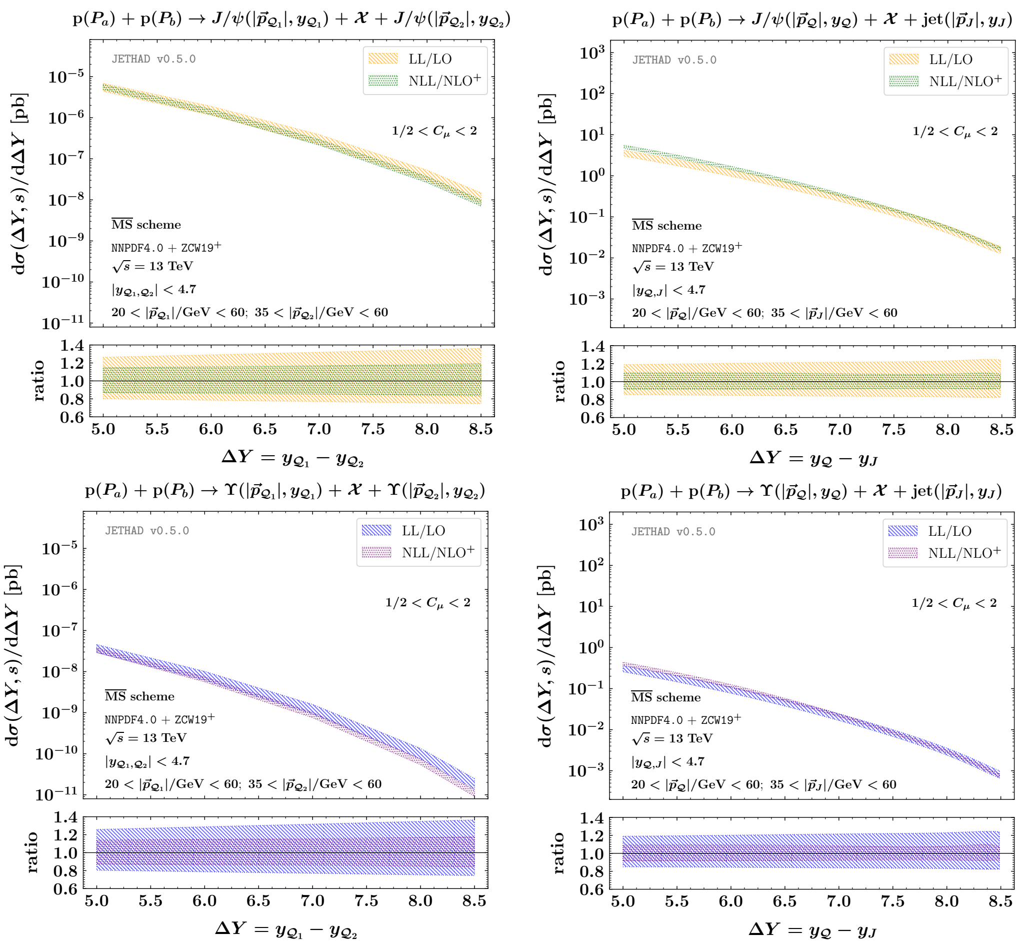

Figure 8. ΔY-distribution for the double vector quarkonium (**left**) and the inclusive vector quarkonium + jet production (**right**) at NLL/NLO$^+$, for $\sqrt{s} = 14$ TeV and in the *extended* rapidity ranges, $\Delta Y < 9.4$. Uncertainty bands carry the combined effects of renormalization- and factorization-scale variation in the $1 < C_\mu < 2$ range and of phase-space numeric multidimensional integrations.

5. Conclusions and Outlook

We investigated the *direct* inclusive hadroproduction of a forward vector quarkonium, J/ψ or Υ, in association with another backward quarkonium or a light-flavored jet in a hybrid high-energy and collinear factorization formalism. We relied upon the single-parton fragmentation approximation, which represents the most adequate tool to describe quarkonium hadronization at large transverse momentum [68,80,81,455]. By starting from a NRQCD input at the initial energy scale for the constituent heavy-quark [78] and the gluon [68] fragmenting into the observed meson, we achieved the first and novel determination of VFNS-consistent, DGLAP-evolving quarkonium FFs, which we named `ZCW19`$^+$. We believe that this FF set can serve as a useful tool for further phenomenological applications lying outside the high-energy domain, as well as a support basis for forthcoming analyses aimed at unveiling the connection between collinear factorization and NRQCD effective theory.

Inspired by recent findings on the inclusive forward emissions of singly heavy-flavored hadrons studied in the context of the NLL/NLO$^{(+)}$ hybrid factorization [194,321], we searched for a stabilization pattern in the high-energy series under higher-order corrections and energy-scale variation. Our key finding is that these effects are present also when vector quarkonia are detected at large transverse momenta and in forward rapidity directions. Notably, the *natural stability* of the ΔY-distributions turns out to be even more manifest when meson tags are tailored in larger rapidity windows, such the ones reachable when endcap detection is allowed. Thus, we provide strong evidence that this remarkable property is an *intrinsic* feature characterizing heavy-flavor emissions, which becomes manifest whenever a heavy-hadron species is detected, independently of the initial-scale input starting from which corresponding collinear FFs are obtained by DGLAP evolution. Following the results presented in this review, we can unambiguously state that the *natural stability* is so strong as to surmount and overpower any possible destabilizing effect coming from other resummation mechanisms, particularly from *threshold* contaminations highly affecting the forward emission domain [434–451].

Our analysis of vector quarkonia from NRQCD single-parton fragmentation constitutes an important step forward in the study of heavy-flavored emissions at NLL/NLO$^{(+)}$, starting from the analytic computation of heavy-quark pair impact factors [266–268]. It also represents the first and most relevant contact point with the high-energy quarkonium phenomenology. Future investigations are needed to address quarkonium production in broader domains, such as the regimes reachable at new-generation colliding machines [456–483].

Another important advancement comes from NLO studies of single-forward or almost back-to-back semi-inclusive emissions in the context of the gluon saturation framework (see, e.g., Refs. [484–495] and references therein). In this context, the impact of soft gluon radiation on angular asymmetries in di-jet production was addressed in Refs. [496–500]. A recent NLO computation [501] will make it possible to perform similar analyses also for diffractive di-hadron detections. Notably, NLO saturation is relevant to access the (un)polarized gluon content of protons and nucleons at small x [502–507]. The authors of Refs. [508–512] investigated quarkonium production in proton–proton and proton–nucleus collisions by combining both NRQCD low-x effects. Future studies will explore the common ground between our method to address quarkonium production via the NLL/NLO$^{(+)}$ hybrid factorization and higher-order calculations for NLO saturation in the exclusive emissions of heavy mesons [513,514].

Finally, in order to reach a higher level of precision in our knowledge of quarkonium fragmentation, we must compare NRQCD-inspired collinear FFs with the determinations of these quantities obtained by extraction via global fits. On this basis, neural network techniques already developed for the extraction of light-flavored hadron FFs [416,515–521] will represent an asset. Another important development will be linking the JETHAD technology to fully automated codes devoted to the study of quarkonium production at NLO. We mainly refer to `MadGraph5_aMC@NLO` [522] and `HELAC-Onia` [116,117] as interfaced with the `NLOAccess` virtual platform [523,524].

Funding: This research received no external funding.

Data Availability Statement: The data produced in this work are summarized in the figures. They can be made available upon request.

Acknowledgments: The author thanks colleagues at the *Quarkonia As Tools* series of conferences for the inspiring discussions and for the warm atmosphere. The author is grateful to Jean-Philippe Lansberg, Charlotte Van Hulse, Hua-Sheng Shao, Cristian Pisano, Valerio Bertone, Andrea Signori, and Michael Fucilla for the fruitful conversations. The author thanks Alessandro Papa for the encouragement. This work is supported by the Atracción de Talento Grant n. 2022-T1/TIC-24176 of the Comunidad Autónoma de Madrid, Spain.

Conflicts of Interest: The author declares no conflicts of interest.

Abbreviations

ABF	Altarelli–Ball–Forte
BFKL	Balitsky–Fadin–Kuraev–Lipatov
BLM	Brodsky–Lepage–Mackenzie
BNL	Brookhaven National Laboratory
BSM	Beyond the Standard Model
CEM	Color Evaporation Model

CO	Color Octet
CP	Charge Parity
CSM	Color Singlet Mechanism
DGLAP	Dokshitzer–Gribov–Lipatov–Altarelli–Parisi
DPS	Double-Parton Scattering
EIC	Electron–Ion Collider
FCNCs	Flavor-Changing Neutral Currents
FFs	Fragmentation Functions
GIM	Glashow–Iliopoulos–Maiani
LDME	Long-Distance Matrix Element
LHC	Large Hadron Collider
LL	Leading Logarithmic
LO	Leading Order
LVM	Light Vector Meson
MPI	Multi-Parton Interaction
NLL	Next-to-Leading Logarithmic
NLO	Next-to-Leading Order
NRQCD	Nonrelativistic QCD
PDFs	Parton Distribution Functions
QCD	Quantum Chromodynamics
SCET	Soft and Collinear Effective Theory
SLAC	Stanford Linear Accelerator Center
SM	Standard Model
TMD	Transverse-Momentum-Dependent
UGD	Unintegrated Gluon Distribution
VFNS	Variable-Flavor Number Scheme

Appendix A. NLO Heavy-Quarkonium Impact Factor

In this appendix, we give the analytic formula for the NLO correction to the impact factor describing the production of a forward quarkonium $\mathcal{Q}$ at large transverse momentum (for the derivation, see Refs. [252]). One has

$$\hat{c}_{\mathcal{Q}}(n,\nu,|\vec{p}_{\mathcal{Q}}|,x_{\mathcal{Q}}) = \frac{1}{\pi}\sqrt{\frac{C_F}{C_A}}\left(|\vec{p}_{\mathcal{Q}}|^2\right)^{i\nu-\frac{1}{2}} \int_{x_{\mathcal{Q}}}^{1}\frac{\mathrm{d}x}{x}\int_{\frac{x_{\mathcal{Q}}}{x}}^{1}\frac{\mathrm{d}v}{v}\left(\frac{xv}{x_{\mathcal{Q}}}\right)^{2i\nu-1} \tag{A1}$$

$$\times\left[\frac{C_A}{C_F}f_g(x)D_g^{\mathcal{Q}}\left(\frac{x_{\mathcal{Q}}}{xv}\right)C_{gg}(x,v) + \sum_{i=q\bar{q}} f_i(x)D_i^{\mathcal{Q}}\left(\frac{x_{\mathcal{Q}}}{xv}\right)C_{qq}(x,v)\right.$$

$$\left.\times\, D_g^{\mathcal{Q}}\left(\frac{x_{\mathcal{Q}}}{xv}\right)\sum_{i=q\bar{q}} f_i(x)C_{qg}(x,v) + \frac{C_A}{C_F}f_g(x)\sum_{i=q\bar{q}} D_i^{\mathcal{Q}}\left(\frac{x_{\mathcal{Q}}}{xv}\right)C_{gq}(x,v)\right],$$

where

$$C_{gg}(x,v) = P_{gg}(v)\left(1+v^{-2\gamma}\right)\ln\left(\frac{|\vec{p}_{\mathcal{Q}}|^2x^2v^2}{\mu_F^2x_{\mathcal{Q}}^2}\right) - \frac{\beta_0}{2}\ln\left(\frac{|\vec{p}_{\mathcal{Q}}|^2x^2v^2}{\mu_R^2x_{\mathcal{Q}}^2}\right) \tag{A2}$$

$$+\,\delta(1-v)\left[C_A\ln\left(\frac{s_0\,x^2}{|\vec{p}_{\mathcal{Q}}|^2\,x_{\mathcal{Q}}^2}\right)\chi(n,\gamma) - C_A\left(\frac{67}{18}-\frac{\pi^2}{2}\right)+\frac{5}{9}n_f\right.$$

$$\left.+\frac{C_A}{2}\left(\psi'\left(1+\gamma+\frac{n}{2}\right)-\psi'\left(\frac{n}{2}-\gamma\right)-\chi^2(n,\gamma)\right)\right] + C_A\left(\frac{1}{v}+\frac{1}{(1-v)_+}-2+v\bar{v}\right)$$

$$\times\left(\chi(n,\gamma)(1+v^{-2\gamma}) - 2(1+2v^{-2\gamma})\ln v + \frac{\bar{v}^2}{v^2}\mathcal{I}_2\right)$$

$$+\,2\,C_A(1+v^{-2\gamma})\left(\left(\frac{1}{v}-2+v\bar{v}\right)\ln\bar{v} + \left(\frac{\ln(1-v)}{1-v}\right)_+\right),$$

$$C_{gq}(x,v) = P_{qg}(v)\left(\frac{C_F}{C_A}+v^{-2\gamma}\right)\ln\left(\frac{|\vec{p}_Q|^2x^2v^2}{\mu_F^2x_Q^2}\right) \tag{A3}$$
$$+2\,v\bar{v}\,T_R\left(\frac{C_F}{C_A}+v^{-2\gamma}\right)+P_{qg}(v)\left(\frac{C_F}{C_A}\chi(n,\gamma)+2v^{-2\gamma}\ln\frac{\bar{v}}{v}+\frac{\bar{v}}{v}\mathcal{I}_3\right),$$

$$C_{qg}(x,v) = P_{gq}(v)\left(\frac{C_A}{C_F}+v^{-2\gamma}\right)\ln\left(\frac{|\vec{p}_Q|^2x^2v^2}{\mu_F^2x_Q^2}\right) \tag{A4}$$
$$+v\Big(C_Fv^{-2\gamma}+C_A\Big)+\frac{1+\bar{v}^2}{v}\left[C_Fv^{-2\gamma}(\chi(n,\gamma)-2\ln v)+2C_A\ln\frac{\bar{v}}{v}+\frac{\bar{v}}{v}\mathcal{I}_1\right],$$

and

$$C_{qq}(x,v) = P_{qq}(v)\Big(1+v^{-2\gamma}\Big)\ln\left(\frac{|\vec{p}_Q|^2x^2v^2}{\mu_F^2x_Q^2}\right)-\frac{\beta_0}{2}\ln\left(\frac{|\vec{p}_Q|^2x^2v^2}{\mu_R^2x_Q^2}\right) \tag{A5}$$
$$+\delta(1-v)\left[C_A\ln\left(\frac{s_0\,x_Q^2}{|\vec{p}_Q|^2\,x^2}\right)\chi(n,\gamma)+C_A\left(\frac{85}{18}+\frac{\pi^2}{2}\right)-\frac{5}{9}n_f-8\,C_F\right.$$
$$\left.+\frac{C_A}{2}\left(\psi'\Big(1+\gamma+\frac{n}{2}\Big)-\psi'\Big(\frac{n}{2}-\gamma\Big)-\chi^2(n,\gamma)\right)\right]+C_F\,\bar{v}\,(1+v^{-2\gamma})$$
$$+\Big(1+v^2\Big)\left[C_A(1+v^{-2\gamma})\frac{\chi(n,\gamma)}{2(1-v)_+}+\Big(C_A-2\,C_F(1+v^{-2\gamma})\Big)\frac{\ln v}{1-v}\right]$$
$$+\left(C_F-\frac{C_A}{2}\right)\Big(1+v^2\Big)\left[2(1+v^{-2\gamma})\left(\frac{\ln(1-v)}{1-v}\right)_+ +\frac{\bar{v}}{v^2}\mathcal{I}_2\right],$$

Here, s_0 stands for an energy normalization scale that naturally arises within the BFKL formalism. We set $s_0 \equiv \mu_C$. Moreover, we define $\bar{v} \equiv 1-v$ and $\gamma \equiv -\frac{1}{2}+i\nu$. The DGLAP $P_{ij}(v)$ splitting kernels are taken at LO:

$$\begin{aligned}
P_{gq}(z) &= C_F\frac{1+(1-z)^2}{z}, \\
P_{qg}(z) &= T_R\Big[z^2+(1-z)^2\Big], \\
P_{qq}(z) &= C_F\left(\frac{1+z^2}{1-z}\right)_+ = C_F\left[\frac{1+z^2}{(1-z)_+}+\frac{3}{2}\delta(1-z)\right], \\
P_{gg}(z) &= 2C_A\left[\frac{1}{(1-z)_+}+\frac{1}{z}-2+z(1-z)\right]+\left(\frac{11}{6}C_A-\frac{n_f}{3}\right)\delta(1-z).
\end{aligned} \tag{A6}$$

The $\mathcal{I}_{2,1,3}$ functions are given by

$$\mathcal{I}_2 = \frac{v^2}{\bar{v}^2}\left[v\left(\frac{{}_2F_1(1,1+\gamma-\frac{n}{2},2+\gamma-\frac{n}{2},v)}{\frac{n}{2}-\gamma-1}-\frac{{}_2F_1(1,1+\gamma+\frac{n}{2},2+\gamma+\frac{n}{2},v)}{\frac{n}{2}+\gamma+1}\right)\right. \tag{A7}$$
$$+v^{-2\gamma}\left(\frac{{}_2F_1(1,-\gamma-\frac{n}{2},1-\gamma-\frac{n}{2},v)}{\frac{n}{2}+\gamma}-\frac{{}_2F_1(1,-\gamma+\frac{n}{2},1-\gamma+\frac{n}{2},v)}{\frac{n}{2}-\gamma}\right)$$
$$\left.+\Big(1+v^{-2\gamma}\Big)(\chi(n,\gamma)-2\ln\bar{v})+2\ln v\right],$$

$$\mathcal{I}_1 = \frac{\bar{v}}{2v}\mathcal{I}_2+\frac{v}{\bar{v}}\left[\ln v+\frac{1-v^{-2\gamma}}{2}(\chi(n,\gamma)-2\ln\bar{v})\right], \tag{A8}$$

and

$$\mathcal{I}_3 = \frac{\bar{v}}{2v}\mathcal{I}_2-\frac{v}{\bar{v}}\left[\ln v+\frac{1-v^{-2\gamma}}{2}(\chi(n,\gamma)-2\ln\bar{v})\right], \tag{A9}$$

whereas ${}_2F_1$ represents the ordinary hypergeometric special function.

The *plus prescription* introduced in Equations (A2) and (A5) reads

$$\int_\zeta^1 \mathrm{d}y \frac{f(y)}{(1-y)_+} = \int_\zeta^1 \mathrm{d}y \frac{f(y)-f(1)}{(1-y)} - \int_0^\zeta \mathrm{d}y \frac{f(1)}{(1-y)}\,, \tag{A10}$$

with $f(y)$ being a generic function behaving regularly when $y=1$.

Appendix B. NLO Light-Jet Impact Factor

Analogously, the formula for the NLO correction to describe the production of a forward light jet in the small-cone limit reads (for the derivation, see Refs. [249,251])

$$\begin{aligned}
\hat{c}_J(n,\nu,|\vec{p}_J|,x_J) &= \frac{1}{\pi}\sqrt{\frac{C_F}{C_A}}\left(|\vec{p}_J|^2\right)^{i\nu-1/2}\int_{x_J}^1 \frac{\mathrm{d}v}{v} v^{-\bar{\alpha}_s(\mu_R)\chi(n,\nu)} \qquad \text{(A11)}\\
&\times\left\{\sum_{i=q,\bar{q}} f_i\left(\frac{x_J}{v}\right)\left[\left(P_{qq}(v)+\frac{C_A}{C_F}P_{gq}(v)\right)\ln\frac{|\vec{p}_J|^2}{\mu_F^2}\right.\right.\\
&-2v^{-2\gamma}\ln\frac{\mathcal{R}}{\max(v,\bar{v})}\left\{P_{qq}(v)+P_{gq}(v)\right\}-\frac{\beta_0}{2}\ln\frac{|\vec{p}_J|^2}{\mu_R^2}\delta(1-v)\\
&+C_A\delta(1-v)\left[\chi(n,\gamma)\ln\frac{s_0}{|\vec{p}_J|^2}+\frac{85}{18}\right.\\
&\left.+\frac{\pi^2}{2}+\frac{1}{2}\left(\psi'\left(1+\gamma+\frac{n}{2}\right)-\psi'\left(\frac{n}{2}-\gamma\right)-\chi^2(n,\gamma)\right)\right]\\
&+(1+v^2)\left\{C_A\left[\frac{(1+v^{-2\gamma})\,\chi(n,\gamma)}{2(1-v)_+}-v^{-2\gamma}\left(\frac{\ln(1-v)}{1-v}\right)_+\right]\right.\\
&\left.+\left(C_F-\frac{C_A}{2}\right)\left[\frac{\bar{v}}{v^2}\mathcal{I}_2-\frac{2\ln v}{1-v}+2\left(\frac{\ln(1-v)}{1-v}\right)_+\right]\right\}\\
&+\delta(1-v)\left(C_F\left(3\ln 2-\frac{\pi^2}{3}-\frac{9}{2}\right)-\frac{5n_f}{9}\right)+C_A v+C_F\bar{v}\\
&\left.+\frac{1+\bar{v}^2}{v}\left(C_A\frac{\bar{v}}{v}\mathcal{I}_1+2C_A\ln\frac{\bar{v}}{v}+C_F v^{-2\gamma}(\chi(n,\gamma)-2\ln\bar{v})\right)\right]\\
&+f_g\left(\frac{x_J}{v}\right)\frac{C_A}{C_F}\left[\left(P_{gg}(v)+2\,n_f\frac{C_F}{C_A}P_{qg}(v)\right)\ln\frac{|\vec{p}_J|^2}{\mu_F^2}\right.\\
&-2v^{-2\gamma}\ln\frac{\mathcal{R}}{\max(v,\bar{v})}\left(P_{gg}(v)+2\,n_f P_{qg}(v)\right)-\frac{\beta_0}{2}\ln\frac{|\vec{p}_J|^2}{4\mu_R^2}\delta(1-v)\\
&+C_A\delta(1-v)\left(\chi(n,\gamma)\ln\frac{s_0}{|\vec{p}_J|^2}+\frac{1}{12}+\frac{\pi^2}{6}\right.\\
&\left.+\frac{1}{2}\left[\psi'\left(1+\gamma+\frac{n}{2}\right)-\psi'\left(\frac{n}{2}-\gamma\right)-\chi^2(n,\gamma)\right]\right)\\
&+2C_A(1-v^{-2\gamma})\left(\left(\frac{1}{v}-2+v\bar{v}\right)\ln\bar{v}+\frac{\ln(1-v)}{1-v}\right)\\
&+C_A\left[\frac{1}{v}+\frac{1}{(1-v)_+}-2+v\bar{v}\right]\left((1+v^{-2\gamma})\chi(n,\gamma)-2\ln v+\frac{\bar{v}^2}{v^2}\mathcal{I}_2\right)\\
&\left.\left.+n_f\left[2v\bar{v}\frac{C_F}{C_A}+(v^2+\bar{v}^2)\left(\frac{C_F}{C_A}\chi(n,\gamma)+\frac{\bar{v}}{v}\mathcal{I}_3\right)-\frac{1}{12}\delta(1-v)\right]\right]\right\}.
\end{aligned}$$

Here, $\mathcal{R}$ denotes the jet–cone radius, while s_0, $\bar{v}$, γ, $P_{ij}(v)$, $\mathcal{I}_{2,1,3}$, and the plus prescriptions were introduced in the previous appendix.

Notes

[1] In a similar way, collinear FFs for $\bar{b}$ and c quarks fragmenting into B_c and B_c^* mesons were obtained at LO [373–375] and NLO [376] (see Refs. [377–379] for applications).

[2] An analogous strategy was applied in Refs. [383,384] to compute the gluon FF to charmed B mesons.

References

1. Gell-Mann, M. Symmetries of baryons and mesons. *Phys. Rev.* **1962**, *125*, 1067–1084. [CrossRef]
2. Gell-Mann, M. A Schematic Model of Baryons and Mesons. *Phys. Lett.* **1964**, *8*, 214–215. [CrossRef]
3. Zweig, G. An SU(3) model for strong interaction symmetry and its breaking. Version 2. In *Developments in the Quark Theory of Hadrons. Vol. 1. 1964–1978*; Lichtenberg, D.B., Rosen, S.P., Eds.; Hadronic Press: Nonantum, MA, USA , 1964; pp. 22–101.
4. Fritzsch, H.; Gell-Mann, M.; Leutwyler, H. Advantages of the Color Octet Gluon Picture. *Phys. Lett. B* **1973**, *47*, 365–368. [CrossRef]
5. Kronfeld, A.S.; Quigg, C. Resource Letter: Quantum Chromodynamics. *Am. J. Phys.* **2010**, *78*, 1081–1116. [CrossRef]
6. Peccei, R.D.; Quinn, H.R. CP Conservation in the Presence of Instantons. *Phys. Rev. Lett.* **1977**, *38*, 1440–1443. [CrossRef]
7. Peccei, R.D.; Quinn, H.R. Constraints Imposed by CP Conservation in the Presence of Instantons. *Phys. Rev. D* **1977**, *16*, 1791–1797. [CrossRef]
8. Peccei, R.D. The Strong CP problem and axions. *Lect. Notes Phys.* **2008**, *741*, 3–17. [CrossRef]
9. Duffy, L.D.; van Bibber, K. Axions as Dark Matter Particles. *New J. Phys.* **2009**, *11*, 105008. [CrossRef]
10. Forestell, L.; Morrissey, D.E.; Sigurdson, K. Cosmological Bounds on Non-Abelian Dark Forces. *Phys. Rev. D* **2018**, *97*, 075029. [CrossRef]
11. Huang, W.C.; Reichert, M.; Sannino, F.; Wang, Z.W. Testing the dark SU(N) Yang-Mills theory confined landscape: From the lattice to gravitational waves. *Phys. Rev. D* **2021**, *104*, 035005. [CrossRef]
12. McLerran, L.; Pisarski, R.D. Phases of cold, dense quarks at large N(c). *Nucl. Phys. A* **2007**, *796*, 83–100. [CrossRef]
13. Hidaka, Y.; McLerran, L.D.; Pisarski, R.D. Baryons and the phase diagram for a large number of colors and flavors. *Nucl. Phys. A* **2008**, *808*, 117–123. [CrossRef]
14. McLerran, L.; Reddy, S. Quarkyonic Matter and Neutron Stars. *Phys. Rev. Lett.* **2019**, *122*, 122701. [CrossRef] [PubMed]
15. Buchmuller, W.; Wyler, D. Effective Lagrangian Analysis of New Interactions and Flavor Conservation. *Nucl. Phys. B* **1986**, *268*, 621–653. [CrossRef]
16. Witten, E. Baryons in the 1/n Expansion. *Nucl. Phys. B* **1979**, *160*, 57–115. [CrossRef]
17. Dudek, J.J.; Edwards, R.G.; Peardon, M.J.; Richards, D.G.; Thomas, C.E. Toward the excited meson spectrum of dynamical QCD. *Phys. Rev. D* **2010**, *82*, 034508. [CrossRef]
18. Afonin, S.S. The effect of higher dimensional QCD operators on the spectroscopy of bottom-up holographic models. *Universe* **2021**, *7*, 102. [CrossRef]
19. Augustin, J.E.; Boyarski, A.; Breidenbach, M; Bulos, F.; Dakin, J.T.; Feldman, G.J.; Fischer, G.E.; Fryberger, D.; Hanson, G.; Jean-Marie, B.; et al. Discovery of a Narrow Resonance in e^+e^- Annihilation. *Phys. Rev. Lett.* **1974**, *33*, 1406–1408. [CrossRef]
20. Aubert J.J.; Becker, U.; Biggs, P.J.; Burger, J.; Chen, M.; Everhart, G.; Goldhagen, P.; Leong, J.; McCorriston, T.; Rhoades, T.G.; et al Experimental Observation of a Heavy Particle J. *Phys. Rev. Lett.* **1974**, *33*, 1404–1406. [CrossRef]
21. Bacci, C.; Balbini Celio, R.; Berna-Rodini, M.; Caton, G.; del Fabbro, R.; G-rilli, M.; Iarocci, E.; Locci, M.; Mencuccini, C.; Murtas, G.P.; et al. Preliminary Result of Frascati (ADONE) on the Nature of a New 3.1-GeV Particle Produced in e+ e- Annihilation. *Phys. Rev. Lett.* **1974**, *33*, 1408; Erratum in *Phys. Rev. Lett.* **1974**, *33*, 1649. [CrossRef]
22. Bjørken, B.; Glashow, S. Elementary particles and SU(4). *Phys. Lett.* **1964**, *11*, 255–257. [CrossRef]
23. Glashow, S.L.; Iliopoulos, J.; Maiani, L. Weak Interactions with Lepton-Hadron Symmetry. *Phys. Rev. D* **1970**, *2*, 1285-t-1292. [CrossRef]
24. Wiss, J.; Goldhaber, G.; Abrams, G.S.; Alam, M.S.; Boyarski, A.; Breidenbach, M.; Carithers, W.C.; Cooper, S.; DeVoe, R.; Dorfan, J.; et al. Evidence for Parity Violation in the Decays of the Narrow States Near 1.87-GeV/c**2. *Phys. Rev. Lett.* **1976**, *37*, 1531–1534. [CrossRef]
25. Herb, S.W.; Hom, D.C.; Lederman, L.M.; Sens, J.C.; Snyder, H.D.; Yoh, J.K.; Appel, J.A.; Brown, B.C.; Brown, C.N.; Innes, W.R.; et al. Observation of a Dimuon Resonance at 9.5-GeV in 400-GeV Proton-Nucleus Collisions. *Phys. Rev. Lett.* **1977**, *39*, 252–255. [CrossRef]
26. Bebek, C.; Haggerty, J.; Izen, J.M.; Loomis, W.A.; Pipkin, F.M.; Rohlf, J.; Tanenbaum, W.M.; Wilson, R.; Sadoff, A.J.; Bridges, D.L.; et al. Evidence for New Flavor Production at the Upsilon (4S). *Phys. Rev. Lett.* **1981**, *46*, 84. [CrossRef]
27. Fabiano, N. Top mesons. *Eur. Phys. J. C* **1998**, *2*, 345–350. [CrossRef]
28. Fadin, V.S.; Khoze, V.A. Threshold Behavior of Heavy Top Production in e+ e- Collisions. *JETP Lett.* **1987**, *46*, 525–529.
29. Fadin, V.S.; Khoze, V.A. Production of a pair of heavy quarks in e+ e- annihilation in the threshold region. *Sov. J. Nucl. Phys.* **1988**, *48*, 309–313.

30. Pancheri, G.; Revol, J.P.; Rubbia, C. Precise measurement of the toponium mass from the observation of its two photon decay at the LHC. *Phys. Lett. B* **1992**, *277*, 518–523. [CrossRef]
31. Kuhn, J.H.; Mirkes, E. Toponium production at hadron colliders. *Phys. Lett. B* **1992**, *296*, 425–429. [CrossRef]
32. Kuhn, J.H.; Mirkes, E. QCD corrections to toponium production at hadron colliders. *Phys. Rev. D* **1993**, *48*, 179–189. [CrossRef] [PubMed]
33. Fabiano, N.; Grau, A.; Pancheri, G. Observability limits for toponium at hadron colliders. *Phys. Rev. D* **1994**, *50*, 3173–3175. [CrossRef] [PubMed]
34. Fabiano, N.; Pancheri, G.; Grau, A. Toponium from different potential models. *Nuovo Cim. A* **1994**, *107*, 2789–2804. [CrossRef]
35. Hagiwara, K.; Sumino, Y.; Yokoya, H. Bound-state Effects on Top Quark Production at Hadron Colliders. *Phys. Lett. B* **2008**, *666*, 71–76. [CrossRef]
36. Kiyo, Y.; Kuhn, J.H.; Moch, S.; Steinhauser, M.; Uwer, P. Top-quark pair production near threshold at LHC. *Eur. Phys. J. C* **2009**, *60*, 375–386. [CrossRef]
37. Sumino, Y.; Yokoya, H. Bound-state effects on kinematical distributions of top quarks at hadron colliders. *J. High Energy Phys.* **2010**, *9*, 034; Erratum in *J. High Energy Phys.* **2016**, *06*, 037. [CrossRef]
38. Ju, W.L.; Wang, G.; Wang, X.; Xu, X.; Xu, Y.; Yang, L.L. Top quark pair production near threshold: single/double distributions and mass determination. *J. High Energy Phys.* **2020**, *6*, 158. [CrossRef]
39. Strassler, M.J.; Peskin, M.E. The Heavy top quark threshold: QCD and the Higgs. *Phys. Rev. D* **1991**, *43*, 1500–1514. [CrossRef]
40. Sumino, Y.; Fujii, K.; Hagiwara, K.; Murayama, H.; Ng, C.K. Top quark pair production near threshold. *Phys. Rev. D* **1993**, *47*, 56–81. [CrossRef]
41. Jezabek, M.; Kuhn, J.H.; Teubner, T. Momentum distributions in t anti-t production and decay near threshold. *Z. Phys. C* **1992**, *56*, 653–660. [CrossRef]
42. Fadin, V.S.; Khoze, V.A.; Sjostrand, T. On the Threshold Behavior of Heavy Top Production. *Z. Phys. C* **1990**, *48*, 613–622. [CrossRef]
43. Fuks, B.; Hagiwara, K.; Ma, K.; Zheng, Y.J. Signatures of toponium formation in LHC run 2 data. *Phys. Rev. D* **2021**, *104*, 034023. [CrossRef]
44. Hagiwara, K.; Ma, K.; Yokoya, H. Probing CP violation in e^+e^- production of the Higgs boson and toponia. *J. High Energy Phys.* **2016**, *6*, 048. [CrossRef]
45. Lansberg, J.P. New Observables in Inclusive Production of Quarkonia. *Phys. Rept.* **2020**, *889*, 1–106. [CrossRef]
46. Scarpa, F. Probing the Gluon Transverse Momentum-Dependent Distributions Inside the Proton through Quarkonium-Pair Production at the LHC. Ph.D. Thesis, University of Groningen , Groningen, The Netherlands, 2020.
47. Fritzsch, H. Producing Heavy Quark Flavors in Hadronic Collisions: A Test of Quantum Chromodynamics. *Phys. Lett. B* **1977**, *67*, 217–221. [CrossRef]
48. Halzen, F. Cvc for Gluons and Hadroproduction of Quark Flavors. *Phys. Lett. B* **1977**, *69*, 105–108. [CrossRef]
49. Lansberg, J.P. J/ψ, ψ' and Y production at hadron colliders: A Review. *Int. J. Mod. Phys. A* **2006**, *21*, 3857–3916. [CrossRef]
50. Brambilla, N.; Eidelman, S.; Heltsley, B.K.; Vogt, R.; Bodwin, G.T.; Eichten, E.; Frawley, A.D.; Meyer, A.B.; Mitchell, R.E.; Papadimitriou, V.; et al. Heavy Quarkonium: Progress, Puzzles, and Opportunities. *Eur. Phys. J. C* **2011**, *71*, 1534. [CrossRef]
51. Einhorn, M.B.; Ellis, S.D. Hadronic Production of the New Resonances: Probing Gluon Distributions. *Phys. Rev. D* **1975**, *12*, 2007. [CrossRef]
52. Chang, C.H. Hadronic Production of J/ψ Associated With a Gluon. *Nucl. Phys. B* **1980**, *172*, 425–434. [CrossRef]
53. Berger, E.L.; Jones, D.L. Inelastic Photoproduction of J/psi and Upsilon by Gluons. *Phys. Rev. D* **1981**, *23*, 1521–1530. [CrossRef]
54. Baier, R.; Ruckl, R. Hadronic Production of J/psi and Upsilon: Transverse Momentum Distributions. *Phys. Lett. B* **1981**, *102*, 364–370. [CrossRef]
55. Barbieri, R.; Gatto, R.; Remiddi, E. Singular Binding Dependence in the Hadronic Widths of 1++ and 1+- Heavy Quark anti-Quark Bound States. *Phys. Lett. B* **1976**, *61*, 465–468. [CrossRef]
56. Bodwin, G.T.; Braaten, E.; Lepage, G.P. Rigorous QCD predictions for decays of P wave quarkonia. *Phys. Rev. D* **1992**, *46*, R1914–R1918. [CrossRef]
57. Caswell, W.E.; Lepage, G.P. Effective Lagrangians for Bound State Problems in QED, QCD, and Other Field Theories. *Phys. Lett. B* **1986**, *167*, 437–442. [CrossRef]
58. Thacker, B.A.; Lepage, G.P. Heavy quark bound states in lattice QCD. *Phys. Rev. D* **1991**, *43*, 196–208. [CrossRef]
59. Bodwin, G.T.; Braaten, E.; Lepage, G.P. Rigorous QCD analysis of inclusive annihilation and production of heavy quarkonium. *Phys. Rev. D* **1995**, *51*, 1125–1171; Erratum in *Phys. Rev. D* **1997**, *55*, 5853. [CrossRef]
60. Cho, P.L.; Leibovich, A.K. Color octet quarkonia production. *Phys. Rev. D* **1996**, *53*, 150–162. [CrossRef] [PubMed]
61. Cho, P.L.; Leibovich, A.K. Color octet quarkonia production. 2. *Phys. Rev. D* **1996**, *53*, 6203–6217. [CrossRef] [PubMed]
62. Leibovich, A.K. Psi-prime polarization due to color octet quarkonia production. *Phys. Rev. D* **1997**, *56*, 4412–4415. [CrossRef]
63. Bodwin, G.T.; Braaten, E.; Lee, J. Comparison of the color-evaporation model and the NRQCD factorization approach in charmonium production. *Phys. Rev. D* **2005**, *72*, 014004. [CrossRef]
64. Halzen, F.; Herzog, F.; Glover, E.W.N.; Martin, A.D. The J/ψ as a Trigger in $\bar{p}p$ Collisions. *Phys. Rev. D* **1984**, *30*, 700. [CrossRef]
65. Mangano, M.L. Phenomenology of quarkonium production in hadronic collisions. *AIP Conf. Proc.* **1996**, *357*, 120–134. [CrossRef]

66. Braaten, E.; Fleming, S.; Yuan, T.C. Production of heavy quarkonium in high-energy colliders. *Ann. Rev. Nucl. Part. Sci.* **1996**, *46*, 197–235. [CrossRef]
67. Artoisenet, P. Quarkonium Production Phenomenology. Ph.D. Thesis, Louvain University, Louvain, Belgium, 2009.
68. Braaten, E.; Yuan, T.C. Gluon fragmentation into heavy quarkonium. *Phys. Rev. Lett.* **1993**, *71*, 1673–1676. [CrossRef]
69. Curci, G.; Furmanski, W.; Petronzio, R. Evolution of Parton Densities Beyond Leading Order: The Nonsinglet Case. *Nucl. Phys. B* **1980**, *175*, 27–92. [CrossRef]
70. Furmanski, W.; Petronzio, R. Singlet Parton Densities Beyond Leading Order. *Phys. Lett. B* **1980**, *97*, 437–442. [CrossRef]
71. Gribov, V.; Lipatov, L. Deep inelastic e p scattering in perturbation theory. *Sov. J. Nucl. Phys.* **1972**, *15*, 438–450.
72. Gribov, V.N.; Lipatov, L.N. e+ e- pair annihilation and deep inelastic e p scattering in perturbation theory. *Sov. J. Nucl. Phys.* **1972**, *15*, 675–684.
73. Lipatov, L.N. The parton model and perturbation theory. *Yad. Fiz.* **1974**, *20*, 181–198.
74. Altarelli, G.; Parisi, G. Asymptotic Freedom in Parton Language. *Nucl. Phys. B* **1977**, *126*, 298–318. [CrossRef]
75. Dokshitzer, Y.L. Calculation of the Structure Functions for Deep Inelastic Scattering and e+ e- Annihilation by Perturbation Theory in Quantum Chromodynamics. *Sov. Phys. JETP* **1977**, *46*, 641–653.
76. Artoisenet, P.; Braaten, E. Gluon fragmentation into quarkonium at next-to-leading order. *J. High Energy Phys.* **2015**, *4*, 121. [CrossRef]
77. Braaten, E.; Cheung, K.M.; Yuan, T.C. Z0 decay into charmonium via charm quark fragmentation. *Phys. Rev. D* **1993**, *48*, 4230–4235. [CrossRef] [PubMed]
78. Zheng, X.C.; Chang, C.H.; Wu, X.G. NLO fragmentation functions of heavy quarks into heavy quarkonia. *Phys. Rev. D* **2019**, *100*, 014005. [CrossRef]
79. Doncheski, M.A.; Fleming, S.; Mangano, M.L. Charmonium production via fragmentation at $p\bar{p}$ colliders. In *Proceedings of the Workshop on Physics at Current Accelerators and the Supercollider*; Argonne National Lab.: Lemont, IL, USA, 1993.
80. Braaten, E.; Doncheski, M.A.; Fleming, S.; Mangano, M.L. Fragmentation production of J/ψ and ψ' at the Tevatron. *Phys. Lett. B* **1994**, *333*, 548–554. [CrossRef]
81. Cacciari, M.; Greco, M. J/ψ production via fragmentation at the Tevatron. *Phys. Rev. Lett.* **1994**, *73*, 1586–1589. [CrossRef]
82. Cacciari, M.; Greco, M.; Mangano, M.L.; Petrelli, A. Charmonium production at the Tevatron. *Phys. Lett. B* **1995**, *356*, 553–560. [CrossRef]
83. Cacciari, M.; Greco, M. Charm photoproduction via fragmentation. *Z. Phys. C* **1996**, *69*, 459–466. [CrossRef]
84. Ma, Y.Q.; Qiu, J.W.; Zhang, H. Heavy quarkonium fragmentation functions from a heavy quark pair. I. *S* wave. *Phys. Rev. D* **2014**, *89*, 094029. [CrossRef]
85. Ma, Y.Q.; Qiu, J.W.; Zhang, H. Heavy quarkonium fragmentation functions from a heavy quark pair. II. *P* wave. *Phys. Rev. D* **2014**, *89*, 094030. [CrossRef]
86. Nayak, G.C.; Qiu, J.W.; Sterman, G.F. Fragmentation, factorization and infrared poles in heavy quarkonium production. *Phys. Lett. B* **2005**, *613*, 45–51. [CrossRef]
87. Nayak, G.C.; Qiu, J.W.; Sterman, G.F. Fragmentation, NRQCD and NNLO factorization analysis in heavy quarkonium production. *Phys. Rev. D* **2005**, *72*, 114012. [CrossRef]
88. Falk, A.F.; Luke, M.E.; Savage, M.J.; Wise, M.B. Heavy quark fragmentation to polarized quarkonium. *Phys. Lett. B* **1993**, *312*, 486–490. [CrossRef]
89. Chen, Y.Q. Perturbative QCD predictions for the fragmentation functions of the P wave mesons with two heavy quarks. *Phys. Rev. D* **1993**, *48*, 5181–5189. [CrossRef]
90. Cho, P.L.; Wise, M.B.; Trivedi, S.P. Gluon fragmentation into polarized charmonium. *Phys. Rev. D* **1995**, *51*, R2039–R2043, [CrossRef]
91. Kang, Z.B.; Qiu, J.W.; Sterman, G. Heavy quarkonium production and polarization. *Phys. Rev. Lett.* **2012**, *108*, 102002. [CrossRef]
92. Kang, Z.B.; Ma, Y.Q.; Qiu, J.W.; Sterman, G. Heavy Quarkonium Production at Collider Energies: Partonic Cross Section and Polarization. *Phys. Rev. D* **2015**, *91*, 014030. [CrossRef]
93. Ma, Y.Q.; Qiu, J.W.; Zhang, H. Fragmentation functions of polarized heavy quarkonium. *J. High Energy Phys.* **2015**, *6*, 021. [CrossRef]
94. Lansberg, J.P. On the mechanisms of heavy-quarkonium hadroproduction. *Eur. Phys. J. C* **2009**, *61*, 693–703. [CrossRef]
95. Kang, Z.B.; Ma, Y.Q.; Qiu, J.W.; Sterman, G. Heavy Quarkonium Production at Collider Energies: Factorization and Evolution. *Phys. Rev. D* **2014**, *90*, 034006. [CrossRef]
96. Mangano, M.L.; Nason, P.; Ridolfi, G. Heavy quark correlations in hadron collisions at next-to-leading order. *Nucl. Phys. B* **1992**, *373*, 295–345. [CrossRef]
97. Krämer, M. QCD corrections to inelastic J/psi photoproduction. *Nucl. Phys. B* **1996**, *459*, 3–50. [CrossRef]
98. Petrelli, A.; Cacciari, M.; Greco, M.; Maltoni, F.; Mangano, M.L. NLO production and decay of quarkonium. *Nucl. Phys. B* **1998**, *514*, 245–309. [CrossRef]
99. Maltoni, F.; Mangano, M.L.; Petrelli, A. Quarkonium photoproduction at next-to-leading order. *Nucl. Phys. B* **1998**, *519*, 361–393. [CrossRef]

100. Klasen, M.; Kniehl, B.A.; Mihaila, L.N.; Steinhauser, M. J/ψ plus jet associated production in two-photon collisions at next-to-leading order. *Nucl. Phys. B* **2005**, *713*, 487–521. [CrossRef]
101. Gong, B.; Li, X.Q.; Wang, J.X. QCD corrections to J/ψ production via color octet states at Tevatron and LHC. *Phys. Lett. B* **2009**, *673*, 197–200; Erratum in *Phys. Lett. B* **2010**, *693*, 612–613. [CrossRef]
102. Maltoni, F.; Spengler, J.; Bargiotti, M.; Bertin, A.; Bruschi, M.; De Castro, S.; Fabbri, L.; Faccioli, P.; Giacobbe, B.; Grimaldi, F.; et al. Analysis of charmonium production at fixed-target experiments in the NRQCD approach. *Phys. Lett. B* **2006**, *638*, 202–208. [CrossRef]
103. Lansberg, J.P.; Shao, H.S. Production of $J/\psi + \eta_c$ versus $J/\psi + J/\psi$ at the LHC: Importance of Real α_s^5 Corrections. *Phys. Rev. Lett.* **2013**, *111*, 122001. [CrossRef]
104. Lansberg, J.P.; Shao, H.S.; Zhang, H.F. η_c' Hadroproduction at Next-to-Leading Order and its Relevance to ψ' Production. *Phys. Lett. B* **2018**, *786*, 342–346. [CrossRef]
105. Lansberg, J.P.; Shao, H.S. Associated production of a quarkonium and a Z boson at one loop in a quark-hadron-duality approach. *J. High Energy Phys.* **2016**, *10*, 153. [CrossRef]
106. Lansberg, J.P.; Shao, H.S.; Yamanaka, N.; Zhang, Y.J.; Noûs, C. Complete NLO QCD study of single- and double-quarkonium hadroproduction in the colour-evaporation model at the Tevatron and the LHC. *Phys. Lett. B* **2020**, *807*, 135559. [CrossRef]
107. Chao, K.T.; Ma, Y.Q.; Shao, H.S.; Wang, K.; Zhang, Y.J. J/ψ Polarization at Hadron Colliders in Nonrelativistic QCD. *Phys. Rev. Lett.* **2012**, *108*, 242004. [CrossRef]
108. Shao, H.S.; Ma, Y.Q.; Wang, K.; Chao, K.T. Polarizations of χ_{c1} and χ_{c2} in prompt production at the LHC. *Phys. Rev. Lett.* **2014**, *112*, 182003. [CrossRef]
109. Shao, H.S.; Han, H.; Ma, Y.Q.; Meng, C.; Zhang, Y.J.; Chao, K.T. Yields and polarizations of prompt J/ψ and $\psi(2S)$ production in hadronic collisions. *J. High Energy Phys.* **2015**, *5*, 103. [CrossRef]
110. Kom, C.H.; Kulesza, A.; Stirling, W.J. Pair Production of J/psi as a Probe of Double Parton Scattering at LHCb. *Phys. Rev. Lett.* **2011**, *107*, 082002. [CrossRef]
111. Lansberg, J.P.; Shao, H.S. J/ψ-pair production at large momenta: Indications for double parton scatterings and large α_s^5 contributions. *Phys. Lett. B* **2015**, *751*, 479–486. [CrossRef]
112. Lansberg, J.P.; Shao, H.S. Towards an automated tool to evaluate the impact of the nuclear modification of the gluon density on quarkonium, D and B meson production in proton–nucleus collisions. *Eur. Phys. J. C* **2017**, *77*, 1. [CrossRef]
113. Kusina, A.; Lansberg, J.P.; Schienbein, I.; Shao, H.S. Gluon Shadowing in Heavy-Flavor Production at the LHC. *Phys. Rev. Lett.* **2018**, *121*, 052004. [CrossRef]
114. Kusina, A.; Lansberg, J.P.; Schienbein, I.; Shao, H.S. Reweighted nuclear PDFs using heavy-flavor production data at the LHC. *Phys. Rev. D* **2021**, *104*, 014010. [CrossRef]
115. Artoisenet, P.; Maltoni, F.; Stelzer, T. Automatic generation of quarkonium amplitudes in NRQCD. *J. High Energy Phys.* **2008**, *2*, 102. [CrossRef]
116. Shao, H.S. HELAC-Onia: An automatic matrix element generator for heavy quarkonium physics. *Comput. Phys. Commun.* **2013**, *184*, 2562–2570. [CrossRef]
117. Shao, H.S. HELAC-Onia 2.0: An upgraded matrix-element and event generator for heavy quarkonium physics. *Comput. Phys. Commun.* **2016**, *198*, 238–259. [CrossRef]
118. Shao, H.S. Boosting perturbative QCD stability in quarkonium production. *J. High Energy Phys.* **2019**, *1*, 112. [CrossRef]
119. Flore, C.; Lansberg, J.P.; Shao, H.S.; Yedelkina, Y. Large-P_T inclusive photoproduction of J/ψ in electron-proton collisions at HERA and the EIC. *Phys. Lett. B* **2020**, *811*, 135926. [CrossRef]
120. Lansberg, J.P.; Ozcelik, M.A. Curing the unphysical behaviour of NLO quarkonium production at the LHC and its relevance to constrain the gluon PDF at low scales. *Eur. Phys. J. C* **2021**, *81*, 497. [CrossRef]
121. Colpani Serri, A.; Feng, Y.; Flore, C.; Lansberg, J.P.; Ozcelik, M.A.; Shao, H.S.; Yedelkina, Y. Revisiting NLO QCD corrections to total inclusive J/ψ and Υ photoproduction cross sections in lepton-proton collisions. *Phys. Lett. B* **2022**, *835*, 137556. [CrossRef]
122. Lansberg, J.P.; Nefedov, M.; Ozcelik, M.A. Matching next-to-leading-order and high-energy-resummed calculations of heavy-quarkonium-hadroproduction cross sections. *J. High Energy Phys.* **2022**, *5*, 083. [CrossRef]
123. Lansberg, J.P.; Nefedov, M.; Ozcelik, M.A. Curing the high-energy perturbative instability of vector-quarkonium-photoproduction cross sections at order $\alpha\alpha_s^3$ with high-energy factorisation. *arXiv* **2023**, arXiv:2306.02425.
124. Kotko, P.; Motyka, L.; Stasto, A. Color Reconnection Effects in J/ψ Hadroproduction. *arXiv* **2023**, arXiv:2303.13128.
125. Gay Ducati, M.B.; Griep, M.T.; Machado, M.V.T. Exclusive photoproduction of J/psi and psi(2S) states in proton-proton collisions at the CERN LHC. *Phys. Rev. D* **2013**, *88*, 017504. [CrossRef]
126. Kniehl, B.A.; Nefedov, M.A.; Saleev, V.A. $\psi(2S)$ and $\Upsilon(3S)$ hadroproduction in the parton Reggeization approach: Yield, polarization, and the role of fragmentation. *Phys. Rev. D* **2016**, *94*, 054007. [CrossRef]
127. Gay Ducati, M.B.; Kopp, F.; Machado, M.V.T.; Martins, S. Photoproduction of Upsilon states in ultraperipheral collisions at the CERN Large Hadron Collider within the color dipole approach. *Phys. Rev. D* **2016**, *94*, 094023. [CrossRef]
128. Gonçalves, V.P.; Machado, M.V.T.; Moreira, B.D.; Navarra, F.S.; dos Santos, G.S. Color dipole predictions for the exclusive vector meson photoproduction in pp, pPb, and PbPb collisions at run 2 LHC energies. *Phys. Rev. D* **2017**, *96*, 094027. [CrossRef]

129. Cisek, A.; Schäfer, W.; Szczurek, A. Production of χ_c pairs with large rapidity separation in k_T factorization. *Phys. Rev. D* **2018**, *97*, 114018. [CrossRef]
130. Cepila, J.; Contreras, J.G.; Krelina, M. Coherent and incoherent J/ψ photonuclear production in an energy-dependent hot-spot model. *Phys. Rev. C* **2018**, *97*, 024901. [CrossRef]
131. Maciuła, R.; Szczurek, A.; Cisek, A. J/ψ-meson production within improved color evaporation model with the k_T-factorization approach for $c\bar{c}$ production. *Phys. Rev. D* **2019**, *99*, 054014. [CrossRef]
132. Gonçalves, V.P.; Navarra, F.S.; Spiering, D. Exclusive ρ and J/Ψ photoproduction in ultraperipheral pA collisions: Predictions of the gluon saturation models for the momentum transfer distributions. *Phys. Lett. B* **2019**, *791*, 299–304. [CrossRef]
133. Babiarz, I.; Goncalves, V.P.; Pasechnik, R.; Schäfer, W.; Szczurek, A. $\gamma^*\gamma^* \to \eta_c(1S, 2S)$ transition form factors for spacelike photons. *Phys. Rev. D* **2019**, *100*, 054018. [CrossRef]
134. Babiarz, I.; Pasechnik, R.; Schäfer, W.; Szczurek, A. Prompt hadroproduction of $\eta_c(1S, 2S)$ in the k_T-factorization approach. *J. High Energy Phys.* **2020**, *2*, 037. [CrossRef]
135. Gonçalves, V.P.; Palota da Silva, R. Exclusive and diffractive quarkonium—Pair production at the LHC and FCC. *Phys. Rev. D* **2020**, *101*, 034025. [CrossRef]
136. Babiarz, I.; Pasechnik, R.; Schäfer, W.; Szczurek, A. Hadroproduction of scalar *P*-wave quarkonia in the light-front k_T -factorization approach. *J. High Energy Phys.* **2020**, *6*, 101. [CrossRef]
137. Babiarz, I.; Pasechnik, R.; Schäfer, W.; Szczurek, A. Central exclusive production of scalar and pseudoscalar charmonia in the light-front k_T-factorization approach. *Phys. Rev. D* **2020**, *102*, 114028. [CrossRef]
138. Kopp, F.; Gay Ducati, M.B.; Machado, M.V.T. Central exclusive $\chi_{c,b}$ production at high energy colliders and gluon saturation approach. *Phys. Lett. B* **2020**, *806*, 135492. [CrossRef]
139. Guzey, V.; Kryshen, E.; Strikman, M.; Zhalov, M. Nuclear suppression from coherent J/ψ photoproduction at the Large Hadron Collider. *Phys. Lett. B* **2021**, *816*, 136202. [CrossRef]
140. Xie, Y.P.; Goncalves, V.P. Near threshold heavy vector meson photoproduction at LHC and EicC. *Eur. Phys. J. C* **2021**, *81*, 645. [CrossRef]
141. Jenkovszky, L.; Libov, V.; Machado, M.V.T. The reggeometric pomeron and exclusive production of J/ψ(2S) in ultraperipheral collisions at the LHC. *Phys. Lett. B* **2022**, *824*, 136836. [CrossRef]
142. Cisek, A.; Schäfer, W.; Szczurek, A. Exclusive production of ρ meson in gamma-proton collisions: dσ/dt and the role of helicity flip processes. *Phys. Lett. B* **2023**, *836*, 137595. [CrossRef]
143. Ferretti, J.; Santopinto, E.; Naeem Anwar, M.; Bedolla, M.A. The baryo-quarkonium picture for hidden-charm and bottom pentaquarks and LHCb $P_c(4380)$ and $P_c(4450)$ states. *Phys. Lett. B* **2019**, *789*, 562–567. [CrossRef]
144. Ferretti, J.; Santopinto, E. Hidden-charm and bottom tetra- and pentaquarks with strangeness in the hadro-quarkonium and compact tetraquark models. *J. High Energy Phys.* **2020**, *4*, 119. [CrossRef]
145. Dubynskiy, S.; Voloshin, M.B. Hadro-Charmonium. *Phys. Lett. B* **2008**, *666*, 344–346. [CrossRef]
146. Guo, F.K.; Hanhart, C.; Meissner, U.G. Implications of heavy quark spin symmetry on heavy meson hadronic molecules. *Phys. Rev. Lett.* **2009**, *102*, 242004. [CrossRef] [PubMed]
147. Nejad, S.M.M.; Amiri, N. Ground state heavy tetraquark production in heavy quark fragmentation. *Phys. Rev. D* **2022**, *105*, 034001. [CrossRef]
148. Feng, F.; Huang, Y.; Jia, Y.; Sang, W.L.; Xiong, X.; Zhang, J.Y. Fragmentation production of fully-charmed tetraquarks at the LHC. *Phys. Rev. D* **2022**, *106*, 114029. [CrossRef]
149. Feng, F.; Huang, Y.; Jia, Y.; Sang, W.L.; Zhang, J.Y. Exclusive radiative production of fully-charmed tetraquarks at *B* Factory. *Phys. Lett. B* **2021**, *818*, 136368. [CrossRef]
150. Feng, F.; Huang, Y.; Jia, Y.; Sang, W.L.; Yang, D.S.; Zhang, J.Y. Inclusive production of fully-charmed tetraquarks at LHC. *arXiv* **2023**, arXiv:2304.11142.
151. Anikin, I.; Ivanov, D.Y.; Pire, B.; Szymanowski, L.; Wallon, S. QCD factorization of exclusive processes beyond leading twist: $\gamma_T^* \to \rho_T$ impact factor with twist three accuracy. *Nucl. Phys. B* **2010**, *828*, 1–68. [CrossRef]
152. Anikin, I.; Besse, A.; Ivanov, D.Y.; Pire, B.; Szymanowski, L.; Wallon, S. A phenomenological study of helicity amplitudes of high energy exclusive leptoproduction of the rho meson. *Phys. Rev. D* **2011**, *84*, 054004. [CrossRef]
153. Besse, A.; Szymanowski, L.; Wallon, S. Saturation effects in exclusive rhoT, rhoL meson electroproduction. *J. High Energy Phys.* **2013**, *11*, 062. [CrossRef]
154. Bolognino, A.D.; Celiberto, F.G.; Ivanov, D.Y.; Papa, A. Unintegrated gluon distribution from forward polarized ρ-electroproduction. *Eur. Phys. J.* **2018**, *C78*, 1023. [CrossRef]
155. Celiberto, F.G. Unraveling the Unintegrated Gluon Distribution in the Proton via ρ-Meson Leptoproduction. *Nuovo Cim.* **2019**, *C42*, 220. [CrossRef]
156. Bolognino, A.D.; Celiberto, F.G.; Ivanov, D.Y.; Papa, A.; Schäfer, W.; Szczurek, A. Exclusive production of ρ-mesons in high-energy factorization at HERA and EIC. *Eur. Phys. J. C* **2021**, *81*, 846. [CrossRef]
157. Motyka, L.; Sadzikowski, M.; Stebel, T. Twist expansion of Drell-Yan structure functions in color dipole approach. *J. High Energy Phys.* **2015**, *5*, 087. [CrossRef]
158. Brzeminski, D.; Motyka, L.; Sadzikowski, M.; Stebel, T. Twist decomposition of Drell-Yan structure functions: phenomenological implications. *J. High Energy Phys.* **2017**, *1*, 005. [CrossRef]

159. Celiberto, F.G.; Gordo Gómez, D.; Sabio Vera, A. Forward Drell-Yan production at the LHC in the BFKL formalism with collinear corrections. *Phys. Lett.* **2018**, *B786*, 201–206. [CrossRef]
160. Suzuki, K.; Hayashigaki, A.; Itakura, K.; Alam, J.; Hatsuda, T. Validity of the color dipole approximation for diffractive production of heavy quarkonium. *Phys. Rev. D* **2000**, *62*, 031501. [CrossRef]
161. Cepila, J.; Nemchik, J.; Krelina, M.; Pasechnik, R. Theoretical uncertainties in exclusive electroproduction of S-wave heavy quarkonia. *Eur. Phys. J. C* **2019**, *79*, 495. [CrossRef]
162. Hentschinski, M.; Padrón Molina, E. Exclusive J/Ψ and $\Psi(2s)$ photo-production as a probe of QCD low x evolution equations. *Phys. Rev. D* **2021**, *103*, 074008. [CrossRef]
163. Mulders, P.J.; Rodrigues, J. Transverse momentum dependence in gluon distribution and fragmentation functions. *Phys. Rev.* **2001**, *D63*, 094021. [CrossRef]
164. Meissner, S.; Metz, A.; Goeke, K. Relations between generalized and transverse momentum dependent parton distributions. *Phys. Rev.* **2007**, *D76*, 034002. [CrossRef]
165. Lorce', C.; Pasquini, B. Structure analysis of the generalized correlator of quark and gluon for a spin-1/2 target. *J. High Energy Phys.* **2013**, *9*, 138. [CrossRef]
166. Boer, D.; Cotogno, S.; van Daal, T.; Mulders, P.J.; Signori, A.; Zhou, Y.J. Gluon and Wilson loop TMDs for hadrons of spin ≤ 1. *J. High Energy Phys.* **2016**, *10*, 013. [CrossRef]
167. D'Alesio, U.; Murgia, F.; Pisano, C.; Taels, P. Azimuthal asymmetries in semi-inclusive J/ψ + jet production at an EIC. *Phys. Rev.* **2019**, *D100*, 094016. [CrossRef]
168. Boer, D.; D'Alesio, U.; Murgia, F.; Pisano, C.; Taels, P. J/ψ meson production in SIDIS: matching high and low transverse momentum. *J. High Energy Phys.* **2020**, *9*, 040. [CrossRef]
169. Bacchetta, A.; Boer, D.; Pisano, C.; Taels, P. Gluon TMDs and NRQCD matrix elements in J/ψ production at an EIC. *Eur. Phys. J. C* **2020**, *80*, 72. [CrossRef]
170. Boer, D.; Pisano, C.; Taels, P. Extracting color octet NRQCD matrix elements from J/ψ production at the EIC. *Phys. Rev. D* **2021**, *103*, 074012. [CrossRef]
171. D'Alesio, U.; Maxia, L.; Murgia, F.; Pisano, C.; Rajesh, S. J/ψ polarization in semi-inclusive DIS at low and high transverse momentum. *J. High Energy Phys.* **2022**, *3*, 037. [CrossRef]
172. D'Alesio, U.; Maxia, L.; Murgia, F.; Pisano, C.; Rajesh, S. J/ψ polarization in large-P_T semi-inclusive deep-inelastic scattering at the EIC. *arXiv* **2023**, arXiv:2301.11987.
173. Boer, D.; Bor, J.; Maxia, L.; Pisano, C.; Yuan, F. Transverse momentum dependent shape function for J/ψ production in SIDIS. *arXiv* **2023**, arXiv:2304.09473.
174. den Dunnen, W.J.; Lansberg, J.P.; Pisano, C.; Schlegel, M. Accessing the Transverse Dynamics and Polarization of Gluons inside the Proton at the LHC. *Phys. Rev. Lett.* **2014**, *112*, 212001. [CrossRef]
175. Boer, D. Gluon TMDs in quarkonium production. *Few Body Syst.* **2017**, *58*, 32. [CrossRef]
176. Lansberg, J.P.; Pisano, C.; Scarpa, F.; Schlegel, M. Pinning down the linearly-polarised gluons inside unpolarised protons using quarkonium-pair production at the LHC. *Phys. Lett. B* **2018**, *784*, 217–222; Erratum in *Phys. Lett. B* **2019**, *791*, 420–421. [CrossRef]
177. Scarpa, F.; Boer, D.; Echevarria, M.G.; Lansberg, J.P.; Pisano, C.; Schlegel, M. Studies of gluon TMDs and their evolution using quarkonium-pair production at the LHC. *Eur. Phys. J. C* **2020**, *80*, 87. [CrossRef]
178. D'Alesio, U.; Maxia, L.; Murgia, F.; Pisano, C.; Rajesh, S. Process dependence of the gluon Sivers function in $p^{\uparrow}p \to J/\psi + X$ within a TMD scheme in NRQCD. *Phys. Rev. D* **2020**, *102*, 094011. [CrossRef]
179. Echevarria, M.G. Proper TMD factorization for quarkonia production: $pp \to \eta_{c,b}$ as a study case. *J. High Energy Phys.* **2019**, *10*, 144. [CrossRef]
180. Fleming, S.; Makris, Y.; Mehen, T. An effective field theory approach to quarkonium at small transverse momentum. *J. High Energy Phys.* **2020**, *4*, 122. [CrossRef]
181. del Castillo, R.F.; Echevarria, M.G.; Makris, Y.; Scimemi, I. TMD factorization for dijet and heavy-meson pair in DIS. *J. High Energy Phys.* **2021**, *1*, 088. [CrossRef]
182. Procura, M.; Stewart, I.W. Quark Fragmentation within an Identified Jet. *Phys. Rev. D* **2010**, *81*, 074009; Erratum in *Phys. Rev. D* **2011**, *83*, 039902. [CrossRef]
183. Baumgart, M.; Leibovich, A.K.; Mehen, T.; Rothstein, I.Z. Probing Quarkonium Production Mechanisms with Jet Substructure. *J. High Energy Phys.* **2014**, *11*, 003. [CrossRef]
184. Bain, R.; Dai, L.; Hornig, A.; Leibovich, A.K.; Makris, Y.; Mehen, T. Analytic and Monte Carlo Studies of Jets with Heavy Mesons and Quarkonia. *J. High Energy Phys.* **2016**, *6*, 121. [CrossRef]
185. Bain, R.; Makris, Y.; Mehen, T. Transverse Momentum Dependent Fragmenting Jet Functions with Applications to Quarkonium Production. *J. High Energy Phys.* **2016**, *11*, 144. [CrossRef]
186. Bain, R.; Dai, L.; Leibovich, A.; Makris, Y.; Mehen, T. NRQCD Confronts LHCb Data on Quarkonium Production within Jets. *Phys. Rev. Lett.* **2017**, *119*, 032002. [CrossRef] [PubMed]
187. Echevarria, M.G.; Makris, Y.; Scimemi, I. Quarkonium TMD fragmentation functions in NRQCD. *J. High Energy Phys.* **2020**, *10*, 164. [CrossRef]

188. Mele, B.; Nason, P. The Fragmentation function for heavy quarks in QCD. *Nucl. Phys. B* **1991**, *361*, 626–644; Erratum in *Nucl. Phys. B* **2017**, *921*, 841–842. [CrossRef]
189. Cacciari, M.; Greco, M. Large p_T hadroproduction of heavy quarks. *Nucl. Phys. B* **1994**, *421*, 530–544. [CrossRef]
190. Celiberto, F.G.; Fucilla, M. Diffractive semi-hard production of a J/ψ or a Υ from single-parton fragmentation plus a jet in hybrid factorization. *Eur. Phys. J. C* **2022**, *82*, 929. [CrossRef]
191. Colferai, D.; Schwennsen, F.; Szymanowski, L.; Wallon, S. Mueller Navelet jets at LHC - complete NLL BFKL calculation. *J. High Energy Phys.* **2010**, *12*, 026. [CrossRef]
192. Celiberto, F.G. Hunting BFKL in semi-hard reactions at the LHC. *Eur. Phys. J. C* **2021**, *81*, 691. [CrossRef]
193. Bolognino, A.D.; Celiberto, F.G.; Fucilla, M.; Ivanov, D.Y.; Papa, A. Inclusive production of a heavy-light dijet system in hybrid high-energy and collinear factorization. *Phys. Rev. D* **2021**, *103*, 094004. [CrossRef]
194. Celiberto, F.G.; Fucilla, M.; Ivanov, D.Y.; Papa, A. High-energy resummation in Λ_c baryon production. *Eur. Phys. J. C* **2021**, *81*, 780. [CrossRef]
195. Celiberto, F.G. High-energy emissions of light mesons plus heavy flavor at the LHC and the Forward Physics Facility. *Phys. Rev. D* **2022**, *105*, 114008. [CrossRef]
196. Deak, M.; Hautmann, F.; Jung, H.; Kutak, K. Forward Jet Production at the Large Hadron Collider. *J. High Energy Phys.* **2009**, *9*, 121. [CrossRef]
197. van Hameren, A.; Kotko, P.; Kutak, K. Resummation effects in the forward production of Z_0+jet at the LHC. *Phys. Rev. D* **2015**, *92*, 054007. [CrossRef]
198. Deak, M.; van Hameren, A.; Jung, H.; Kusina, A.; Kutak, K.; Serino, M. Calculation of the Z+jet cross section including transverse momenta of initial partons. *Phys. Rev. D* **2019**, *99*, 094011. [CrossRef]
199. Van Haevermaet, H.; Van Hameren, A.; Kotko, P.; Kutak, K.; Van Mechelen, P. Trijets in k_T-factorisation: Matrix elements vs parton shower. *Eur. Phys. J. C* **2020**, *80*, 610. [CrossRef]
200. van Hameren, A.; Motyka, L.; Ziarko, G. Hybrid k_T-factorization and impact factors at NLO. *J. High Energy Phys.* **2022**, *11*, 103. [CrossRef]
201. Bonvini, M.; Marzani, S. Double resummation for Higgs production. *Phys. Rev. Lett.* **2018**, *120*, 202003. [CrossRef] [PubMed]
202. Silvetti, F.; Bonvini, M. Differential heavy quark pair production at small x. *Eur. Phys. J. C* **2023**, *83*, 267. [CrossRef]
203. Bonvini, M.; Marzani, S.; Peraro, T. Small-x resummation from HELL. *Eur. Phys. J. C* **2016**, *76*, 597. [CrossRef]
204. Bonvini, M.; Marzani, S.; Muselli, C. Towards parton distribution functions with small-x resummation: HELL 2.0. *J. High Energy Phys.* **2017**, *12*, 117. [CrossRef]
205. Bonvini, M. Small-x phenomenology at the LHC and beyond: HELL 3.0 and the case of the Higgs cross section. *Eur. Phys. J. C* **2018**, *78*, 834. [CrossRef]
206. Ball, R.D.; Forte, S. Summation of leading logarithms at small x. *Phys. Lett. B* **1995**, *351*, 313–324. [CrossRef]
207. Ball, R.D.; Forte, S. Asymptotically free partons at high-energy. *Phys. Lett. B* **1997**, *405*, 317–326. [CrossRef]
208. Altarelli, G.; Ball, R.D.; Forte, S. Factorization and resummation of small x scaling violations with running coupling. *Nucl. Phys. B* **2002**, *621*, 359–387. [CrossRef]
209. Altarelli, G.; Ball, R.D.; Forte, S. An Anomalous dimension for small x evolution. *Nucl. Phys. B* **2003**, *674*, 459–483. [CrossRef]
210. Altarelli, G.; Ball, R.D.; Forte, S. Perturbatively stable resummed small x evolution kernels. *Nucl. Phys. B* **2006**, *742*, 1–40. [CrossRef]
211. Altarelli, G.; Ball, R.D.; Forte, S. Small x Resummation with Quarks: Deep-Inelastic Scattering. *Nucl. Phys. B* **2008**, *799*, 199–240. [CrossRef]
212. White, C.; Thorne, R. A Global Fit to Scattering Data with NLL BFKL Resummations. *Phys. Rev. D* **2007**, *75*, 034005. [CrossRef]
213. Catani, S.; Ciafaloni, M.; Hautmann, F. Gluon Contributions to Small x Heavy Flavor Production. *Phys. Lett. B* **1990**, *242*, 97–102. [CrossRef]
214. Catani, S.; Ciafaloni, M.; Hautmann, F. High-energy factorization and small x heavy flavor production. *Nucl. Phys. B* **1991**, *366*, 135–188. [CrossRef]
215. Collins, J.C.; Ellis, R. Heavy quark production in very high-energy hadron collisions. *Nucl. Phys. B* **1991**, *360*, 3–30. [CrossRef]
216. Catani, S.; Ciafaloni, M.; Hautmann, F. High-energy factorization in QCD and minimal subtraction scheme. *Phys. Lett. B* **1993**, *307*, 147–153. [CrossRef]
217. Catani, S.; Hautmann, F. Quark anomalous dimensions at small x. *Phys. Lett. B* **1993**, *315*, 157–163. [CrossRef]
218. Catani, S.; Hautmann, F. High-energy factorization and small x deep inelastic scattering beyond leading order. *Nucl. Phys. B* **1994**, *427*, 475–524. [CrossRef]
219. Ball, R.D. Resummation of Hadroproduction Cross-sections at High Energy. *Nucl. Phys. B* **2008**, *796*, 137–183. [CrossRef]
220. Caola, F.; Forte, S.; Marzani, S. Small x resummation of rapidity distributions: The Case of Higgs production. *Nucl. Phys. B* **2011**, *846*, 167–211. [CrossRef]
221. Boussarie, R.; Ducloué, B.; Szymanowski, L.; Wallon, S. Forward J/ψ and very backward jet inclusive production at the LHC. *Phys. Rev. D* **2018**, *97*, 014008. [CrossRef]

222. Hagler, P.; Kirschner, R.; Schafer, A.; Szymanowski, L.; Teryaev, O.V. Towards a solution of the charmonium production controversy: k^- perpendicular factorization versus color octet mechanism. *Phys. Rev. Lett.* **2001**, *86*, 1446–1449. [CrossRef]
223. Kniehl, B.A.; Vasin, D.V.; Saleev, V.A. Charmonium production at high energy in the k_T -factorization approach. *Phys. Rev. D* **2006**, *73*, 074022. [CrossRef]
224. Gribov, L.V.; Levin, E.M.; Ryskin, M.G. Semihard Processes in QCD. *Phys. Rept.* **1983**, *100*, 1–150. [CrossRef]
225. Celiberto, F.G. High-Energy Resummation in Semi-Hard Processes at the LHC. Ph.D. Thesis, Università della Calabria and INFN-Cosenza, Rende, Italy.
226. Bolognino, A.D. From Semi-Hard Processes to the Unintegrated Gluon Distribution: A Phenomenological Path in the High-Energy Framework. Ph.D. Thesis, Università della Calabria and INFN-Cosenza, Rende, Italy, 2021.
227. Celiberto, F.G.; Fucilla, M.; Papa, A. The high-energy limit of perturbative QCD: Theory and phenomenology. *EPJ Web Conf.* **2022**, *270*, 00001. [CrossRef]
228. Fadin, V.S.; Kuraev, E.; Lipatov, L. On the Pomeranchuk Singularity in Asymptotically Free Theories. *Phys. Lett. B* **1975**, *60*, 50–52. [CrossRef]
229. Kuraev, E.A.; Lipatov, L.N.; Fadin, V.S. Multi - Reggeon Processes in the Yang-Mills Theory. *Sov. Phys. JETP* **1976**, *44*, 443–450.
230. Kuraev, E.; Lipatov, L.; Fadin, V.S. The Pomeranchuk Singularity in Nonabelian Gauge Theories. *Sov. Phys. JETP* **1977**, *45*, 199–204.
231. Balitsky, I.; Lipatov, L. The Pomeranchuk Singularity in Quantum Chromodynamics. *Sov. J. Nucl. Phys.* **1978**, *28*, 822–829.
232. Fadin, V.S.; Lipatov, L.N. BFKL pomeron in the next-to-leading approximation. *Phys. Lett. B* **1998**, *429*, 127–134. [CrossRef]
233. Ciafaloni, M.; Camici, G. Energy scale(s) and next-to-leading BFKL equation. *Phys. Lett. B* **1998**, *430*, 349–354. [CrossRef]
234. Fadin, V.S.; Fiore, R.; Papa, A. The Quark part of the nonforward BFKL kernel and the 'bootstrap' for the gluon Reggeization. *Phys. Rev. D* **1999**, *60*, 074025. [CrossRef]
235. Fadin, V.S.; Gorbachev, D.A. Nonforward color octet BFKL kernel. *JETP Lett.* **2000**, *71*, 222–226. [CrossRef]
236. Fadin, V.S.; Gorbachev, D.A. Nonforward color-octet kernel of the Balitsky-Fadin-Kuraev-Lipatov equation. *Phys. Atom. Nucl.* **2000**, *63*, 2157–2172. [CrossRef]
237. Fadin, V.S.; Fiore, R. Non-forward BFKL pomeron at next-to-leading order. *Phys. Lett. B* **2005**, *610*, 61–66; Erratum in *Phys. Lett. B* **2005**, *621*, 320. [CrossRef]
238. Fadin, V.S.; Fiore, R. Non-forward NLO BFKL kernel. *Phys. Rev. D* **2005**, *72*, 014018. [CrossRef]
239. Caola, F.; Chakraborty, A.; Gambuti, G.; von Manteuffel, A.; Tancredi, L. Three-Loop Gluon Scattering in QCD and the Gluon Regge Trajectory. *Phys. Rev. Lett.* **2022**, *128*, 212001. [CrossRef]
240. Falcioni, G.; Gardi, E.; Maher, N.; Milloy, C.; Vernazza, L. Disentangling the Regge Cut and Regge Pole in Perturbative QCD. *Phys. Rev. Lett.* **2022**, *128*, 132001. [CrossRef]
241. Del Duca, V.; Marzucca, R.; Verbeek, B. The gluon Regge trajectory at three loops from planar Yang-Mills theory. *J. High Energy Phys.* **2022**, *1*, 149. [CrossRef]
242. Byrne, E.P.; Del Duca, V.; Dixon, L.J.; Gardi, E.; Smillie, J.M. One-loop central-emission vertex for two gluons in $\mathcal{N}$ = 4 super Yang-Mills theory. *J. High Energy Phys.* **2022**, *8*, 271. [CrossRef]
243. Fadin, V.S.; Fucilla, M.; Papa, A. One-loop Lipatov vertex in QCD with higher ϵ-accuracy. *J. High Energy Phys.* **2023**, *4*, 137. [CrossRef]
244. Fadin, V.S.; Fiore, R.; Kotsky, M.I.; Papa, A. The Gluon impact factors. *Phys. Rev. D* **2000**, *61*, 094005. [CrossRef]
245. Fadin, V.S.; Fiore, R.; Kotsky, M.I.; Papa, A. The Quark impact factors. *Phys. Rev. D* **2000**, *61*, 094006. [CrossRef]
246. Bartels, J.; Colferai, D.; Vacca, G.P. The NLO jet vertex for Mueller-Navelet and forward jets: The Quark part. *Eur. Phys. J. C* **2002**, *24*, 83–99. [CrossRef]
247. Bartels, J.; Colferai, D.; Vacca, G.P. The NLO jet vertex for Mueller-Navelet and forward jets: The Gluon part. *Eur. Phys. J. C* **2003**, *29*, 235–249. [CrossRef]
248. Caporale, F.; Ivanov, D.Y.; Murdaca, B.; Papa, A.; Perri, A. The next-to-leading order jet vertex for Mueller-Navelet and forward jets revisited. *J. High Energy Phys.* **2012**, *2*, 101. [CrossRef]
249. Caporale, F.; Ivanov, D.Y.; Murdaca, B.; Papa, A. Mueller-Navelet small-cone jets at LHC in next-to-leading BFKL. *Nucl. Phys. B* **2013**, *877*, 73–94. [CrossRef]
250. Ivanov, D.Y.; Papa, A. The next-to-leading order forward jet vertex in the small-cone approximation. *J. High Energy Phys.* **2012**, *5*, 086. [CrossRef]
251. Colferai, D.; Niccoli, A. The NLO jet vertex in the small-cone approximation for kt and cone algorithms. *J. High Energy Phys.* **2015**, *4*, 071. [CrossRef]
252. Ivanov, D.Y.; Papa, A. Inclusive production of a pair of hadrons separated by a large interval of rapidity in proton collisions. *J. High Energy Phys.* **2012**, *7*, 045. [CrossRef]
253. Ivanov, D.Y.; Kotsky, M.I.; Papa, A. The Impact factor for the virtual photon to light vector meson transition. *Eur. Phys. J. C* **2004**, *38*, 195–213. [CrossRef]
254. Bartels, J.; Gieseke, S.; Qiao, C.F. The (gamma* —> q anti-q) Reggeon vertex in next-to-leading order QCD. *Phys. Rev. D* **2001**, *63*, 056014; Erratum in *Phys. Rev. D* **2002**, *65*, 079902. [CrossRef]
255. Bartels, J.; Gieseke, S.; Kyrieleis, A. The Process gamma*(L) + q —> (q anti-q g) + q: Real corrections to the virtual photon impact factor. *Phys. Rev. D* **2002**, *65*, 014006. [CrossRef]

256. Bartels, J.; Colferai, D.; Gieseke, S.; Kyrieleis, A. NLO corrections to the photon impact factor: Combining real and virtual corrections. *Phys. Rev. D* **2002**, *66*, 094017. [CrossRef]
257. Bartels, J.; Kyrieleis, A. NLO corrections to the gamma* impact factor: First numerical results for the real corrections to gamma*(L). *Phys. Rev. D* **2004**, *70*, 114003. [CrossRef]
258. Fadin, V.S.; Ivanov, D.Y.; Kotsky, M.I. Photon Reggeon interaction vertices in the NLA. *Phys. Atom. Nucl.* **2002**, *65*, 1513–1527. [CrossRef]
259. Balitsky, I.; Chirilli, G.A. Photon impact factor and k_T-factorization for DIS in the next-to-leading order. *Phys. Rev. D* **2013**, *87*, 014013. [CrossRef]
260. Hentschinski, M.; Kutak, K.; van Hameren, A. Forward Higgs production within high energy factorization in the heavy quark limit at next-to-leading order accuracy. *Eur. Phys. J. C* **2021**, *81*, 112; Erratum in *Eur. Phys. J. C* **2021**, *81*, 262. [CrossRef]
261. Nefedov, M.A. Computing one-loop corrections to effective vertices with two scales in the EFT for Multi-Regge processes in QCD. *Nucl. Phys. B* **2019**, *946*, 114715. [CrossRef]
262. Celiberto, F.G.; Fucilla, M.; Ivanov, D.Y.; Mohammed, M.M.A.; Papa, A. The next-to-leading order Higgs impact factor in the infinite top-mass limit. *J. High Energy Phys.* **2022**, *8*, 092. [CrossRef]
263. Hentschinski, M. Forward Higgs production at NLO using Lipatov's high energy effective action. *SciPost Phys. Proc.* **2022**, *8*, 136. [CrossRef]
264. Fucilla, M. The Higgs impact factor at next-to-leading order. *arXiv* **2022**, arXiv:2212.01794
265. Hentschinski, M.; Salas, C. Forward Drell-Yan plus backward jet as a test of BFKL evolution. In Proceedings of the 20th International Workshop on Deep-Inelastic Scattering and Related Subjects, Bonn, Germany, 26–30 March 2012. [CrossRef]
266. Celiberto, F.G.; Ivanov, D.Y.; Murdaca, B.; Papa, A. High-energy resummation in heavy-quark pair photoproduction. *Phys. Lett. B* **2018**, *777*, 141–150. [CrossRef]
267. Bolognino, A.D.; Celiberto, F.G.; Fucilla, M.; Ivanov, D.Y.; Murdaca, B.; Papa, A. Inclusive production of two rapidity-separated heavy quarks as a probe of BFKL dynamics . *Proceeds Sci.* **2019**, *DIS2019*, 067. [CrossRef]
268. Bolognino, A.D.; Celiberto, F.G.; Fucilla, M.; Ivanov, D.Y.; Papa, A. High-energy resummation in heavy-quark pair hadroproduction. *Eur. Phys. J. C* **2019**, *79*, 939. [CrossRef]
269. Boussarie, R.; Ducloué, B.; Szymanowski, L.; Wallon, S. Production of a forward J/psi and a backward jet at the LHC. In Proceedings of the International Conference on the Structure and Interactions of the Photon and 21st International Workshop on Photon-Photon Collisions and International Workshop on High Energy Photon Linear Colliders, Novosibirsk, Russia, 15–19 June 2015.
270. Boussarie, R.; Ducloue, B.; Szymanowski, L.; Wallon, S. Production of a forward J/ψ and a backward jet at the LHC. *Proceeds Sci.* **2016**, *DIS2016*, 204. [CrossRef]
271. Boussarie, R.; Ducloué, B.; Szymanowski, L.; Wallon, S. QCD resummation effects in forward J/ψ and very backward jet inclusive production at the LHC. *Proceeds Sci.* **2018**, *DIS2017*, 063. [CrossRef]
272. Pire, B.; Szymanowski, L.; Wallon, S. Double diffractive rho-production in gamma* gamma* collisions. *Eur. Phys. J. C* **2005**, *44*, 545–558. [CrossRef]
273. Segond, M.; Szymanowski, L.; Wallon, S. Diffractive production of two rho0(L) mesons in e+e- collisions. *Eur. Phys. J. C* **2007**, *52*, 93–112. [CrossRef]
274. Enberg, R.; Pire, B.; Szymanowski, L.; Wallon, S. BFKL resummation effects in gamma* gamma* —> rho rho. *Eur. Phys. J. C* **2006**, *45*, 759–769; Erratum in *Eur. Phys. J. C* **2007**, *51*, 1015. [CrossRef]
275. Ivanov, D.Y.; Papa, A. Electroproduction of two light vector mesons in the next-to-leading approximation. *Nucl. Phys. B* **2006**, *732*, 183–199. [CrossRef]
276. Ivanov, D.Y.; Papa, A. Electroproduction of two light vector mesons in next-to-leading BFKL: Study of systematic effects. *Eur. Phys. J. C* **2007**, *49*, 947–955. [CrossRef]
277. Mueller, A.H.; Navelet, H. An Inclusive Minijet Cross-Section and the Bare Pomeron in QCD. *Nucl. Phys. B* **1987**, *282*, 727–744. [CrossRef]
278. Ducloué, B.; Szymanowski, L.; Wallon, S. Confronting Mueller-Navelet jets in NLL BFKL with LHC experiments at 7 TeV. *J. High Energy Phys.* **2013**, *5*, 096. [CrossRef]
279. Ducloué, B.; Szymanowski, L.; Wallon, S. Evidence for high-energy resummation effects in Mueller-Navelet jets at the LHC. *Phys. Rev. Lett.* **2014**, *112*, 082003. [CrossRef]
280. Caporale, F.; Murdaca, B.; Sabio Vera, A.; Salas, C. Scale choice and collinear contributions to Mueller-Navelet jets at LHC energies. *Nucl. Phys. B* **2013**, *875*, 134–151. [CrossRef]
281. Caporale, F.; Ivanov, D.Y.; Murdaca, B.; Papa, A. Mueller–Navelet jets in next-to-leading order BFKL: Theory versus experiment. *Eur. Phys. J. C* **2014**, *74*, 3084; Erratum in *Eur. Phys. J. C* **2015**, *75*, 535. [CrossRef]
282. Caporale, F.; Ivanov, D.Y.; Murdaca, B.; Papa, A. Brodsky-Lepage-Mackenzie optimal renormalization scale setting for semihard processes. *Phys. Rev. D* **2015**, *91*, 114009. [CrossRef]
283. Ducloué, B.; Szymanowski, L.; Wallon, S. Evaluating the double parton scattering contribution to Mueller-Navelet jets production at the LHC. *Phys. Rev. D* **2015**, *92*, 076002. [CrossRef]
284. Celiberto, F.G.; Ivanov, D.Y.; Murdaca, B.; Papa, A. Mueller–Navelet Jets at LHC: BFKL Versus High-Energy DGLAP. *Eur. Phys. J. C* **2015**, *75*, 292. [CrossRef]

285. Celiberto, F.G.; Ivanov, D.Y.; Murdaca, B.; Papa, A. Mueller–Navelet Jets at the LHC: Discriminating BFKL from DGLAP by Asymmetric Cuts. *Acta Phys. Polon. Suppl.* **2015**, *8*, 935. [CrossRef]
286. Celiberto, F.G.; Ivanov, D.Y.; Murdaca, B.; Papa, A. Mueller–Navelet jets at 13 TeV LHC: Dependence on dynamic constraints in the central rapidity region. *Eur. Phys. J. C* **2016**, *76*, 224. [CrossRef]
287. Celiberto, F.G.; Ivanov, D.Y.; Murdaca, B.; Papa, A. BFKL effects and central rapidity dependence in Mueller-Navelet jet production at 13 TeV LHC. *Proceeds Sci.* **2016**, *DIS2016*, 176. [CrossRef]
288. Caporale, F.; Celiberto, F.G.; Chachamis, G.; Gordo Gómez, D.; Sabio Vera, A. Inclusive dijet hadroproduction with a rapidity veto constraint. *Nucl. Phys. B* **2018**, *935*, 412–434. [CrossRef]
289. de León, N.B.; Chachamis, G.; Sabio Vera, A. Average minijet rapidity ratios in Mueller–Navelet jets. *Eur. Phys. J. C* **2021**, *81*, 1019. [CrossRef]
290. Celiberto, F.G.; Papa, A. Mueller-Navelet jets at the LHC: Hunting data with azimuthal distributions. *Phys. Rev. D* **2022**, *106*, 114004. [CrossRef]
291. Celiberto, F.G.; Ivanov, D.Y.; Murdaca, B.; Papa, A. High energy resummation in dihadron production at the LHC. *Phys. Rev. D* **2016**, *94*, 034013. [CrossRef]
292. Celiberto, F.G.; Ivanov, D.Y.; Murdaca, B.; Papa, A. Dihadron Production at LHC: BFKL Predictions for Cross Sections and Azimuthal Correlations. *AIP Conf. Proc.* **2017**, *1819*, 060005. [CrossRef]
293. Celiberto, F.G.; Ivanov, D.Y.; Murdaca, B.; Papa, A. Dihadron production at the LHC: Full next-to-leading BFKL calculation. *Eur. Phys. J. C* **2017**, *77*, 382. [CrossRef]
294. Celiberto, F.G.; Ivanov, D.Y.; Murdaca, B.; Papa, A. Inclusive charged light di-hadron production at 7 and 13 TeV LHC in the full NLA BFKL approach. *arXiv* **2017**, arXiv:1709.01128.
295. Celiberto, F.G.; Ivanov, D.Y.; Murdaca, B.; Papa, A. Inclusive dihadron production at the LHC in NLA BFKL. In Proceedings of the 17th conference on Elastic and Diffractive Scattering, Prague, Czech Republic, 26–30 June 2017.
296. Caporale, F.; Chachamis, G.; Murdaca, B.; Sabio Vera, A. Balitsky-Fadin-Kuraev-Lipatov Predictions for Inclusive Three Jet Production at the LHC. *Phys. Rev. Lett.* **2016**, *116*, 012001. [CrossRef]
297. Caporale, F.; Celiberto, F.G.; Chachamis, G.; Sabio Vera, A. Multi-Regge kinematics and azimuthal angle observables for inclusive four-jet production. *Eur. Phys. J. C* **2016**, *76*, 165. [CrossRef]
298. Caporale, F.; Celiberto, F.G.; Chachamis, G.; Gordo Gómez, D.; Sabio Vera, A. BFKL azimuthal imprints in inclusive three-jet production at 7 and 13 TeV. *Nucl. Phys. B* **2016**, *910*, 374–386. [CrossRef]
299. Caporale, F.; Celiberto, F.G.; Chachamis, G.; Sabio Vera, A. Inclusive four-jet production: A study of Multi-Regge kinematics and BFKL observables. *Proceeds Sci.* **2016**, *DIS2016*, 177. [CrossRef]
300. Caporale, F.; Celiberto, F.G.; Chachamis, G.; Gordo Gómez, D.; Sabio Vera, A. Inclusive Four-jet Production at 7 and 13 TeV: Azimuthal Profile in Multi-Regge Kinematics. *Eur. Phys. J. C* **2017**, *77*, 5. [CrossRef]
301. Celiberto, F.G. BFKL phenomenology: resummation of high-energy logs in semi-hard processes at LHC. *Frascati Phys. Ser.* **2016**, *63*, 43–48.
302. Caporale, F.; Celiberto, F.G.; Chachamis, G.; Gordo Gómez, D.; Sabio Vera, A. Inclusive three- and four-jet production in multi-Regge kinematics at the LHC. *AIP Conf. Proc.* **2017**, *1819*, 060009. [CrossRef]
303. Caporale, F.; Celiberto, F.G.; Chachamis, G.; Gordo Gomez, D.; Murdaca, B.; Sabio Vera, A. High energy effects in multi-jet production at LHC. *arXiv* **2017**, arXiv:1610.04765.
304. Chachamis, G.; Caporale, F.; Celiberto, F.G.; Gomez, D.G.; Sabio Vera, A. Inclusive three jet production at the LHC at 7 and 13 TeV collision energies. *Proceeds Sci.* **2016**, *DIS2016*, 178. [CrossRef]
305. Caporale, F.; Celiberto, F.G.; Chachamis, G.; Gordo Gómez, D.; Sabio Vera, A. Probing the BFKL dynamics in inclusive three jet production at the LHC. *EPJ Web Conf.* **2017**, *164*, 07027. [CrossRef]
306. Caporale, F.; Celiberto, F.G.; Chachamis, G.; Gordo Gómez, D.; Sabio Vera, A. Stability of Azimuthal-angle Observables under Higher Order Corrections in Inclusive Three-jet Production. *Phys. Rev. D* **2017**, *95*, 074007. [CrossRef]
307. Caporale, F.; Celiberto, F.G.; Gordo Gomez, D.; Sabio Vera, A.; Chachamis, G. Multi-jet production in the high energy limit at LHC. *arXiv*, **2017**, arXiv:1801.00014.
308. Chachamis, G.; Caporale, F.; Celiberto, F.G.; Gordo Gomez, D.; Sabio Vera, A. Azimuthal-angle Observables in Inclusive Three-jet Production. *Proceeds Sci.* **2018**, *DIS2017*, 067. [CrossRef]
309. Bolognino, A.D.; Celiberto, F.G.; Ivanov, D.Y.; Mohammed, M.M.A.; Papa, A. Hadron-jet correlations in high-energy hadronic collisions at the LHC. *Eur. Phys. J. C* **2018**, *78*, 772. [CrossRef]
310. Bolognino, A.D.; Celiberto, F.G.; Ivanov, D.Y.; Mohammed, M.M.A.; Papa, A. High-energy effects in forward inclusive dijet and hadron-jet production. *Proceeds Sci.* **2019**, *DIS2019*, 049. [CrossRef]
311. Bolognino, A.D.; Celiberto, F.G.; Ivanov, D.Y.; Mohammed, M.M.A.; Papa, A. Inclusive hadron-jet production at the LHC. *Acta Phys. Polon. Suppl.* **2019**, *12*, 773. [CrossRef]
312. Celiberto, F.G.; Ivanov, D.Y.; Papa, A. Diffractive production of Λ hyperons in the high-energy limit of strong interactions. *Phys. Rev. D* **2020**, *102*, 094019. [CrossRef]
313. Celiberto, F.G. Emergence of high-energy dynamics from cascade-baryon detections at the LHC. *Eur. Phys. J. C* **2023**, *83*, 332. [CrossRef]

314. Celiberto, F.G.; Ivanov, D.Y.; Mohammed, M.M.A.; Papa, A. High-energy resummed distributions for the inclusive Higgs-plus-jet production at the LHC. *Eur. Phys. J. C* **2021**, *81*, 293. [CrossRef]
315. Celiberto, F.G.; Ivanov, D.Y.; Mohammed, M.M.A.; Papa, A. High-energy resummation in inclusive hadroproduction of Higgs plus jet. *SciPost Phys. Proc.* **2022**, *8*, 039. [CrossRef]
316. Celiberto, F.G.; Fucilla, M.; Papa, A.; Ivanov, D.Y.; Mohammed, M.M.A. Higgs-plus-jet inclusive production as stabilizer of the high-energy resummation. *Proceeds Sci.* **2022**, *EPS-HEP2021*, 589. [CrossRef]
317. Celiberto, F.G.; Fucilla, M.; Ivanov, D.Y.; Mohammed, M.M.A.; Papa, A. Higgs boson production in the high-energy limit of pQCD. *Proceeds Sci.* **2022**, *PANIC2021*, 352. [CrossRef]
318. Celiberto, F.G.; Fucilla, M.; Ivanov, D.Y.; Mohammed, M.M.A.; Papa, A. BFKL phenomenology: Resummation of high-energy logs in inclusive processes. *SciPost Phys. Proc.* **2022**, *10*, 002. [CrossRef]
319. Bolognino, A.D.; Celiberto, F.G.; Fucilla, M.; Ivanov, D.Y.; Papa, A. Hybrid high-energy/collinear factorization in a heavy-light dijets system reaction. *SciPost Phys. Proc.* **2022**, *8*, 068. [CrossRef]
320. Golec-Biernat, K.; Motyka, L.; Stebel, T. Forward Drell-Yan and backward jet production as a probe of the BFKL dynamics. *J. High Energy Phys.* **2018**, *12*, 091. [CrossRef]
321. Celiberto, F.G.; Fucilla, M.; Ivanov, D.Y.; Mohammed, M.M.A.; Papa, A. Bottom-flavored inclusive emissions in the variable-flavor number scheme: A high-energy analysis. *Phys. Rev. D* **2021**, *104*, 114007. [CrossRef]
322. Bolognino, A.D.; Celiberto, F.G.; Fucilla, M.; Ivanov, D.Y.; Papa, A. Heavy flavored emissions in hybrid collinear/high energy factorization. *Proceeds Sci.* **2022**, *EPS-HEP2021*, 389. [CrossRef]
323. Celiberto, F.G. Stabilizing BFKL via Heavy-flavor and NRQCD Fragmentation. *Acta Phys. Polon. Suppl.* **2023**, *16*, 41. [CrossRef]
324. Bolognino, A.D.; Celiberto, F.G.; Fucilla, M.; Ivanov, D.Y.; Mohammed, M.M.A.; Papa, A. High-energy Signals from Heavy-flavor Physics. *Acta Phys. Polon. Suppl.* **2023**, *16*, 17. [CrossRef]
325. Celiberto, F.G. The high-energy spectrum of QCD from inclusive emissions of charmed B-mesons. *Phys. Lett. B* **2022**, *835*, 137554. [CrossRef]
326. Celiberto, F.G.; Fucilla, M.; Mohammed, M.M.A.; Papa, A. Ultraforward production of a charmed hadron plus a Higgs boson in unpolarized proton collisions. *Phys. Rev. D* **2022**, *105*, 114056. [CrossRef]
327. Celiberto, F.G.; Fucilla, M. Inclusive J/ψ and Υ emissions from single-parton fragmentation in hybrid high-energy and collinear factorization. *arXiv* **2022**, arXiv:2208.07206.
328. Bolognino, A.D.; Celiberto, F.G.; Ivanov, D.Y.; Papa, A. ρ-meson leptoproduction as testfield for the unintegrated gluon distribution in the proton. *Frascati Phys. Ser.* **2018**, *67*, 76–82.
329. Bolognino, A.D.; Celiberto, F.G.; Ivanov, D.Y.; Papa, A. Leptoproduction of ρ-mesons as discriminator for the unintegrated gluon distribution in the proton. *Acta Phys. Polon. Suppl.* **2019**, *12*, 891. [CrossRef]
330. Bolognino, A.D.; Szczurek, A.; Schaefer, W. Exclusive production of ϕ meson in the $\gamma^* p \to \phi p$ reaction at large photon virtualities within k_T-factorization approach. *Phys. Rev. D* **2020**, *101*, 054041. [CrossRef]
331. Łuszczak, A.; Łuszczak, M.; Schäfer, W. Unintegrated gluon distributions from the color dipole cross section in the BGK saturation model. *Phys. Lett. B* **2022**, *835*, 137582. [CrossRef]
332. Bolognino, A.D.; Celiberto, F.G.; Ivanov, D.Y.; Papa, A. Exclusive emissions of rho-mesons and the unintegrated gluon distribution. *SciPost Phys. Proc.* **2022**, *8*, 089. [CrossRef]
333. Bolognino, A.D.; Celiberto, F.G.; Fucilla, M.; Ivanov, D.Y.; Papa, A.; Schäfer, W.; Szczurek, A. Hadron structure at small-x via unintegrated gluon densities. *arXiv* **2022**, arXiv:2202.02513
334. Celiberto, F.G. Phenomenology of the hadronic structure at small-x. *arXiv* **2022**, arXiv:2202.04207.
335. Bolognino, A.D.; Celiberto, F.G.; Ivanov, D.Y.; Papa, A.; Schäfer, W.; Szczurek, A. Exclusive emissions of polarized ρ mesons at the EIC and the proton content at low x. *arXiv* **2022**, arXiv:2207.05726.
336. Bautista, I.; Fernandez Tellez, A.; Hentschinski, M. BFKL evolution and the growth with energy of exclusive J/ψ and Υ photoproduction cross sections. *Phys. Rev. D* **2016**, *94*, 054002. [CrossRef]
337. Arroyo Garcia, A.; Hentschinski, M.; Kutak, K. QCD evolution based evidence for the onset of gluon saturation in exclusive photo-production of vector mesons. *Phys. Lett. B* **2019**, *795*, 569–575. [CrossRef]
338. Motyka, L.; Sadzikowski, M.; Stebel, T. Lam-Tung relation breaking in Z^0 hadroproduction as a probe of parton transverse momentum. *Phys. Rev.* **2017**, *D95*, 114025. [CrossRef]
339. Ball, R.D.; Bertone, V.; Bonvini, M.; Marzani, S.; Rojo, J.; Rottoli, L. Parton distributions with small-x resummation: Evidence for BFKL dynamics in HERA data. *Eur. Phys. J.* **2018**, *C78*, 321. [CrossRef]
340. Abdolmaleki, H.; Bertone, V.; Britzger, D.; Camarda, S.; Cooper-Sarkar, A.; Giuli, F.; Glazov, A.; Kusina, A.; Luszczak, A.; Olness, F.; et al. Impact of low-x resummation on QCD analysis of HERA data. *Eur. Phys. J. C* **2018**, *78*, 621. [CrossRef]
341. Bonvini, M.; Giuli, F. A new simple PDF parametrization: improved description of the HERA data. *Eur. Phys. J. Plus* **2019**, *134*, 531. [CrossRef]
342. Bacchetta, A.; Celiberto, F.G.; Radici, M.; Taels, P. Transverse-momentum-dependent gluon distribution functions in a spectator model. *Eur. Phys. J. C* **2020**, *80*, 733. [CrossRef]
343. Celiberto, F.G. 3D tomography of the nucleon: Transverse-momentum-dependent gluon distributions. *Nuovo Cim.* **2021**, *C44*, 36. [CrossRef]

344. Bacchetta, A.; Celiberto, F.G.; Radici, M.; Taels, P. A spectator-model way to transverse-momentum-dependent gluon distribution functions. *SciPost Phys. Proc.* **2022**, *8*, 040. [CrossRef]
345. Bacchetta, A.; Celiberto, F.G.; Radici, M. Toward twist-2 T-odd transverse-momentum-dependent gluon distributions: The f-type Sivers function. *Proceeds Sci.* **2022**, *EPS-HEP2021*, 376. [CrossRef]
346. Bacchetta, A.; Celiberto, F.G.; Radici, M. Toward twist-2 T-odd transverse-momentum-dependent gluon distributions: The f-type linearity function. *Proceeds Sci.* **2022**, *PANIC2021*, 378. [CrossRef]
347. Bacchetta, A.; Celiberto, F.G.; Radici, M. Towards Leading-twist T-odd TMD Gluon Distributions. *JPS Conf. Proc.* **2022**, *37*, 020124. [CrossRef]
348. Bacchetta, A.; Celiberto, F.G.; Radici, M. Unveiling the proton structure via transverse-momentum-dependent gluon distributions. *arXiv* **2022**, arXiv:2206.07815.
349. Bacchetta, A.; Celiberto, F.G.; Radici, M.; Signori, A. Phenomenology of gluon TMDs from $\eta_{b,c}$ production. *arXiv* **2022**, arXiv:2208.06252.
350. Celiberto, F.G. A Journey into the Proton Structure: Progresses and Challenges. *Universe* **2022**, *8*, 661. [CrossRef]
351. Nefedov, M. Sudakov resummation from the BFKL evolution. *Phys. Rev. D* **2021**, *104*, 054039. [CrossRef]
352. Hentschinski, M. Transverse momentum dependent gluon distribution within high energy factorization at next-to-leading order. *Phys. Rev. D* **2021**, *104*, 054014. [CrossRef]
353. Boroun, G.R. The dipole cross section by the unintegrated gluon distribution at small x. *arXiv* **2023**, arXiv:2301.01083.
354. Brodsky, S.J.; Hautmann, F.; Soper, D.E. Probing the QCD pomeron in e+ e- collisions. *Phys. Rev. Lett.* **1997**, *78*, 803–806; Erratum in *Phys. Rev. Lett.* **1997**, *79*, 3544. [CrossRef]
355. Brodsky, S.J.; Hautmann, F.; Soper, D.E. Virtual photon scattering at high-energies as a probe of the short distance pomeron. *Phys. Rev. D* **1997**, *56*, 6957–6979. [CrossRef]
356. Brodsky, S.J.; Fadin, V.S.; Kim, V.T.; Lipatov, L.N.; Pivovarov, G.B. The QCD pomeron with optimal renormalization. *JETP Lett.* **1999**, *70*, 155–160. [CrossRef]
357. Brodsky, S.J.; Fadin, V.S.; Kim, V.T.; Lipatov, L.N.; Pivovarov, G.B. High-energy QCD asymptotics of photon-photon collisions. *JETP Lett.* **2002**, *76*, 249–252. [CrossRef]
358. Mohammed, M.M.A. Hunting Stabilization Effects of the High-Energy Resummation at the LHC. Ph.D. Thesis, Università della Calabria and INFN-Cosenza, Rende, Italy.
359. Celiberto, F.G.; Papa, A. The high-energy QCD dynamics from Higgs-plus-jet correlations at the FCC. *arXiv* **2023**, arXiv:2305.00962.
360. Celiberto, F.G.; Delle Rose, L.; Fucilla, M.; Gatto, G.; Papa, A. High-energy resummed Higgs-plus-jet distributions at NLL/NLO* with POWHEG+JETHAD. In Proceedings of the 57th Rencontres de Moriond on QCD and High Energy Interactions, La Thuile, Italy, 25 March–1 April 2023.
361. Celiberto, F.G.; Fucilla, M.; Ivanov, D.Y.; Mohammed, M.M.A.; Papa, A. Higgs boson production at next-to-leading logarithmic accuracy. In Proceedings of the 57th Rencontres de Moriond on QCD and High Energy Interactions, La Thuile, Italy, 25 March–1 April 2023.
362. Binosi, D.; Collins, J.; Kaufhold, C.; Theussl, L. JaxoDraw: A Graphical user interface for drawing Feynman diagrams. Version 2.0 release notes. *Comput. Phys. Commun.* **2009**, *180*, 1709–1715. [CrossRef]
363. Bardeen, W.A.; Buras, A.J.; Duke, D.W.; Muta, T. Deep-inelastic scattering beyond the leading order in asymptotically free gauge theories. *Phys. Rev. D* **1978**, *18*, 3998–4017. [CrossRef]
364. Kotikov, A.V.; Lipatov, L.N. NLO corrections to the BFKL equation in QCD and in supersymmetric gauge theories. *Nucl. Phys. B* **2000**, *582*, 19–43. [CrossRef]
365. Furman, M. Study of a Nonleading {QCD} Correction to Hadron Calorimeter Reactions. *Nucl. Phys. B* **1982**, *197*, 413–445. [CrossRef]
366. Aversa, F.; Chiappetta, P.; Greco, M.; Guillet, J.P. QCD Corrections to Parton-Parton Scattering Processes. *Nucl. Phys. B* **1989**, *327*, 105. [CrossRef]
367. Ball, R.D.; Carrazza, S.; Cruz-Martinez, J.; Del Debbio, L.; Forte, S.; Giani, T.; Iranipour, S.; Kassabov, Z.; Latorre, J.I.; Nocera, E.R.; et al. An open-source machine learning framework for global analyses of parton distributions. *Eur. Phys. J. C* **2021**, *81*, 958.
368. Ball, R.D.; Carrazza, S.; Cruz-Martinez, J.; Del Debbio, L.; Forte, S.; Giani, T.; Iranipour, S.; Kassabov, Z.; Latorre, J.I.; Nocera, E.R.; et al. The path to proton structure at 1% accuracy. *Eur. Phys. J. C* **2022**, *82*, 428. [CrossRef]
369. Buckley, A.; Ferrando, J.; Lloyd, S.; Nordström, K.; Page, B.; Rüfenacht, M.; Schönherr, M.; Watt, G. LHAPDF6: Parton density access in the LHC precision era. *Eur. Phys. J. C* **2015**, *75*, 132. [CrossRef]
370. Forte, S.; Garrido, L.; Latorre, J.I.; Piccione, A. Neural network parametrization of deep inelastic structure functions. *J. High Energy Phys.* **2002**, *5*, 062. [CrossRef]
371. Ball, R.D.; Forte, S.; Stegeman, R. Correlation and combination of sets of parton distributions. *Eur. Phys. J. C* **2021**, *81*, 1046. [CrossRef]
372. Bugge, L. Experimental Heavy Quarkonium Physics: Introduction and Survey. In *Lectures Presented at the Trondheim Workshop 1984 in Theoretical Physics: Quantum ChromoDynamics in Theory and Experiment. Trondheim, Norway; Report Number: OSLO-86-20*; 1986. Available online: https://cds.cern.ch/record/171748/files/Oslo-86-20.pdf (accessed on 30 June 2023).
373. Chang, C.H.; Chen, Y.Q. The Production of B(c) or anti-B(c) meson associated with two heavy quark jets in Z0 boson decay. *Phys. Rev. D* **1992**, *46*, 3845; Erratum in *Phys. Rev. D* **1994**, *50*, 6013. [CrossRef]

374. Braaten, E.; Cheung, K.M.; Yuan, T.C. Perturbative QCD fragmentation functions for B_c and B_c * production. *Phys. Rev. D* **1993**, *48*, R5049. [CrossRef] [PubMed]
375. Ma, J.P. Calculating fragmentation functions from definitions. *Phys. Lett. B* **1994**, *332*, 398–404. [CrossRef]
376. Zheng, X.C.; Chang, C.H.; Feng, T.F.; Wu, X.G. QCD NLO fragmentation functions for c or b$^-$ quark to Bc or Bc* meson and their application. *Phys. Rev. D* **2019**, *100*, 034004. [CrossRef]
377. Zheng, X.C.; Chang, C.H.; Wu, X.G.; Zeng, J.; Huang, X.D. Next-to-leading order QCD corrections to the production of B_c and B_c^* through W^+-boson decays. *Phys. Rev. D* **2020**, *101*, 034029. [CrossRef]
378. Dadfar, S.; Zarrin, S. The production cross section of the Bc and Bc$*$ mesons via the fragmentation of b$^-$ quark at the next-to-leading-order accuracy. *Phys. Lett. B* **2022**, *835*, 137538. [CrossRef]
379. Zheng, X.C.; Wu, X.G.; Zhan, X.J.; Wang, G.Y.; Li, H.T. Higgs boson decays to Bc meson in the fragmentation-function approach. *Phys. Rev. D* **2023**, *107*, 074005. [CrossRef]
380. Eichten, E.J.; Quigg, C. Mesons with beauty and charm: Spectroscopy. *Phys. Rev. D* **1994**, *49*, 5845–5856. [CrossRef]
381. Landau, L.D. On the angular momentum of a system of two photons. *Dokl. Akad. Nauk SSSR* **1948**, *60*, 207–209. [CrossRef]
382. Yang, C.N. Selection Rules for the Dematerialization of a Particle Into Two Photons. *Phys. Rev.* **1950**, *77*, 242–245. [CrossRef]
383. Zheng, X.C.; Chang, C.H.; Wu, X.G. Fragmentation functions for gluon into B_c or B_c^* meson. *J. High Energy Phys.* **2022**, *5*, 036. [CrossRef]
384. Feng, F.; Jia, Y.; Yang, D. Gluon fragmentation into $B_c^{(*)}$ in NRQCD factorization. *arXiv* **2021**, arXiv:2112.15569.
385. Braaten, E.; Yuan, T.C. Gluon fragmentation into spin triplet S wave quarkonium. *Phys. Rev. D* **1995**, *52*, 6627–6629. [CrossRef] [PubMed]
386. Yuan, T.C. Perturbative QCD fragmentation functions for production of P wave mesons with charm and beauty. *Phys. Rev. D* **1994**, *50*, 5664–5675. [CrossRef] [PubMed]
387. Vogt, A. Efficient evolution of unpolarized and polarized parton distributions with QCD-PEGASUS. *Comput. Phys. Commun.* **2005**, *170*, 65–92. [CrossRef]
388. Salam, G.P.; Rojo, J. A Higher Order Perturbative Parton Evolution Toolkit (HOPPET). *Comput. Phys. Commun.* **2009**, *180*, 120–156. [CrossRef]
389. Botje, M. QCDNUM: Fast QCD Evolution and Convolution. *Comput. Phys. Commun.* **2011**, *182*, 490–532. [CrossRef]
390. Bertone, V.; Carrazza, S.; Rojo, J. APFEL: A PDF Evolution Library with QED corrections. *Comput. Phys. Commun.* **2014**, *185*, 1647–1668. [CrossRef]
391. Carrazza, S.; Ferrara, A.; Palazzo, D.; Rojo, J. APFEL Web: A web-based application for the graphical visualization of parton distribution functions. *J. Phys. G* **2015**, *42*, 057001. [CrossRef]
392. Bertone, V. APFEL++: A new PDF evolution library in C++. *Proceeds Sci.* **2018**, *DIS2017*, 201. [CrossRef]
393. Candido, A.; Hekhorn, F.; Magni, G. EKO: evolution kernel operators. *Eur. Phys. J. C* **2022**, *82*, 976. [CrossRef]
394. Kniehl, B.A.; Kramer, G.; Schienbein, I.; Spiesberger, H. Inclusive D*+- production in p anti-p collisions with massive charm quarks. *Phys. Rev. D* **2005**, *71*, 014018. [CrossRef]
395. Kniehl, B.A.; Kramer, G. D0, D+, D+(s), and Lambda+(c) fragmentation functions from CERN LEP1. *Phys. Rev. D* **2005**, *71*, 094013. [CrossRef]
396. Kniehl, B.A.; Kramer, G. Charmed-hadron fragmentation functions from CERN LEP1 revisited. *Phys. Rev. D* **2006**, *74*, 037502. [CrossRef]
397. Kneesch, T.; Kniehl, B.A.; Kramer, G.; Schienbein, I. Charmed-meson fragmentation functions with finite-mass corrections. *Nucl. Phys. B* **2008**, *799*, 34–59. [CrossRef]
398. Corcella, G.; Ferrera, G. Charm-quark fragmentation with an effective coupling constant. *J. High Energy Phys.* **2007**, *12*, 029. [CrossRef]
399. Anderle, D.P.; Kaufmann, T.; Stratmann, M.; Ringer, F.; Vitev, I. Using hadron-in-jet data in a global analysis of D^* fragmentation functions. *Phys. Rev. D* **2017**, *96*, 034028. [CrossRef]
400. Salajegheh, M.; Moosavi Nejad, S.M.; Soleymaninia, M.; Khanpour, H.; Atashbar Tehrani, S. NNLO charmed-meson fragmentation functions and their uncertainties in the presence of meson mass corrections. *Eur. Phys. J. C* **2019**, *79*, 999. [CrossRef]
401. Salajegheh, M.; Moosavi Nejad, S.M.; Delpasand, M. Determination of D_s^+ meson fragmentation functions through two different approaches. *Phys. Rev. D* **2019**, *100*, 114031. [CrossRef]
402. Soleymaninia, M.; Khanpour, H.; Moosavi Nejad, S.M. First determination of D^{*+}-meson fragmentation functions and their uncertainties at next-to-next-to-leading order. *Phys. Rev. D* **2018**, *97*, 074014. [CrossRef]
403. Kniehl, B.A.; Kramer, G.; Schienbein, I.; Spiesberger, H. $\Lambda_c^{\pm}$ production in pp collisions with a new fragmentation function. *Phys. Rev. D* **2020**, *101*, 114021. [CrossRef]
404. Delpasand, M.; Moosavi Nejad, S.M.; Soleymaninia, M. Λ_c^+ fragmentation functions from pQCD approach and the Suzuki model. *Phys. Rev. D* **2020**, *101*, 114022. [CrossRef]
405. Binnewies, J.; Kniehl, B.A.; Kramer, G. Inclusive B meson production in e^+e^- and $p\bar{p}$ collisions. *Phys. Rev. D* **1998**, *58*, 034016. [CrossRef]
406. Kniehl, B.A.; Kramer, G.; Schienbein, I.; Spiesberger, H. Finite-mass effects on inclusive B meson hadroproduction . *Phys. Rev. D* **2008**, *77*, 014011. [CrossRef]

407. Kniehl, B.A.; Kramer, G.; Schienbein, I.; Spiesberger, H. Inclusive B-Meson Production at the LHC in the GM-VFN Scheme. *Phys. Rev. D* **2011**, *84*, 094026. [CrossRef]
408. Kniehl, B.A.; Kramer, G.; Moosavi Nejad, S.M. Bottom-Flavored Hadrons from Top-Quark Decay at Next-to-Leading order in the General-Mass Variable-Flavor-Number Scheme. *Nucl. Phys. B* **2012**, *862*, 720–736. [CrossRef]
409. Kramer, G.; Spiesberger, H. b-hadron production in the general-mass variable-flavour-number scheme and LHC data. *Phys. Rev. D* **2018**, *98*, 114010. [CrossRef]
410. Kramer, G.; Spiesberger, H. Λ_b^0-baryon production in pp collisions in the general-mass variable-flavour-number scheme and comparison with CMS and LHCb data. *Chin. Phys. C* **2018**, *42*, 083102. [CrossRef]
411. Salajegheh, M.; Moosavi Nejad, S.M.; Khanpour, H.; Kniehl, B.A.; Soleymaninia, M. B-hadron fragmentation functions at next-to-next-to-leading order from a global analysis of e^+e^- annihilation data. *Phys. Rev. D* **2019**, *99*, 114001. [CrossRef]
412. Kniehl, B.A.; Moosavi Nejad, S.M. Angular analysis of bottom-flavored hadron production in semileptonic decays of polarized top quarks. *Phys. Rev. D* **2021**, *103*, 034015. [CrossRef]
413. Bowler, M.G. e+ e- Production of Heavy Quarks in the String Model. *Z. Phys. C* **1981**, *11*, 169. [CrossRef]
414. Kartvelishvili, V.G.; Likhoded, A.K. Structure Functions and Leptonic Widths of Heavy Mesons. *Yad. Fiz.* **1985**, *42*, 1306–1308.
415. Albino, S.; Kniehl, B.A.; Kramer, G. AKK Update: Improvements from New Theoretical Input and Experimental Data. *Nucl. Phys. B* **2008**, *803*, 42–104. [CrossRef]
416. Soleymaninia, M.; Hashamipour, H.; Khanpour, H.; Spiesberger, H. Fragmentation Functions for $\Xi^-/\bar{\Xi}^+$ Using Neural Networks. *Nucl. Phys. A* **2022**, *2023*, 01. [CrossRef]
417. Salam, G.P. A Resummation of large subleading corrections at small x. *J. High Energy Phys.* **1998**, *7*, 019. [CrossRef]
418. Ciafaloni, M.; Colferai, D.; Salam, G.P.; Stasto, A.M. Renormalization group improved small x Green's function. *Phys. Rev. D* **2003**, *68*, 114003. [CrossRef]
419. Ciafaloni, M.; Colferai, D.; Colferai, D.; Salam, G.P.; Stasto, A.M. Extending QCD perturbation theory to higher energies. *Phys. Lett. B* **2003**, *576*, 143–151. [CrossRef]
420. Ciafaloni, M.; Colferai, D.; Salam, G.P. On factorization at small x. *J. High Energy Phys.* **2000**, *7*, 054. [CrossRef]
421. Ciafaloni, M.; Colferai, D.; Salam, G.P. Renormalization group improved small x equation. *Phys. Rev. D* **1999**, *60*, 114036. [CrossRef]
422. Ciafaloni, M.; Colferai, D. The BFKL equation at next-to-leading level and beyond. *Phys. Lett. B* **1999**, *452*, 372–378. [CrossRef]
423. Sabio Vera, A. An 'All-poles' approximation to collinear resummations in the Regge limit of perturbative QCD. *Nucl. Phys. B* **2005**, *722*, 65–80. [CrossRef]
424. [The CMS collaboration] Azimuthal decorrelation of jets widely separated in rapidity in pp collisions at $\sqrt{s} = 7$ TeV. *J. High Energy Phys.* **2016**, *8*, 139. [CrossRef]
425. Mueller, A.; Xiao, B.W.; Yuan, F. Sudakov Resummation in Small-x Saturation Formalism. *Phys. Rev. Lett.* **2013**, *110*, 082301. [CrossRef]
426. Mueller, A.; Xiao, B.W.; Yuan, F. Sudakov double logarithms resummation in hard processes in the small-x saturation formalism. *Phys. Rev. D* **2013**, *88*, 114010. [CrossRef]
427. Marzani, S. Combining Q_T and small-x resummations. *Phys. Rev. D* **2016**, *93*, 054047. [CrossRef]
428. Mueller, A.; Szymanowski, L.; Wallon, S.; Xiao, B.W.; Yuan, F. Sudakov Resummations in Mueller-Navelet Dijet Production. *J. High Energy Phys.* **2016**, *3*, 096. [CrossRef]
429. Xiao, B.W.; Yuan, F. BFKL and Sudakov Resummation in Higgs Boson Plus Jet Production with Large Rapidity Separation. *Phys. Lett. B* **2018**, *782*, 28–33. [CrossRef]
430. Andersen, J.R.; Del Duca, V.; Frixione, S.; Schmidt, C.R.; Stirling, W.J. Mueller-Navelet jets at hadron colliders. *J. High Energy Phys.* **2001**, *2*, 007. [CrossRef]
431. Fontannaz, M.; Guillet, J.P.; Heinrich, G. Is a large intrinsic k(T) needed to describe photon + jet photoproduction at HERA? *Eur. Phys. J. C* **2001**, *22*, 303–315. [CrossRef]
432. Ducloué, B.; Szymanowski, L.; Wallon, S. Violation of energy–momentum conservation in Mueller–Navelet jets production. *Phys. Lett. B* **2014**, *738*, 311–316. [CrossRef]
433. [The CMS collaboration] Measurement of the Λ_b cross section and the $_{\bar{\Lambda}_b}$ to Λ_b ratio with $J/\Psi\Lambda$ decays in pp collisions at $\sqrt{s} = 7$ TeV. *Phys. Lett. B* **2012**, *714*, 136–157. [CrossRef]
434. Sterman, G.F. Summation of Large Corrections to Short Distance Hadronic Cross-Sections. *Nucl. Phys. B* **1987**, *281*, 310–364. [CrossRef]
435. Catani, S.; Trentadue, L. Resummation of the QCD Perturbative Series for Hard Processes. *Nucl. Phys. B* **1989**, *327*, 323–352. [CrossRef]
436. Catani, S.; Mangano, M.L.; Nason, P.; Trentadue, L. The Resummation of soft gluons in hadronic collisions. *Nucl. Phys. B* **1996**, *478*, 273–310. [CrossRef]
437. Bonciani, R.; Catani, S.; Mangano, M.L.; Nason, P. Sudakov resummation of multiparton QCD cross-sections. *Phys. Lett. B* **2003**, *575*, 268–278. [CrossRef]
438. de Florian, D.; Kulesza, A.; Vogelsang, W. Threshold resummation for high-transverse-momentum Higgs production at the LHC. *J. High Energy Phys.* **2006**, *2*, 047. [CrossRef]

439. Ahrens, V.; Becher, T.; Neubert, M.; Yang, L.L. Renormalization-Group Improved Prediction for Higgs Production at Hadron Colliders. *Eur. Phys. J. C* **2009**, *62*, 333–353. [CrossRef]
440. de Florian, D.; Grazzini, M. Higgs production at the LHC: updated cross sections at $\sqrt{s} = 8$ TeV. *Phys. Lett. B* **2012**, *718*, 117–120. [CrossRef]
441. Forte, S.; Ridolfi, G.; Rota, S. Threshold resummation of transverse momentum distributions beyond next-to-leading log. *J. High Energy Phys.* **2021**, *8*, 110. [CrossRef]
442. Mukherjee, A.; Vogelsang, W. Threshold resummation for W-boson production at RHIC. *Phys. Rev. D* **2006**, *73*, 074005. [CrossRef]
443. Bolzoni, P. Threshold resummation of Drell-Yan rapidity distributions. *Phys. Lett. B* **2006**, *643*, 325–330. [CrossRef]
444. Becher, T.; Neubert, M. Threshold resummation in momentum space from effective field theory. *Phys. Rev. Lett.* **2006**, *97*, 082001. [CrossRef]
445. Becher, T.; Neubert, M.; Xu, G. Dynamical Threshold Enhancement and Resummation in Drell-Yan Production. *J. High Energy Phys.* **2008**, *7*, 030. [CrossRef]
446. Bonvini, M.; Forte, S.; Ridolfi, G. Soft gluon resummation of Drell-Yan rapidity distributions: Theory and phenomenology. *Nucl. Phys. B* **2011**, *847*, 93–159. [CrossRef]
447. Ahmed, T.; Mandal, M.K.; Rana, N.; Ravindran, V. Higgs Rapidity Distribution in $b\bar{b}$ Annihilation at Threshold in N^3LO QCD. *J. High Energy Phys.* **2015**, *2*, 131. [CrossRef]
448. Banerjee, P.; Das, G.; Dhani, P.K.; Ravindran, V. Threshold resummation of the rapidity distribution for Drell-Yan production at NNLO+NNLL. *Phys. Rev. D* **2018**, *98*, 054018. [CrossRef]
449. Duhr, C.; Mistlberger, B.; Vita, G. Soft integrals and soft anomalous dimensions at N^3LO and beyond. *J. High Energy Phys.* **2022**, *9*, 155. [CrossRef]
450. Shi, Y.; Wang, L.; Wei, S.Y.; Xiao, B.W. Pursuing the Precision Study for Color Glass Condensate in Forward Hadron Productions. *Phys. Rev. Lett.* **2022**, *128*, 202302. [CrossRef] [PubMed]
451. Wang, L.; Chen, L.; Gao, Z.; Shi, Y.; Wei, S.Y.; Xiao, B.W. Forward inclusive jet productions in pA collisions. *Phys. Rev. D* **2023**, *107*, 016016. [CrossRef]
452. Lansberg, J.P.; Shao, H.S.; Yamanaka, N. Indication for double parton scatterings in $W+$ prompt J/ψ production at the LHC. *Phys. Lett. B* **2018**, *781*, 485–491. [CrossRef]
453. d'Enterria, D.; Snigirev, A.M. Triple parton scatterings in high-energy proton-proton collisions. *Phys. Rev. Lett.* **2017**, *118*, 122001. [CrossRef]
454. Shao, H.S.; Zhang, Y.J. Triple prompt J/ψ hadroproduction as a hard probe of multiple-parton scatterings. *Phys. Rev. Lett.* **2019**, *122*, 192002. [CrossRef]
455. Roy, D.P.; Sridhar, K. Fragmentation contribution to quarkonium production in hadron collision. *Phys. Lett. B* **1994**, *339*, 141–147. [CrossRef]
456. Chapon, E.; d'Enterria, D.; Ducloue, B.; Echevarria, M.G.; Gossiaux, P.B.; Kartvelishvili, V.; Kasemets, T.; Lansberg, J.P.; McNulty, R.; Price, D.D.; et al. Prospects for quarkonium studies at the high-luminosity LHC. *Prog. Part. Nucl. Phys.* **2022**, *122*, 103906. [CrossRef]
457. Anchordoqui, L.A.; Ariga, A.; Ariga, T.; Bai, W.D.; Balazs, K.; Batell, B.; Boyd, J.; Bramante, J.; Campanelli, M.; Carmona, A.; et al. The Forward Physics Facility: Sites, experiments, and physics potential. *Phys. Rept.* **2022**, *968*, 1–50. [CrossRef]
458. Feng, J.L.; Kling, F.; Reno, M.H.; Rojo, J.; Soldin, D.; Anchordoqui, L.A.; Boyd, J.; Ismail, A.; Harland-Lang, L.; Kelly, K.J.; et al. The Forward Physics Facility at the High-Luminosity LHC. *J. Phys. G* **2023**, *50*, 030501. [CrossRef]
459. Hentschinski, M.; Royon, C.; Peredo, M.A.; Baldenegro, C.; Bellora, A.; Boussarie, R.; Celiberto, F.G.; Cerci, S.; Chachamis, G.; Contreras, J.G.; et al. White Paper on Forward Physics, BFKL, Saturation Physics and Diffraction. *Acta Phys. Polon. B* **2023**, *54*, 2. [CrossRef]
460. Accardi, A.; Albacete, J.L.; Anselmino, M.; Armesto, N.; Aschenauer, E.C.; Bacchetta, A.; Boer, D.; Brooks, W.K.; Burton, T.; Chang, N.B.; et al. Electron Ion Collider: The Next QCD Frontier: Understanding the glue that binds us all. *Eur. Phys. J. A* **2016**, *52*, 268. [CrossRef]
461. Khalek, R.A.; Accardi, A.; Adam, J.; Adamiak, D.; Akers, W.; Albaladejo, M.; Al-bataineh, A.; Alexeev, M.G.; Ameli, F.; Antonioli, P.; et al. Science Requirements and Detector Concepts for the Electron-Ion Collider: EIC Yellow Report. *Nucl. Phys. A* **2022**, *1026*, 122447. [CrossRef]
462. Khalek, R.A.; D'Alesio, U.; Arratia, M.; Bacchetta, A.; Battaglieri, M.; Begel, M.; Boglione, M.; Boughezal, R.; Boussarie, R.; Bozzi, G.; et al. Snowmass 2021 White Paper: Electron Ion Collider for High Energy Physics. In Proceedings of the 2022 Snowmass Summer Study, Seattle, WA, USA, 17–26 July 2022.
463. Acosta, D.; Barberis, E.; Hurley, N.; Li, W.; Colin, O.M.; Wood, D.; Zuo, X. The Potential of a TeV-Scale Muon-Ion Collider. In Proceedings of the 2022 Snowmass Summer Study, Seattle, WA, USA, 17–26 July 2022.
464. Aryshev, A.; Behnke, T.; Berggren, M.; Brau, J.; Craig, N.; Freitas, A.; Gaede, F.; Gessner, S.; Gori, S.; Grojean, C.; et al. The International Linear Collider: Report to Snowmass 2021. *arXiv* **2022**, arXiv:2203.07622.
465. Brunner, O.; Burrows, P.N.; Calatroni, S.; Lasheras, N.C.; Corsini, R.; D'Auria, G.; Doebert, S.; Faus-Golfe, A.; Grudiev, A.; Latina, A.; et al. The CLIC project. *arXiv* **2022**, arXiv:2203.09186.

466. Arbuzov, A.; Bacchetta, A.; Butenschoen, M.; Celiberto, F.G.; D'Alesio, U.; Deka, M.; Denisenko, I.; Echevarria, M.G.; Efremov, A.; Ivanov, N.Y.; et al. On the physics potential to study the gluon content of proton and deuteron at NICA SPD. *Prog. Part. Nucl. Phys.* **2021**, *119*, 103858. [CrossRef]
467. Abazov, V.M. et al. [The SPD collaboration] Conceptual design of the Spin Physics Detector. *arXiv* **2021**. arXiv:2102.00442.
468. Bernardi, G.; Brost, E.; Denisov, D.; Landsberg, G.; Aleksa, M.; d'Enterria, D.; Janot, P.; Mangano, M.L.; Selvaggi, M.; Zimmermann, F.; et al. The Future Circular Collider: A Summary for the US 2021 Snowmass Process. *arXiv* **2022**, arXiv:2203.06520.
469. Amoroso, S.; Apyan, A.; Armesto, N.; Ball, R.D.; Bertone, V.; Bissolotti, C.; Bluemlein, J.; Boughezal, R.; Bozzi, G.; Britzger, D.; et al. Snowmass 2021 whitepaper: Proton structure at the precision frontier. *Acta Phys. Polon. B* **2022**, *53*, A1. [CrossRef]
470. Celiberto, F.G.; Fucilla, M.; Ivanov, D.Y.; Mohammed, M.M.A.; Papa, A. High-energy QCD at colliders: Semi-hard reactions and unintegrated gluon densities: Letter of Interest for SnowMass 2021. In Proceedings of the 2022 Snowmass Summer Study, Seattle, WA, USA, 17–26 July 2022.
471. Klein, S.; Takaki, D.T.; Adam, J.; Aidala, C.; Angerami, A.; Audurier, B.; Bertulani, C.; Bierlich, C.; Blok, B.; Brandenburg, J.D.; et al. New opportunities at the photon energy frontier. *arXiv* **2020**, arXiv:2009.03838.
472. Canepa, A.; D'Onofrio, M. Future Accelerator Projects: New Physics at the Energy Frontier (FERMILAB-PUB-22-248-PPD). *arXiv* **2022**, arXiv:2306.12897.
473. de Blas, J.; Buttazzo, D.; Capdevilla, R.M.; Curtin, D.; Franceschini, R.; Maltoni, F.; Meade, P.R.; Meloni, F.; Su, S.F.; Vryonidou, E.; et al. The physics case of a 3 TeV muon collider stage. *arXiv* **2022**, arXiv:2203.07261.
474. Aimè, C.; Apyan, A.; Mahmoud, M.A.; Bartosik, N.; Batsch, F.; Bertolin, A.; Bonesini, M.; Bottaro, S.; Buttazzo, D.; Capdevilla, R.M.; et al. Muon Collider Physics Summary. *arXiv* **2022**, arXiv:2203.07256.
475. Bartosik, N.; Krizka, K.; Griso, S.P.; Aimè, C.; Apyan, A.; Agashe, K.; Allanach, B.C.; Andreetto, P.; Asadi, P.; Mahmoud, M.A.; et al. Simulated Detector Performance at the Muon Collider. In Proceedings of the 2022 Snowmass Summer Study, Seattle, WA, USA, 17–26 July 2022.
476. Accettura, C.; Adams, D.; Agarwal, R.; Ahdida, C.; Aimè, C.; Amapane, N.; Amorim, D.; Andreetto, P.; Anulli, F.; Appleby, R.; et al. Towards a Muon Collider. *arXiv* **2023**, arXiv:2303.08533.
477. Vignaroli, N. Charged resonances and MDM bound states at a multi-TeV muon collider. *arXiv* **2023**, arXiv:2304.12362.
478. Black, K.M.; Jindariani, S.; Li, D.; Maltoni, F.; Meade, P.; Stratakis, D.; Acosta, D.; Agarwal, R.; Agashe, K.; Aimè, C.; et al. Muon Collider Forum Report. *arXiv* **2022**, arXiv:2209.01318.
479. Dawson, S.; Meade, P.; Ojalvo, I.; Vernieri, C.; Adhikari, S.; Abu-Ajamieh, F.; Alberta, A.; Bahl, H.; Barman, R.; Basso, M.; et al. Report of the Topical Group on Higgs Physics for Snowmass 2021: The Case for Precision Higgs Physics. In Proceedings of the 2022 Snowmass Summer Study, Seattle, WA, USA, 17–26 July 2022.
480. Bose, T.; Boveia, A.; Doglioni, C.; Griso, S.P.; Hirschauer, J.; Lipeles, E.; Liu, Z.; Shah, N.R.; Wang, L.T.; Agashe, K.; et al. Report of the Topical Group on Physics Beyond the Standard Model at Energy Frontier for Snowmass 2021. In Proceedings of the 2022 Snowmass Summer Study, Seattle, WA, USA, 17–26 July 2022.
481. Begel, M.; Hoeche, S.; Schmitt, M.; Lin, H.W.; Nadolsky, P.M.; Royon, C.; Lee, Y.J.; Mukherjee, S.; Baldenegro, C.; Campbell, J.; et al. Precision QCD, Hadronic Structure & Forward QCD, Heavy Ions: Report of Energy Frontier Topical Groups 5, 6, 7 submitted to Snowmass 2021. *arXiv* **2022**, arXiv:2209.14872.
482. Abir, R.; Akushevich, I.; Altinoluk, T.; Anderle, D.P.; Aslan, F.P.; Bacchetta, A.; Balantekin, B.; Barata, J.; Battaglieri, M.; Bertulani, C.A.; et al. The case for an EIC Theory Alliance: Theoretical Challenges of the EIC. *arXiv* **2023**, arXiv:2305.14572.
483. Accardi, A.; Achenbach, P.; Adhikari, D.; Afanasev, A.; Akondi, C.S.; Akopov, N.; Albaladejo, M.; Albataineh H.; Albrecht, M.; Almeida-Zamora, B.; et al. Strong Interaction Physics at the Luminosity Frontier with 22 GeV Electrons at Jefferson Lab. *arXiv* **2023**, arXiv:2306.09360.
484. Gelis, F.; Iancu, E.; Jalilian-Marian, J.; Venugopalan, R. The Color Glass Condensate. *Ann. Rev. Nucl. Part. Sci.* **2010**, *60*, 463–489. [CrossRef]
485. Kovchegov, Y.V.; Levin, E. *Quantum Chromodynamics at High Energy*; Cambridge University Press: Cambridge, UK, 2012; Volume 33. [CrossRef]
486. Chirilli, G.A.; Xiao, B.W.; Yuan, F. Inclusive Hadron Productions in pA Collisions. *Phys. Rev. D* **2012**, *86*, 054005. [CrossRef]
487. Boussarie, R.; Grabovsky, A.V.; Szymanowski, L.; Wallon, S. Impact factor for high-energy two and three jets diffractive production. *J. High Energy Phys.* **2014**, *9*, 026. [CrossRef]
488. Benic, S.; Fukushima, K.; Garcia-Montero, O.; Venugopalan, R. Probing gluon saturation with next-to-leading order photon production at central rapidities in proton-nucleus collisions. *J. High Energy Phys.* **2017**, *1*, 115. [CrossRef]
489. Benić, S.; Fukushima, K.; Garcia-Montero, O.; Venugopalan, R. Constraining unintegrated gluon distributions from inclusive photon production in proton–proton collisions at the LHC. *Phys. Lett. B* **2019**, *791*, 11–16. [CrossRef]
490. Roy, K.; Venugopalan, R. NLO impact factor for inclusive photon+dijet production in $e + A$ DIS at small x. *Phys. Rev. D* **2020**, *101*, 034028. [CrossRef]
491. Roy, K.; Venugopalan, R. Extracting many-body correlators of saturated gluons with precision from inclusive photon+dijet final states in deeply inelastic scattering. *Phys. Rev. D* **2020**, *101*, 071505. [CrossRef]
492. Beuf, G.; Hänninen, H.; Lappi, T.; Mäntysaari, H. Color Glass Condensate at next-to-leading order meets HERA data. *Phys. Rev. D* **2020**, *102*, 074028. [CrossRef]

493. Iancu, E.; Mueller, A.H.; Triantafyllopoulos, D.N. Probing Parton Saturation and the Gluon Dipole via Diffractive Jet Production at the Electron-Ion Collider. *Phys. Rev. Lett.* **2022**, *128*, 202001. [CrossRef] [PubMed]
494. Iancu, E.; Mueller, A.H.; Triantafyllopoulos, D.N.; Wei, S.Y. Probing gluon saturation via diffractive jets in ultra-peripheral nucleus-nucleus collisions. *arXiv* **2023**, arXiv:2304.12401.
495. Wallon, S. The QCD shockwave approach at NLO: Towards precision physics in gluonic saturation. In Proceedings of the Diffraction and Low-x 2022, Corigliano Calabro, Italy, 24–30 September 2023.
496. Hatta, Y.; Xiao, B.W.; Yuan, F.; Zhou, J. Anisotropy in Dijet Production in Exclusive and Inclusive Processes. *Phys. Rev. Lett.* **2021**, *126*, 142001. [CrossRef]
497. Hatta, Y.; Xiao, B.W.; Yuan, F.; Zhou, J. Azimuthal angular asymmetry of soft gluon radiation in jet production. *Phys. Rev. D* **2021**, *104*, 054037. [CrossRef]
498. Caucal, P.; Salazar, F.; Venugopalan, R. Dijet impact factor in DIS at next-to-leading order in the Color Glass Condensate. *J. High Energy Phys.* **2021**, *11*, 222. [CrossRef]
499. Caucal, P.; Salazar, F.; Schenke, B.; Venugopalan, R. Back-to-back inclusive dijets in DIS at small x: Sudakov suppression and gluon saturation at NLO. *J. High Energy Phys.* **2022**, *11*, 169. [CrossRef]
500. Taels, P.; Altinoluk, T.; Beuf, G.; Marquet, C. Dijet photoproduction at low x at next-to-leading order and its back-to-back limit. *J. High Energy Phys.* **2022**, *10*, 184. [CrossRef]
501. Fucilla, M.; Grabovsky, A.V.; Li, E.; Szymanowski, L.; Wallon, S. NLO computation of diffractive di-hadron production in a saturation framework. *J. High Energy Phys.* **2023**, *3*, 159. [CrossRef]
502. Kotko, P.; Kutak, K.; Marquet, C.; Petreska, E.; Sapeta, S.; van Hameren, A. Improved TMD factorization for forward dijet production in dilute-dense hadronic collisions. *J. High Energy Phys.* **2015**, *9*, 106. [CrossRef]
503. van Hameren, A.; Kotko, P.; Kutak, K.; Marquet, C.; Petreska, E.; Sapeta, S. Forward di-jet production in p+Pb collisions in the small-x improved TMD factorization framework. *J. High Energy Phys.* **2016**, *12*, 034; Erratum in *J. High Energy Phys.* **2019**, *02*, 158. [CrossRef]
504. Altinoluk, T.; Boussarie, R.; Marquet, C.; Taels, P. Photoproduction of three jets in the CGC: Gluon TMDs and dilute limit. *arXiv* **2020**, arXiv:2001.00765.
505. Altinoluk, T.; Marquet, C.; Taels, P. Low-x improved TMD approach to the lepto- and hadroproduction of a heavy-quark pair. *J. High Energy Phys.* **2021**, *6*, 085. [CrossRef]
506. Boussarie, R.; Mäntysaari, H.; Salazar, F.; Schenke, B. The importance of kinematic twists and genuine saturation effects in dijet production at the Electron-Ion Collider. *J. High Energy Phys.* **2021**, *9*, 178. [CrossRef]
507. Caucal, P.; Salazar, F.; Schenke, B.; Stebel, T.; Venugopalan, R. Back-to-back inclusive di-jets in DIS at small x_{Bj}: Gluon Weizsäcker-Williams distribution at NLO. *arXiv* **2023**, arXiv:2304.03304.
508. Kang, Z.B.; Ma, Y.Q.; Venugopalan, R. Quarkonium production in high energy proton-nucleus collisions: CGC meets NRQCD. *J. High Energy Phys.* **2014**, *1*, 056. [CrossRef]
509. Ma, Y.Q.; Venugopalan, R. Comprehensive Description of J/ψ Production in Proton-Proton Collisions at Collider Energies. *Phys. Rev. Lett.* **2014**, *113*, 192301. [CrossRef]
510. Ma, Y.Q.; Venugopalan, R.; Zhang, H.F. J/ψ production and suppression in high energy proton-nucleus collisions. *Phys. Rev. D* **2015**, *92*, 071901. [CrossRef]
511. Ma, Y.Q.; Stebel, T.; Venugopalan, R. J/ψ polarization in the CGC+NRQCD approach. *J. High Energy Phys.* **2018**, *12*, 057. [CrossRef]
512. Stebel, T.; Watanabe, K. $J\psi$ polarization in high multiplicity pp and pA collisions: CGC + NRQCD approach. *Phys. Rev. D* **2021**, *104*, 034004. [CrossRef]
513. Mäntysaari, H.; Penttala, J. Exclusive heavy vector meson production at next-to-leading order in the dipole picture. *Phys. Lett. B* **2021**, *823*, 136723. [CrossRef]
514. Mäntysaari, H.; Penttala, J. Complete calculation of exclusive heavy vector meson production at next-to-leading order in the dipole picture. *J. High Energy Phys.* **2022**, *8*, 247. [CrossRef]
515. Nocera, E.R. Towards a Neural Network Determination of Charged Pion Fragmentation Functions. In Proceedings of the 22nd International Symposium on Spin Physics, Urbana, IL, USA, 25–30 September 2016.
516. Bertone, V.; Carrazza, S.; Nocera, E.R.; Hartland, N.P.; Rojo, J. Towards a Neural Network determination of Pion Fragmentation Functions. In Proceedings of the Parton Radiation and Fragmentation from LHC to FCC-ee: CERN, Geneva, Switzerland, 22–23 November 2016; pp. 19–25.
517. Bertone, V.; Carrazza, S.; Hartland, N.P.; Nocera, E.R.; Rojo, J. A determination of the fragmentation functions of pions, kaons, and protons with faithful uncertainties. *Eur. Phys. J. C* **2017**, *77*, 516. [CrossRef]
518. Bertone, V.; Hartland, N.P.; Nocera, E.R.; Rojo, J.; Rottoli, L. Charged hadron fragmentation functions from collider data. *Eur. Phys. J. C* **2018**, *78*, 651. [CrossRef]
519. Khalek, R.A.; Bertone, V.; Nocera, E.R. Determination of unpolarized pion fragmentation functions using semi-inclusive deep-inelastic-scattering data. *Phys. Rev. D* **2021**, *104*, 034007. [CrossRef]
520. Abdul Khalek, R.; Bertone, V.; Khoudli, A.; Nocera, E.R. Pion and kaon fragmentation functions at next-to-next-to-leading order. *Phys. Lett. B* **2022**, *834*, 137456. [CrossRef]

521. Soleymaninia, M.; Hashamipour, H.; Khanpour, H. Neural network QCD analysis of charged hadron fragmentation functions in the presence of SIDIS data. *Phys. Rev. D* **2022**, *105*, 114018. [CrossRef]
522. Alwall, J.; Frederix, R.; Frixione, S.; Hirschi, V.; Maltoni, F.; Mattelaer, O.; Shao, H.S.; Stelzer, T.; Torrielli, P.; Zaro, M. The automated computation of tree-level and next-to-leading order differential cross sections, and their matching to parton shower simulations. *J. High Energy Phys.* **2014**, *7*, 079. [CrossRef]
523. Safronov, A.; Flore, C.; Kikola, D.; Kusina, A.; Lansberg, J.P.; Mattelaer, O.; Shao, H.S. A tool for automated perturbative cross section computations of asymmetric hadronic collisions at next-to-leading order using the MadGraph5_aMC@NLO framework. *Proceeds Sci.* **2022**, *ICHEP2022*, 494. [CrossRef]
524. Flore, C. NLOAccess: automated online computations for collider physics. *Eur. Phys. J. A* **2023**, *59*, 46. [CrossRef]